ADVANCED MOTION CONTROL IN ROBOTIC PATIENT POSITIONING SYSTEM FOR BRAIN CANCER RADIOSURGERY

Thesis for the Degree of Doctor of Philosophy (PhD)

by:
Alaa Saadah

Supervisor:
Dr. Géza Husi

UNIVERSITY OF DEBRECEN
Doctoral Council of Natural Sciences and Information Technology
Doctoral School of Informatics
Debrecen, 2024

Hereby I declare that I prepared this thesis within the Doctoral Council of Natural Sciences and Information Technology, Doctoral School of Informatics, University of Debrecen in order to obtain a PhD Degree in Informatics at Debrecen University.

The results published in the thesis are not reported in any other PhD theses.

Debrecen, 2024/06/12. ……..
signature of the candidate

Hereby I confirm that, Alaa Saadah candidate conducted her studies with my supervision within the Informatics Doctoral Program of the Doctoral School of University of Debrecen between 2019 and 2024 The independent studies and research work of the candidate significantly contributed to the results published in the thesis.
I also declare that the results published in the thesis are not reported in any other theses.
I support the acceptance of the thesis.

Debrecen, 2024/06/12 . ……..
signature of the supervisor

ADVANCED MOTION CONTROL IN ROBOTIC PATIENT POSITIONING SYSTEM FOR BRAIN CANCER RADIOSURGERY

Dissertation submitted in partial fulfilment of the requirements for the doctoral (PhD) degree in Informatics

Written by Alaa Saadah certified in Technical Engineering.

Prepared in the framework of the Informatics doctoral school of the University of Debrecen
(Industrial and Scientific Applications of Informatics)

Dissertation advisor: Dr. Géza Husi.

The official opponents of the dissertation:

Dr. …….

Dr. …….

The evaluation committee:

chairperson: Dr. …….

members: Dr. …….

Dr. …….

Dr. …….

Dr. …….

The date of the dissertation defense: 2024

"The aim of science is not to open the door to infinite wisdom, but to set a limit to infinite error"

Bertolt Brecht

"The good physician treats the disease, the great physician treats the patient who has the disease"

William Osler

DEBRECEN UNIVERSITY

Abstract

Doctoral School of Informatics

Advanced Motion Control in Robotic Patient Positioning System for Brain Cancer Radiosurgery

by Alaa SAADAH

The dissertation presents a comprehensive analysis of the Robotic Patient Positioning System (PPS), pivotal for enhancing the accuracy and safety of Stereotactic Radiosurgery (SRS). With an innovative design pending patent approval, the PPS targets an unparalleled precision of 0.1mm, which is vital for the efficacy of treatments, particularly in brain cancer therapies where the margin for error is negligible.

Aiming to fill a critical gap in the current literature, the study delves into the unexplored kinematic and control mechanisms integral to the PPS's function. The research is significant for its meticulous evaluation of these systems, providing a kinematic study that steers clear of overly complex design specifics while spotlighting the motion control science essential to the PPS's operation.

Objectives are strategically set to include an in-depth kinematic study to comprehend the system's movement characteristics, an investigation into the motion control components like servo motors and drives, and a rigorous examination of the control algorithms, specifically comparing single-loop and dual-loop systems. Validation plays a key role, employing MATLAB and CAD-based simulations complemented by empirical testing using the OptiTrack system, which offers a high-precision method for real-world motion tracking.

The outcomes are poised to contribute significantly to the field of SRS by bolstering the precision and safety protocols within PPS technologies, thereby potentially improving patient outcomes in cancer treatments. This dissertation stands as an essential reference for future interdisciplinary research and development in medical robotics and patient care systems.

Acknowledgements

Firstly, I must express my heartfelt thanks to Dr. Géza Husi. Beyond his expertise, his continuous patience and unwavering faith in me have been guiding forces.

I'd also like to extend my appreciation to everyone at Spinotron Company. It wasn't just about work there; it was a hub for collaboration and personal growth.

To my father and mother: You two are the wings that have always let me soar, pushing me higher towards my dreams. Your prayers have been my guiding light, leading me every step of the way.

To my pillars of strength, my sisters Nour and Bayan: Words fall short when I try to thank you. Through the ups and downs you two have been the wind beneath my wings.

To my nephews, Kareem and Hazem: The world, through your eyes, seems brighter, and filled with hope.

To Salah and Bisher: You've become like true brothers to me in every sense.

For Moafak, my dear godson: your faith in me has always been my compass, guiding my steps.

To the friends that became family - Sandy and Raghad: Your support, both before and during this journey, has kept me strong. Our shared memories, laughter, and encouragement have been invaluable.

In this journey, I've found a family away from home, a group of kindred spirits who've made every success sweeter and every challenge easier to face to Ayham, Maria, Rachael and Lamas.

To Ammar: Your support and understanding have meant the world to me. Knowing you've got my back makes every tough moment easier.

To Alaa and Mohammad: Thank you for always being there, through every high and low, and for making this journey so much easier with your love and support.

Lastly, to everyone who's been a part of this journey, no matter how briefly: Every chat, every moment, every guidance has shaped my path and every piece of advice has molded the person I've become today.

From the depths of my heart, I thank each one of you for leaving an indelible mark on the pages of my life's story...

Contents

List of Figures

List of Tables

List of Abbreviations

SRS	**S**tereotactic **R**adio **S**urgery
SBRT	**S**tereotactic **B**ody **R**adio **T**herapy
PPS	**P**atient **P**ositionning **S**ystem
PPT	**P**atient **P**ositionning **T**able
BDP	**B**eam **D**elivery **P**latform
PRTH	**P**recision **R**obotic **T**reatment **H**ead
TPS	**T**reatment **P**laning**S**ystem
FDA	**F**ood (and) **D**rug **A**dministration
IEC	**I**nternational **E**lectrotechnical **C**ommission
CT	**C**omputed **T**omography
BCE	**B**efore **C**ommen **E**ra
BC	**B**efore **C**hrist
AD	**A**nno **D**omini
XRT	E**X**ternal **R**adiation **T**herapy
LDR	**L**ow **D**ose **R**ate
LINAC	**LIN**ear **AC**celerator
IMRT	**I**ntensity **M**odulated **R**adiation**T**herapy
MRI	**M**agnetic **R**esonance **I**maging
GK	**G**amma **K**nife
CGK	**C**yber **G**amma **K**nife
DOF	**D**egree **O**f **F**reedom
MIC	**M**echanical **I**so **C**enter
FK	**F**orward **K**inematics
IK	**I**nverse **K**inematics
CP	**C**ontrolled **P**oint
TP	**T**arget **P**oint
ROM	**R**ange **O**f **M**otion
OTS	**O**ptical **T**racking **S**ystem
SIS	**S**tereotactic **I**mmobilization **S**ystem

To my father . . .
This is for you – the dream you started -
I now fulfill . . .

Chapter 1

Introduction

1.1 Background

Brain cancer is a serious health issue that needs better treatment options. This research focuses on the Patient Positioning System (PPS), which helps position patients very accurately during treatment. The PPS can achieve precision up to 0.1 mm, ensuring that the tumor is targeted effectively while minimizing damage to healthy tissues. This accuracy is crucial for improving treatment success. .

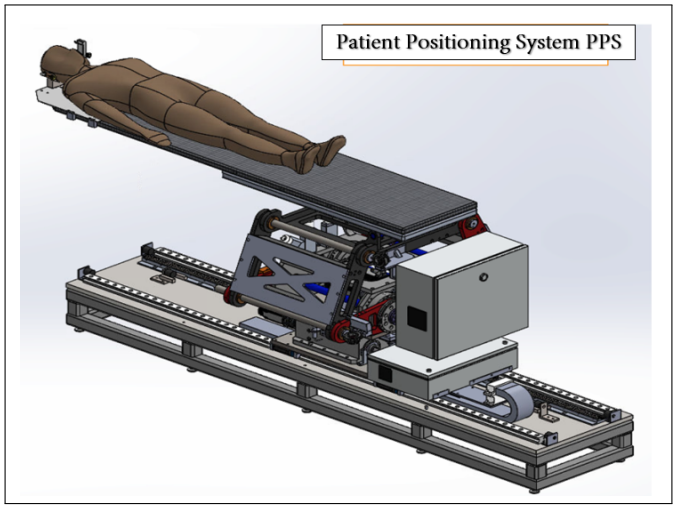

FIGURE 1.1: Patient Positioning Table

This research focuses on the Patient Positioning System (PPS). The PPS helps to place the patient in the right position for treatment. It uses a camera system for super-accurate positioning—up to 0.1mm. The system can also make small adjustments during treatment, which helps in targeting the tumor more effectively.

Our aim is to study the PPS in detail to understand how it can make brain cancer treatment more accurate and maybe even help treat other types of cancer in the future.

1.2 Significance of the Research

The Patient Positioning System (PPS), which is currently in the patent application phase, presents a groundbreaking design with the potential to revolutionize Stereotactic Radiosurgery (SRS) treatments. Engineered for unparalleled positioning accuracy of up to 0.1mm through advanced motion control systems, this innovation could set new standards in medical precision.

This dissertation aims to provide an evaluation of the PPS, focusing on its effectiveness, safety, and alignment with regulatory standards. Specifically, it assesses compliance with guidelines set by the Food and Drug Administration (FDA) and the International Electrotechnical Commission (IEC), including the IEC 60601 standard for the safety and effectiveness of medical electrical equipment. Through an in-depth study of the system's kinematics and control mechanisms, this research seeks to confirm that the PPS is not only highly precise but also meets essential safety standards, ensuring its suitability for both patients and healthcare providers.

1.3 The Importance of Robotic PPS

The Patient Positioning System (PPS) is integral to the success of modern cancer therapies. It offers the Patient Positioning Table (PPT) a remarkable 6-degree-of-freedom mobility, allowing it to move up and down, left and right, as well as to tilt for optimal alignment. This feature is particularly invaluable for specialized treatments such as brain cancer, where even minor inaccuracies can adversely affect healthy tissue. By facilitating such precise adjustments, the PPS focuses the radiation solely on the tumor, thus sparing the surrounding healthy tissue.

Therefore, optimizing the 6-degree-of-freedom function in the PPS is a key area of focus for enhancing both the precision and safety of cancer treatments.

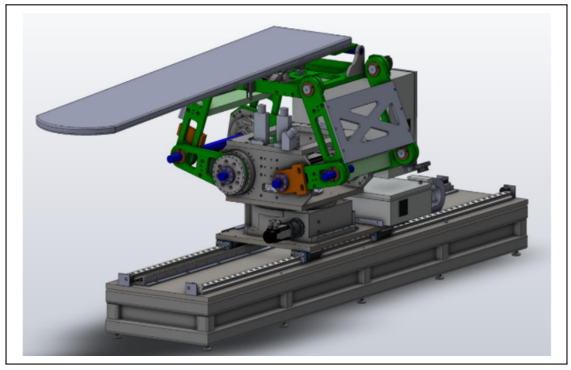

FIGURE 1.2: Patient Positioning Table (PPT) CAD model

1.4 Problem Statement

The Patient Positioning System (PPS) represents a breakthrough in Stereotactic Radiosurgery (SRS), aiming for an exceptional positioning accuracy of 0.1 mm. While the PPS is designed to meet stringent safety and accuracy standards, its intricate mechanism poses several challenges:

1. **Complex Mechanism**: The PPS consists of multiple subsystems, such as a linear rail system, a linkage system operating as a parallel robot, and a tabletop. These elements require an in-depth kinematic study for effective control.

2. **Precision Target**: The targeted accuracy for positioning is extremely narrow, set at 0.1 mm. Any minor miscalculation or mechanical issue, such as gear backlash, could compromise this precision.

3. **Advanced Motion Control**: Implementing control over each motor axis with 3-phase servo motors requires advanced control algorithms and high-resolution encoders. Fine-tuning these control systems is crucial for achieving the intended level of precision.

4. **Safety Compliance**: Given the medical application of the PPS, adherence to safety standards is imperative. Advanced control algorithms and system configurations must work seamlessly to mitigate any risks associated with patient positioning.

This dissertation aims to dissect and address these challenges, ultimately contributing to the optimization of the PPS for SRS treatments, in compliance with applicable safety standards.

1.5 Objectives

The primary objective of this dissertation is to comprehensively evaluate the Robotic Patient Positioning System (PPS), with a focus on the following key aspects:

1. Conduct a detailed kinematic study to understand the motion characteristics of the system.

2. Investigate the types of servo motors and drives utilized and assess their suitability for achieving a targeted positioning accuracy of 0.1 mm.

3. Examine the control algorithms responsible for the system's motion, particularly in the context of single-loop and dual-loop control mechanisms.

4. Validate the findings through testing and measurements.

1.6 Scope

This dissertation will specifically delve into:

1. The kinematic properties of the PPS, avoiding intricate design details but focusing on the motion science.
2. The motion controller, servo motors, Encoders and drives used in the system, elucidating their roles in achieving the system's targeted accuracy.
3. The control mechanisms, comparing the effectiveness of single-loop and dual-loop systems in the context of Stereotactic Radiosurgery (SRS) for brain cancer treatments.
4. Measurement and validation methods involving MATLAB and CAD models, followed by real-world testing using a three-camera OptiTrack system to measure markers on controlled points.

   The outcomes will be compared against calculated results for validation.

This dissertation aims to align with the IEC Standard 60601, focusing on assessing the system's safety and reliability. The focus will not be on the intricate details of the design but rather on the kinematics and control systems that make the PPS functional for its intended medical applications.

1.7 Research Gap

Despite the considerable advancements in Stereotactic Radiosurgery (SRS) technologies, a comprehensive study focusing on the kinematics and control mechanisms of Patient Positioning Systems (PPS) is notably lacking. While existing literature extensively covers the technological components used in SRS—such as linear accelerators (LINAC), Gamma Knife, and CyberKnife—few delve into the precise control and positioning systems that significantly affect treatment outcomes.

The lack of specialized studies becomes particularly glaring when considering the high accuracy levels required in SRS, where even minor misalignments can lead to suboptimal treatment or, worse, damage to healthy tissue. As PPS technologies continue to evolve, particularly with new designs aiming for accuracies up to 0.1mm, there is an unmet need for detailed research in this domain.

This dissertation aims to fill this existing research gap by conducting an in-depth examination of the kinematics and control systems behind advanced PPS technologies, with an emphasis on their safety, effectiveness, and alignment with regulatory standards.

Through this focused inquiry, the research seeks to make a substantive contribution to the existing literature, while also providing practical insights for engineers, medical physicists, and clinicians engaged in SRS treatments.

1.8 Methodology Overview

This dissertation adopts a multi-faceted methodology to comprehensively evaluate the Robotic Patient Positioning System (PPS). The key elements of the methodology are as follows:

- **Kinematic Analysis:** A kinematic model of the PPS will be developed using MATLAB to understand the theoretical motion characteristics of the system.
- **Control Systems Analysis:** Examination of the control algorithms implemented in single-loop and dual-loop control systems to identify the most effective mechanisms for achieving the targeted positional accuracy of up to 0.1 mm.
- **Hardware Specifications:** A detailed review of the servo motors and drives will be conducted to evaluate their suitability for achieving the high levels of accuracy required.
- **Measurement and Validation:**
  - **Simulated Testing:** MATLAB simulation results will be compared against a CAD model of the PPS to assess theoretical performance.
  - **Real-world Testing:** An OptiTrack system, equipped with three cameras, will be employed to measure the markers at controlled points on the PPS.
- **Comparative Analysis:** A comparison between the results of the simulations and real-world tests will be carried out to validate the system's performance and reliability.
- **Regulatory Compliance:** The study will assess the system's alignment with IEC Standard 60601, focusing on the aspects of safety and reliability pertinent to medical applications.

This methodology aims to provide a thorough and rigorous evaluation of the Robotic PPS, contributing to both academic understanding and practical advancements in the field of SRS.

1.9 Organization of the Dissertation

This dissertation provides an in-depth analysis of the Patient Positioning System (PPS) used in Stereotactic Radiosurgery (SRS), addressing significant gaps in kinematics and control systems as highlighted by the literature. The dissertation is structured into the following chapters:

- **Chapter 1: Introduction** - Sets the stage by outlining the research objectives, the significance of the study within the context of SRS, and the scope of the research.
- **Chapter 2: Literature Review** - Reviews the evolution of cancer treatment technologies, focusing particularly on advancements in patient positioning systems. It emphasizes the critical role of precision in SRS and concludes by identifying research gaps in the kinematics and control systems of PPS.
- **Chapter 3: Problem Formulation and State-of-the-Art Context** - This chapter serves multiple purposes:
  - **Problem Formulation** - Clearly defines the specific problems that the dissertation seeks to address within the domain of patient positioning in SRS. It outlines the practical challenges faced by current systems and the need for improved kinematic and control solutions.
  - **PPS Characteristics** - Describes in detail the design, operational parameters, and coordinate systems of the PPS used in the study. This includes a technical breakdown of the system's components and functionalities, establishing a foundational understanding that supports the subsequent methodologies and experiments.
- **Chapter 4: Scientific and Engineering Methodology** - Outlines the rigorous methodologies employed in the research:
  - **Kinematic Study** - Provides an in-depth kinematic analysis of the PPS, addressing significant gaps in existing research.
  - **System Components** - Details the system's components, such as controllers, servos, and drives, and the integration of measurement systems like the OptiTrack.
  - **Control Algorithms** - Explores various control strategies implemented, focusing on single-loop and dual-loop configurations to enhance precision and stability.
  - **Safety Protocols** - Discusses safety measures and fault management in the PPS, essential for patient safety and system reliability.
  - **Testing and Measurement** - Describes testing methodologies and techniques used to validate the system's accuracy and performance.

- **Chapter 5: Results and Validation** - Presents results from the testing of the PPS, analyzing its performance across various parameters and configurations to evaluate precision, error margins, and operational consistency.
- **Chapter 6: Conclusions and Future Work** - Synthesizes the research findings, discusses their implications for the field of SRS, and outlines potential areas for future research. Emphasizes the need for cross-disciplinary cooperation to advance the field of patient positioning systems.
- **Appendices** - Includes supplementary materials such as motors specifications and detailed tuning steps.

This dissertation aims to not only fill identified gaps in the existing research but also provide actionable insights for future interdisciplinary collaborations in the field of SRS.

1.10 Human and Ethical Aspects of the Research

This research is conducted with a commitment to adhere to the highest ethical standards, even though it does not involve human subjects or animal testing. The study focuses on the kinematic and control aspects of the Patient Positioning System (PPS) in Stereotactic Radiosurgery (SRS). Here are the key ethical aspects considered:

- **Data Integrity** - All data will be reported accurately, without manipulation or fabrication.
- **Transparency** - All methods and procedures will be clearly outlined to enable peer review and replication of the study.
- **Confidentiality** - Any proprietary or sensitive information related to the PPS technology, especially as it is in the patent application phase, will be treated with strict confidentiality.
- **Compliance** - The research aims to evaluate compliance with the Food and Drug Administration (FDA) and International Electrotechnical Commission (IEC) guidelines, respecting their roles in ensuring public safety.
- **Conflict of Interest** - Any potential conflicts of interest will be declared to maintain the transparency and integrity of the research.

The ethical considerations aim to contribute positively to the broader scientific community by promoting rigorous, transparent, and responsible research.

Chapter 2

Literature Review

2.1 Introduction

From ancient texts like the Edwin Smith Papyrus [1] to modern research, people have been trying to understand and treat cancer for ages. While early methods were simple, technological advancements have given us powerful tools like X-rays, CT scans, and even robotic radiosurgery systems. Among these, the Gamma Knife stands out as particularly effective for treating brain tumors.

This review explores the evolution of cancer treatment, with a special focus on radiosurgery. We'll delve into how this technique has become a game-changer in treating difficult cases, especially those involving the brain. We'll also look at the gaps in current research and the future of radiosurgery, highlighting areas where further advancements can be made.

The aim is to outline how far we have come in the battle against cancer and how we can continue to improve treatment methods.

2.2 A Historical Perspective on Cancer Diagnosis

Tracing the history of cancer diagnosis begins with the Edwin Smith Papyrus from around 1600 BCE, likely a reproduction of earlier texts from 3000-2500 BCE, which provides the earliest documented mention of breast cancer, describing it as incurable [2, 3]. Complementing this, the Ebers Papyrus details various cancers including those of the skin, uterus, stomach, and rectum [4]. This foundation was built upon during the Greek and Roman era when Hippocrates introduced the term "karcinos" to describe tumors, linking the disease to an excess of black bile, a concept later elaborated by Roman physicians such as Aulus Celsus and Claudius Galen [5, 6].

The understanding of cancer was significantly advanced during the Islamic Golden Age, as Islamic scholars like Avicenna synthesized and expanded the Greco-Roman medical knowledge, further classifying and differentiating between benign and malignant tumors [7, 8, 9, 10, 11]. Despite advancements during the Renaissance to the Enlightenment, the comprehensive understanding of cancer lagged

until the establishment of specialized institutions such as the London Cancer Hospital in 1851, which marked a major step in specialized cancer care [12].

The invention of the microscope in the 19th century revolutionized the field, allowing Rudolf Virchow to establish the cellular basis of disease, making precise diagnoses possible through biopsies [13, 14]. The same century saw the creation of cancer registries, enhancing the ability to track and understand the epidemiology of cancer [15]. The 20th century marked an era of dramatic advancements with the development of diagnostic technologies such as X-ray radiography and mammography, and treatments like chemotherapy and hormonal therapies that transformed the landscape of cancer treatment [16, 17, 18, 19, 20, 21, 22, 23, 24].

Now, in the 21st century, cancer treatment has become increasingly personalized, driven by innovations in genomics, immunology, nanotechnology, and minimally invasive surgical techniques. These advances are significantly shaping current approaches to cancer care, with targeted therapies, immunotherapies, and enhanced chemotherapy and radiation treatments offering new hope and capabilities for precision medicine [25, 26, 27, 28, 29, 30, 31, 32].

2.3 Radiation Oncology: Past, Present, and Future

Radiation oncology has evolved significantly since Wilhelm Conrad Roentgen's discovery of X-rays in 1895, which catalyzed the initial use of radiation for treating a variety of conditions, including both malignant and benign diseases. Initially, radiation treatments involved single, large exposures using low-energy cathode-ray tubes or radium-filled glass tubes placed close to tumors. However, these early treatments often resulted in extensive damage to normal tissues surrounding the tumors due to the high doses employed.

By 1911, the concept of fractionation in external beam radiotherapy (XRT) and slow, continuous low-dose-rate (LDR) radium treatments were developed, allowing for more controlled and less harmful treatments. The decades between 1930 and 1950 witnessed further advancements with the introduction of brachytherapy and supervoltage X-ray treatment, significantly improving the precision and safety of radiation treatments for deep-seated cancers.

The period from 1950 to 1980 marked a revolution in radiotherapeutic technology, characterized by the introduction of Cobalt teletherapy and powerful linear accelerators. Cobalt-60 therapy, emerging in the 1950s, utilized gamma rays to target and destroy cancer cells, becoming a staple in external beam radiotherapy. Despite its effectiveness, the transition toward more sophisticated technologies like linear accelerators began as they offered enhanced control and reduced the need for specialist support.

The advancements continued into the late 1970s and 1980s with the exploration of proton beam therapy, an approach that leveraged computer-assisted accelerators for targeting tumors with unprecedented precision. This period also saw the integration of radiation physics with emerging computer technologies, enhancing the

precision of treatments through techniques such as Conformal Radiation Therapy (CRT) and Intensity-Modulated Radiation Therapy (IMRT). These methods utilize detailed imaging and software to meticulously control the radiation dose delivered to cancerous tissues while sparing healthy ones.

The culmination of these technological advancements has led to the development of what is now known as "radiation surgery," a term that encompasses non-invasive, high-precision radiation treatments using sophisticated equipment like the Gamma Knife, CyberKnife, and modern linear accelerators. These systems represent the cutting-edge of radiation oncology, delivering precise radiation doses to targeted areas without the need for actual surgical incisions, thereby reducing recovery times and improving outcomes for patients.

2.4 Gamma Knife

Gamma Knife technology has been at the forefront of neurosurgery and oncology since its inception in the 1960s by Lars Leksell [31]. Known for its high precision in delivering ionizing radiation, this technology has been a cornerstone in the treatment of brain tumors and other intracranial conditions. With the advent of Cyber Gamma Knife, this tool has seen significant improvements in efficiency and effectiveness. This review aims to summarize the current literature on Gamma Knife, its evolving technology, and its pivotal role in brain cancer and tumor treatment.

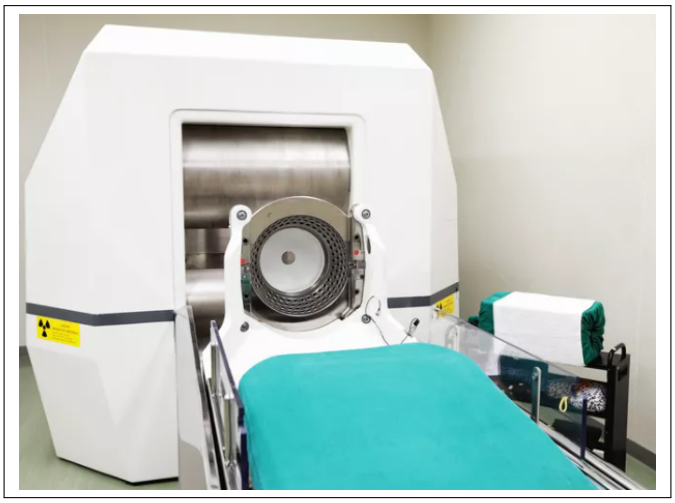

FIGURE 2.1: Gamma Knife Machine

2.4.1 Importance in Brain Cancer and Tumor Treatment

Gamma Knife radiosurgery offers a non-invasive alternative to traditional neurosurgery, providing a high dose of radiation with extreme accuracy [32]. This technique minimizes damage to surrounding healthy tissue, making it especially useful for treating brain tumors that are either hard to reach or are close to critical structures like the optic nerve [33]. Several studies have demonstrated the clinical effectiveness of Gamma Knife in treating various types of brain tumors, including meningiomas, pituitary adenomas, and metastatic tumors [34].

2.4.2 Mechanisms of Gamma Knife Radiosurgery

One of the key components that contribute to the high precision and effectiveness of Gamma Knife radiosurgery is its unique helmet and head frame system. This technology functions as the foundation upon which the entire radiosurgery process is built, ensuring stability and accuracy throughout the treatment [35].

2.4.3 The Head Frame

The head frame, typically made of lightweight yet sturdy materials like titanium, is securely fastened to the patient's skull before the procedure. It serves as both a stabilizing and a reference structure. Local anesthesia is applied to minimize discomfort during the frame application. Once affixed, the head frame prevents any movement of the head, thereby eliminating the possibility of even the slightest error due to involuntary motions such as breathing or muscle twitching. In addition, the head frame is equipped with fiducial markers, which help in calibrating the Gamma Knife machine for individualized treatment planning [36].

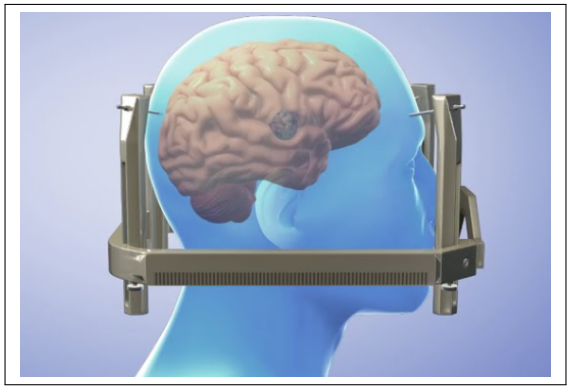

FIGURE 2.2: Gamma Knife Head Frame

2.4.4 The Helmet

The helmet, on the other hand, is an essential part of the Gamma Knife machine itself. It consists of up to 201 small holes through which gamma rays are directed towards the target tissue. Each of these holes is oriented in such a way that all the rays converge at a single focal point [37].

FIGURE 2.3: Gamma Knife Helmet 1

This unique configuration allows for the delivery of a high dose of ionizing radiation with extraordinary precision, minimizing the exposure of surrounding healthy tissues.

FIGURE 2.4: Gamma Knife Helmet 2

2.4.5 Harmony Between Helmet and Head Frame

The interplay between the helmet and the head frame is meticulously coordinated. The head frame is aligned with the helmet, guiding the gamma rays to the precise

location of the tumor. Advanced imaging techniques, often involving magnetic resonance imaging (MRI) or computed tomography (CT) scans, are used in conjunction with the fiducial markers on the head frame to establish the exact coordinates of the tumor. Treatment planning software then calculates the optimal radiation dose and the best angles for gamma ray delivery [38].

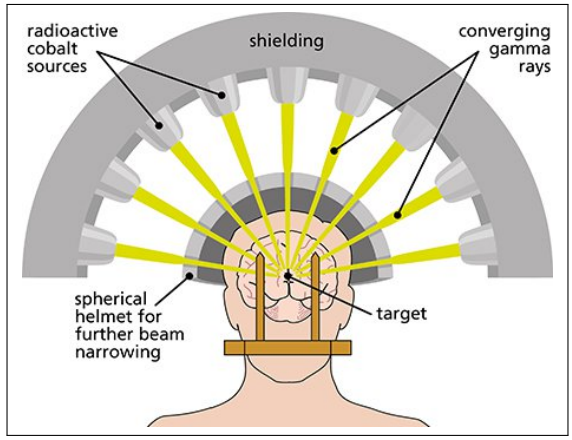

FIGURE 2.5: Gamma Knife procedure explain

2.4.6 Real-Time Monitoring and Adaptation

During the treatment, real-time monitoring systems keep track of the head frame's position relative to the helmet, making any necessary adjustments to ensure that the radiation is continually focused on the target area. This seamless integration between the helmet and head frame enables the Gamma Knife to achieve its unparalleled accuracy and effectiveness [39].

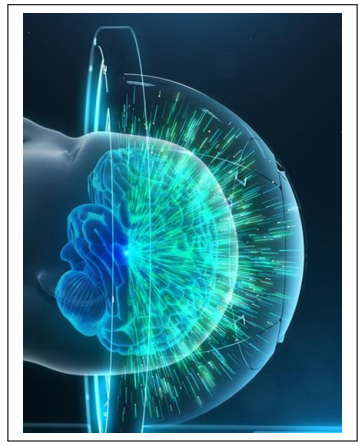

FIGURE 2.6: Beams inside the Helmet

2.4.7 Patient Experience and Quality of Life

Gamma Knife treatments often result in shorter hospital stays and quicker recovery times compared to traditional surgical procedures [32]. This has significant implications for the patient's quality of life, reducing both physical and emotional stress associated with prolonged hospitalization and recovery.

2.4.8 Clinical Studies and Outcomes

Several randomized clinical trials have further substantiated the effectiveness of Gamma Knife radiosurgery. These trials indicate not only high rates of tumor control but also lower incidences of post-operative complications, strengthening its position as a preferred treatment modality [34].

2.4.9 Gamma Knife Technological Advancements

Over the years, the Gamma Knife has undergone several technological advancements aimed at improving its precision and expanding its applications. These include improved imaging techniques, streamlined treatment planning software, and more sophisticated dose-planning algorithms [40]. Such improvements allow for even greater accuracy in targeting tumors while sparing adjacent healthy tissues.

2.4.10 Comparative Analysis with Other Treatments

While Gamma Knife is highly effective, as mentioned before it is not the only option for treating brain tumors. Other methods like LINACs and Proton Therapy also effective, each with their own advantages and limitations. However, Gamma Knife often stands out for its extreme precision and lower side effect profile [41].

2.4.11 Cyber Gamma Knife

One of the most exciting developments in this field is the introduction of Cyber Gamma Knife, which incorporates robotic technology to enhance treatment planning and delivery [42]. This innovation allows for real-time imaging and adaptive dose delivery, ensuring that the treatment remains as precise as possible even if the patient moves during the procedure. Cyber Gamma Knife has shown promising results in terms of treatment outcomes and reduced side effects [43].

2.5 Treatment in Debrecen: The Rotating Gamma System

Since its founding in 2007, the Rotating Gamma Institute in Debrecen, Hungary, has been a cornerstone in the field of stereotactic radiosurgery. Utilizing the groundbreaking RGS Vertex 360^{TM} technology from American Radiosurgery Inc.[44], the

institute offers advanced treatments for a variety of medical conditions, including tumors, vascular malformations, and trigeminal neuralgia.

FIGURE 2.7: Gamma Center Debrecen 2010

2.5.1 Technology Overview

The efficacy of the Rotating Gamma System (RGS Vertex 360^{TM}) lies in its blend of geometric flexibility and precision targeting [45]. This state-of-the-art system rotates around the patient, administering concentrated doses of radiation to the affected areas while sparing the surrounding healthy tissues. It has proven effective in various forms of cancer treatment, including those for the brain, lungs, and spine.

2.5.2 Treatment Planning and Procedure

The patient journey at the Rotating Gamma Institute begins with meticulous treatment planning. Utilizing a multidisciplinary team of oncologists, radiologists, and medical physicists, the institute employs cutting-edge imaging technologies such as MRI and CT scans to design a tailored treatment plan. The RGS Vertex 360^{TM} technology brings these comprehensive plans to fruition, often within a single session, thereby reducing the need for multiple visits to the hospital.

2.5.3 Innovative Treatment Options at Debrecen

The Rotating Gamma Institute is unique in Hungary for housing the state-of-the-art Gamma ART 6000 unit. Developed by American Radiosurgery Incorporated, this FDA-approved machine surpasses traditional technologies like the Gamma Knife. It offers a broader range of treatment capabilities, thereby extending the treatment possibilities for patients who might otherwise not have been candidates for Gamma Knife procedures.

2.5.4 Clinical Outcomes

Since its inception, the Rotating Gamma Institute has amassed a considerable amount of experience, with preliminary data indicating promising clinical outcomes. A high rate of success is often reported, with numerous patients experiencing significant reductions in tumor size and alleviation of symptoms. The non-invasive nature of these treatments also tends to result in fewer complications and quicker recovery times compared to traditional surgical methods [46].

In the featured case study 2.8, the treatment and post-operative care at Debrecen's Gamma Center demonstrate long-term effectiveness for the patient under study. After the completion of radiosurgery, a stringent follow-up regimen was established. During the first year, clinical and contrast-enhanced Magnetic Resonance Imaging (MRI) evaluations were conducted every three months. This frequency was reduced to bi-annual assessments in the second year, followed by annual reviews thereafter. Notably, five years post-stereotactic irradiation, the patient's tumor size has remarkably decreased from an initial volume of 7.99 cm to a mere 0.2 cm, accounting for a 97.46% shrinkage. Currently, the patient is asymptomatic, and the tumor remains in a stabilized condition. These outcomes underscore the successful treatment and vigilant post-operative care provided at the Debrecen Gamma Center.

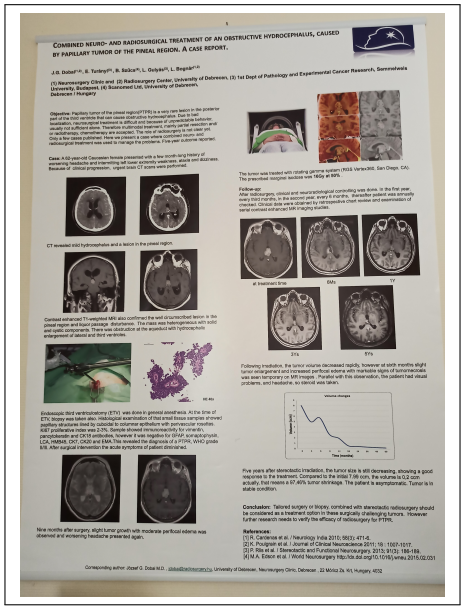

FIGURE 2.8: five years of treatment (Case Study)

2.6 Future Prospects and Challenges in Stereotactic Radiosurgery

As the field of Stereotactic Radiosurgery evolves, exciting advancements in Patient Positioning Systems (PPS) and control algorithms are expected. These developments aim to heighten the precision and effectiveness of treatments. However, these promising innovations also pose challenges, as rigorous validation methods are essential to ascertain the safety and efficacy of these new technologies. In the collective fight against cancer, an interdisciplinary approach is vital. Engineers, medical physicists, and clinicians must collaborate closely to develop, validate, and implement these groundbreaking technologies effectively.

2.7 The Need for Better Patient Positioning System

In Stereotactic Radiosurgery (SRS), placing the patient in the right position is very important. Even a small mistake can cause harm to healthy parts of the body. That's why tables, beds, or couches that position the patient need to be very accurate.

Robotic Patient Positioning Systems (PPS) are now being used more and more to help with this. Studies show that using robots can make positioning up to 20% more accurate compared to doing it by hand. These robotic systems can move the patient very precisely, making sure that the treatment is as effective as possible.

However, there's still room for improvement. Some of these robotic systems could be even better at controlling complicated movements. This means we need more research to make these systems perfect.

In the future, using advanced PPS like this will be a key part of making SRS treatments safer and more effective.

2.8 Research Gaps in Robotic Patient Positioning Systems

Although many studies have looked into new designs for Robotic Patient Positioning Systems (PPS), the kinematics—the science of motion—behind these designs is often not thoroughly explored. There is also a lack of research in advanced control methods that make sure the patient is positioned correctly and safely during radiation therapy.

In other words, while we have new models and designs, the motion and safety controls of these systems need more attention.

More research is needed to fully understand how to best control the complex movements involved in patient positioning, especially to ensure the safety and effectiveness of gamma radiation treatments for brain cancer.

2.9 Conclusion

From the ancient diagnostic techniques of the Egyptian era to the introduction of X-rays and CT scans in the 20th and 21st centuries, the evolution of cancer treatment has been monumental. Advances in technology have brought us to an era where robotics and precise imaging play pivotal roles in surgical procedures. In particular, within the domain of radiation therapy, innovations like the Gamma Knife and linear accelerators (LINAC) have been groundbreaking.

The Gamma Knife technology, discussed in detail from an engineering standpoint, highlights the importance of precise positioning in the effective treatment of brain cancer. This literature review also included a focused discussion on the treatment modalities available at the Gamma Center in Debrecen, Hungary, showcasing the latest advancements in stereotactic radiosurgery. The recent introduction of Cyber Gamma Knife offers a more nuanced understanding of radiosurgery's potential and opens up avenues for future advancements, notably in the area of Patient Positioning Systems (PPS).

However, existing research is not without its gaps. There is a noticeable absence of comprehensive studies that delve into the kinematics behind the PPS and the control mechanisms required for maintaining high levels of precision and safety during the treatment process. This lack of focused research underlines the opportunity—and need—for further study, which will be the central theme of this thesis.

As we look toward the future, it is essential for engineers, medical physicists, and clinicians to work side by side. Their collective expertise is vital for developing new robotic technologies that can fill the existing gaps, thereby optimizing the treatment of cancer, especially brain tumors, through advanced and safer radiation therapies.

Chapter 3

Problem Formulation and State-of-the-Art Context

3.1 Introduction

As the need for precision in SRS grows, the limitations of existing systems become more apparent, necessitating a deeper investigation into their kinematic and control capabilities. This chapter begins by defining the exact nature of these limitations and the consequent research questions that drive this dissertation. Following this, it provides a description for the current state-of-the-art in patient positioning system and it is characteristics.

3.2 Problem Formulation

In the field of Stereotactic Radiosurgery (SRS), precision and reliability in patient positioning are paramount for successful treatment outcomes. The essence of effective cancer treatment lies in the precise targeting of defective cells, leading them to self-destruct through a process called apoptosis. Cancer cells, however, lose this capability, leading to uncontrolled division and the accumulation of abnormal cells.

Radiotherapy, a cornerstone of cancer treatment, uses energy beams to damage the DNA of cancer cells, triggering apoptosis because the damaged cells cannot repair themselves. Despite its precision, radiotherapy sometimes affects healthy cells adjacent to the cancer cells, exposing them to radiation. This inadvertent exposure underscores the critical need for highly precise patient positioning systems.

Current designs often fall short in providing the necessary accuracy and do not integrate the Patient Positioning System (PPS) as a subsystem working seamlessly with the entire machine design. This lack of integration and precision can lead to suboptimal radiation delivery, potentially affecting treatment efficacy and patient safety.

Our state-of-the-art research aims to address these issues by enhancing how we position patients. By achieving greater accuracy in targeting tumors, we can treat the cancer more effectively while minimizing damage to healthy tissues. This is not just about building a better machine—it's about making a real difference in the lives of people fighting brain cancer. Our goal is to help these patients receive the best possible care with the least risk of side effects.

3.3 PPS Characteristics and Coordinate System

To provide a foundational understanding necessary for the ensuing discussion on innovations and improvements, this section describes the operational characteristics and coordinate systems of typical Patient Positioning Systems used in SRS. It includes detailed descriptions of system components, operational parameters, and the technical specifications that are critical for achieving the high levels of accuracy required in radiosurgery. This detailed exposition not only clarifies the technical baseline from which this research departs but also supports the need for advancements in kinematic studies and control systems explored later in this dissertation.

3.3.1 Patient Positioning System Characteristics

As a 6-degree-of-freedom (DOF) robotic patient bed, it has been ingeniously engineered to position patients accurately and precisely. It does so by aligning the clinical targets with the Mechanical Isocenter (MIC), ensuring an accurate delivery of the prescribed radiation. The PPS operates as a comprehensive unit, comprised of three key elements: a Linear Rail System, a Linkage System, and a Tabletop.

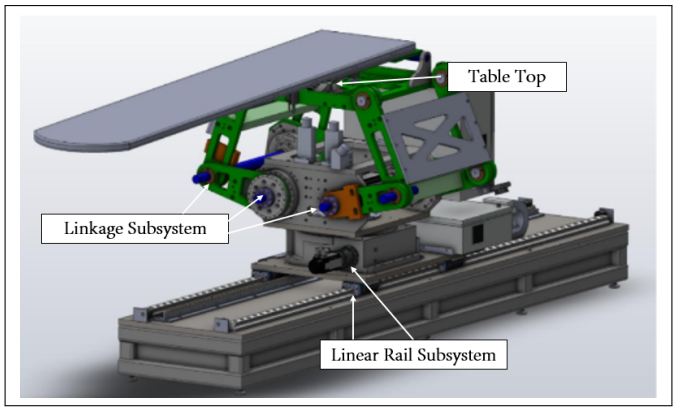

FIGURE 3.1: Patient Positioning Table (PPT) Subsystems

3.3.2 Design Overview

This subsection gives a quick look at the key parts and choices that form our system.

The Linear Rail System

Forms the foundation of the PPS, tasked with controlling movement across two axes. It maneuvers the main plate in relation to the bottom base plate along a rail system and employs a rotary table to effectuate the rotation of the Linkage System relative to the main plate. This linear motion capability offers the flexibility to move the patient in and out of the operating area conveniently.

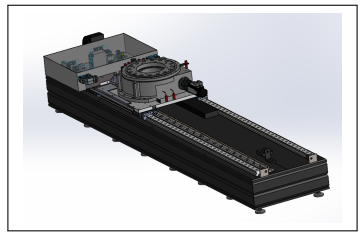

FIGURE 3.2: Linear Rail System

The Linkage System

As the centerpiece of the PPS, includes four linkage arms, three active and one passive. This system is anchored to a stationary weldment directly linked to the rotary table. Precision driven shafts connect the two primary arms, while another driven shaft connects the remaining pair. Each pair of adjacent arms is interconnected by independent shafts. The active arms, driven by three motors, facilitate motion in a 2D plane and of-fer a sizable envelope size. The servo-driven gearbox propels the movements of three out of four linkage arms. Notably, the Linkage System can be adjusted to varying heights for accommodating elderly or disabled patients and can be raised to the necessary height for treatment. To ensure precision for minute motor movements, such as correcting tumor misalignment during patient positioning, the motors are redundantly encoded.

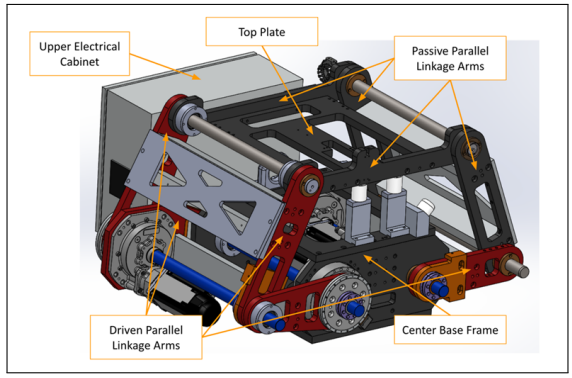

FIGURE 3.3: Linkage Major Components

Tabletop

Completes the system with its capacity to create pitching movements. This functionality is achieved through a helical cam following system, driven by a servo motor 3.5.

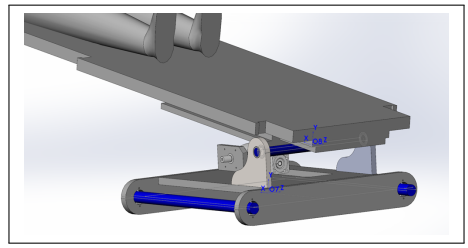

FIGURE 3.4: Table Top Pitching Axis

The Helical Cam's shape is designed such that the radius – as measured from the axis of rotation to the outer surface - and the angle of rotation have a linear relationship.

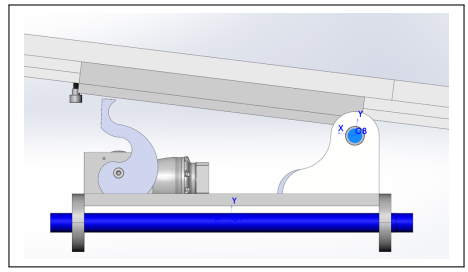

FIGURE 3.5: Side view of Pitching Helical Cam

The PPS, through its distinctive components and operational capabilities, manifests an intricate control system for the patient's position and orientation, fulfilling the exacting demands of radiosurgery treatment. It represents a tangible and pivotal achievement in realizing our goal of developing an effective motion control system for PPS. The 6-DOF in the 3D space of the PPS, represented by positional (x, y, z) and orientation data [pitch (α), yaw (β), and roll (γ)], makes this system a comprehensive solution for precise patient positioning in the field of radiosurgery.

3.3.3 Patient Positioning System Coordinate System

The origin of the coordinate system coincides with the Mechanical Isocenter (MIC), which is a virtual point in space that lies on the z-axis. A description of each axis of the coordinate system is shown in the table below in table 3.1.

TABLE 3.1: PPS Coordinate System

Axis	Description
X	Left and Right
Y	Up and Down
Z	Along the patient axis
Roll	Rotation about Z axis
Pitch	Rotation about X axis
Yaw	Rotation about Y axis

Figure 3.6 showcases the subsystems of the PPS, along with the associated coordinate frame.

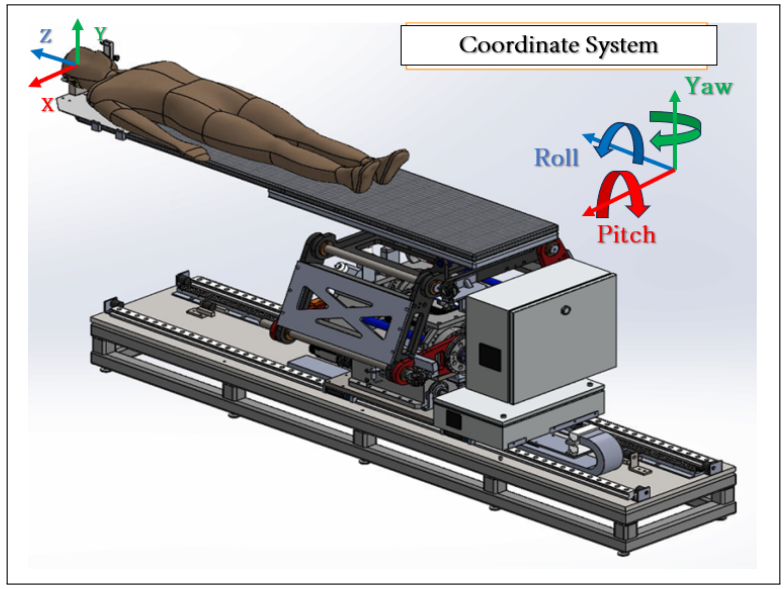

FIGURE 3.6: Patient Positioning Coordinate System

Note: In our frame visualizations, the axes are color-coded for clarity:

- X-axis is represented by the Red color (R).
- Y-axis is represented by the Green color (G).
- Z-axis is represented by the Blue color (B).

The PPS dimensions and mass are summarized in the table 3.2.

TABLE 3.2: PPS Dimensions and Mass

Length[1](z) [mm]	Width[2](x) [mm]	Height[3](y) [mm]	Mass (kg)
3098.8	1179.3	3022.6	2000

[1]Length recorded of the Base Frame only as these values change depending on the location of the Horizontal Rail Assembly.

[2]Width is recorded as the maximum width of the linkage system when the center of the phantom overlaps the MIC position as this changes with the orientation of the Linkage Assembly.

[3]Height recorded where the center of the phantom overlaps the MIC position as this changes with the orientation of the Linkage & Table Top Assemblies.

Chapter 4

Scientific and Engineering Methodology

4.1 Introduction

This chapter outlines the comprehensive scientific and engineering methodologies employed in the development and analysis of the Patient Positioning System (PPS) for Stereotactic Radiosurgery (SRS). Building upon the gaps identified in the literature review and the challenges articulated in Chapter 3, this chapter delves into the kinematic study, system components, control strategies, safety protocols, and testing procedures that underpin the design and functionality of the PPS.

The methodologies presented here are integral to achieving the precision and reliability required in SRS. They encompass a range of disciplines, including mechanical engineering, systems control, and applied mathematics, reflecting the interdisciplinary nature of designing sophisticated medical devices. Each section within this chapter is designed to not only explain the 'how' but also the 'why' behind each methodological choice, providing a clear link between the identified problems, proposed solutions, and the ultimate performance outcomes of the PPS.

- **Kinematic Study** - The chapter begins by exploring the kinematic aspects of the PPS, crucial for understanding the system's motion and ensuring it meets the stringent requirements of precision and flexibility needed in radiosurgery.
- **System Components** - Following the kinematic analysis, this section details the core components that constitute the PPS, explaining how each part contributes to the overall system's efficacy and reliability.
- **Control Algorithms** - The control mechanisms implemented are discussed in-depth, showcasing the application of both traditional and innovative control theories to enhance system responsiveness and stability.
- **Safety Protocols** - Given the critical nature of SRS, this section emphasizes the safety measures integrated into the PPS, detailing the fault detection and management strategies essential for patient safety.

- **Testing and Measurement** - The chapter concludes with an overview of the testing protocols and measurement techniques used to validate and refine the PPS, ensuring that the system performs as intended under real-world conditions.

Through a detailed exposition of these methodologies, this chapter not only reflects the technical depth of the research but also illustrates the practical applications of these innovations in enhancing the safety and effectiveness of patient positioning in radiosurgery.

4.2 Kinematic Study for Patient Positioning System

4.2.1 Forward Kinematics

Forward kinematics, a foundational concept in robotics and mechanical systems, revolves around the determination of the end effector's position and orientation based on given joint parameters and link lengths. Unlike its counterpart, inverse kinematics, which seeks to find joint parameters given a desired end effector position, forward kinematics is a direct mapping from the joint space to the workspace [47]. This computational model becomes essential in scenarios where it's necessary to predict the movement outcome based on joint values[48].

Homogeneous Transformation Matrix

The fundamental concept in the modeling of robots revolves around understanding the dynamics of their frames and how these frames undergo transformations as they transition between different positions [49]. The homogeneous transformation matrix serves as a crucial tool for describing the interplay between translation and rotation motions within the robot's framework. It effectively captures the essence of points, vectors, and motions that occur between individual links. The homogeneous transformation matrix is represented as a comprehensive matrix that encompasses all the necessary information [50].

In the kinematics study for our PPS, we utilize the homogeneous transformation matrix, a 4×4 construct, to seamlessly represent both rotation and translation between coordinate frames. This matrix is pivotal in capturing the spatial relationships required for precise patient positioning.

$$T = \begin{bmatrix} R & d \\ 0 & 1 \end{bmatrix} \tag{4.1}$$

Denavit Hartenberg (DH)

One of the most important methods to manipulate a robot based on the kinematics modeling is Denavit-Hartenberg (DH) it is a prominent approach in kinematic modeling for robot manipulation, plays a vital role in achieving effective control over robotic systems [51]. This method enables the traversal from the base frame to the end effector frame (In our study target Point) by sequentially transitioning through intermediate frames, irrespective of the robot's dynamics or specific characteristics. It delineates the transformations required, encompassing both rotational and translational motions of the manipulator, as illustrated in Figure 4.1, in order to obtain the transformation matrix.

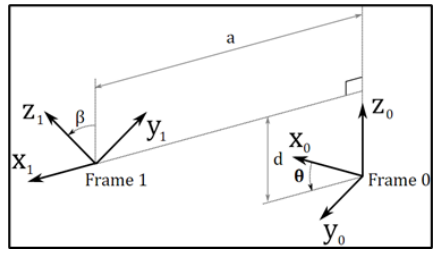

FIGURE 4.1: Denavit Hartenberg (DH)

Starting from that we can generate the (4.4) matrix of our robot after determining the assignment of the manipulator frames -which is defined in 4.1 as [48]:

$$T_i = \text{Rot}\,(z, \theta_i)\,\text{Trans}\,(d_i)\,\text{Trans}\,(a_i)\,\text{Rot}\,(x, \alpha_i) \tag{4.2}$$

Ti Final matrix will be the result of multiple of those matrixes

$$T_i = \begin{bmatrix} c\theta_i & -s\theta_i & 0 & 0 \\ s\theta_i & c\theta_i & 0 & 0 \\ 0 & 0 & 1 & d_i \\ 0 & 0 & 0 & 1 \end{bmatrix} \begin{bmatrix} 1 & 0 & 0 & a_i \\ 0 & c\alpha_i & -s\alpha_i & 0 \\ 0 & s\alpha_i & c\alpha_i & 0 \\ 0 & 0 & 0 & 1 \end{bmatrix} \tag{4.3}$$

This equation can be translated into matrices and by multiplying them we get the final Ti as:

$$T_i = \begin{bmatrix} \cos\theta_i & -\cos\alpha_i \sin\theta_i & \sin\alpha_i \sin\theta_i & a_i \cos\theta_i \\ \sin\theta_i & \cos\alpha_i \cos\theta_i & -\sin\alpha_i \cos\theta_i & a_i \sin\theta_i \\ 0 & \sin\alpha_i & \cos\alpha_i & d_i \\ 0 & 0 & 0 & 1 \end{bmatrix} \tag{4.4}$$

where:

- a_i: The distance between the z_i and z_{i+1} axes along the x_i axis.
- α_i: The angle between the z_i and z_{i+1} axes along the x_i axis.
- d_i: The distance between the x_i and x_{i+1} axes along the z_i axis.
- θ_i: The angle between the x_i and x_{i+1} axes along the z_i axis .

PPS subsystems functionality description and coordinate frame assignment

This vital system plays a crucial role in facilitating precise patient alignment in a variety of medical scenarios. Its construction and functionality embody several distinctive features that contribute to its effective performance. These characteristics span across the system's three main components: the Linear Rail System, the Linkage System, and the Table Assembly. Each component introduces unique attributes that, when combined, result in a highly efficient, versatile, and patient-friendly positioning system.

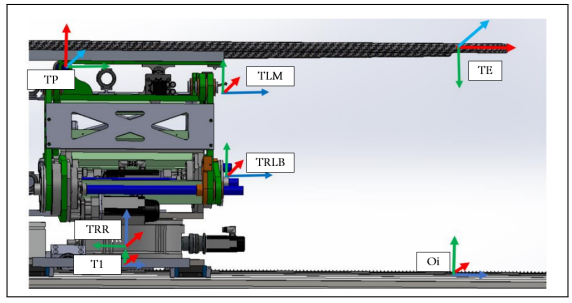

FIGURE 4.2: PPS Frame Assignment

Frame Assignments for the PPS

The Patient Positioning System (PPS) utilizes specific frame assignments to capture its distinct components and their movements as shown in the following figure 4.2:

- **Base Frame (O_i)**: Located at the junction of the main rails.
- **Linear Rail Frame (T_{RR})**: Positioned at the end of the linear rail.
- **Lower Linkage System Frame (T_{RLB})**: At the midpoint of the lower linkage arm.

- **Upper Linkage System Frame (T_{LM})**: At the midpoint of the upper linkage arm.
- **Table Rod Frame (T_P)**: Centered on the table rod.
- **Tabletop Frame (T_E)**: Centered on the tabletop.

Linkage frames shown in figure 4.3 These frame assignments are essential for precise kinematic evaluations in the PPS.

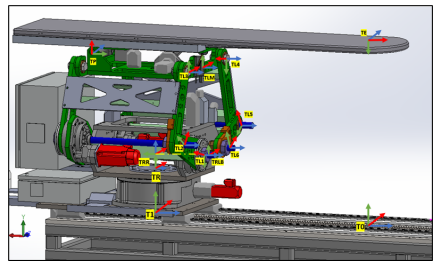

FIGURE 4.3: PPS Frame Assignment with (Linkage Frames)

Linear Rail System from T0 to TRR

This subsystem governs the bidirectional movement of the PPS. It facilitates both the translational motion of the main plate relative to the base plate along a rail system, and the rotational movement of the Linkage System around the main plate, courtesy of a rotary table. The linear motion enables the patient to be safely introduced and withdrawn from the operational area. In rooms equipped with a CT scanner, the rotary table allows a complete 180° rotation of the patient for imaging purposes. Encoded mo-tors drive both movements, ensuring the precise positioning required for such medical devices.

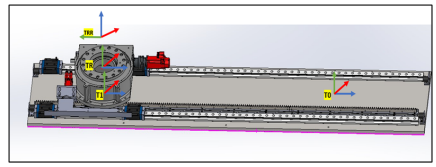

FIGURE 4.4: Linear Rail Frame Assignment (2)

Linkage System from TRLB To TLM

Representing the heart of the PPS, the Linkage System comprises four pairs of two-arm linkages that connect the PPS to the plate on the rotary table. To maintain patient stability and alignment, precision shafts interconnect two of these four pairs. The system harnesses the power of three encoded motors to maneuver three joints, positioning the PPS within a 2D plane that spans a substantial envelope size. This robust design enables the table to be adjusted vertically to accommodate patient needs, from a lowered position facilitating access for elderly patients, to an elevated state suitable for treatment procedures [52].

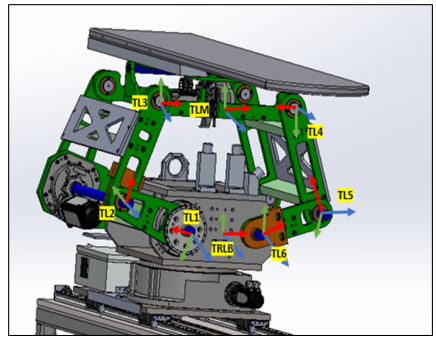

FIGURE 4.5: Linkage Frame Assignment

Table Tob TLM to TE

Located at the top of the system, the Table Assembly is linked to the top plate of the Linkage Assembly. The table, a product of Siemens, features a carbon fiber exterior filled with resin to minimize radio interference during treatment. Given the cantilevered design of the tabletop and the associated gravitational deflection, a pitch adjustment mechanism has been integrated into the Table Assembly. This mechanism actively counteracts gravity, ensuring a consistently level operating area.

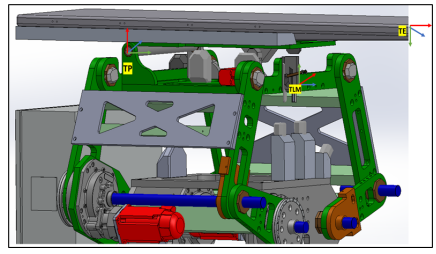

FIGURE 4.6: Table Top Frame Assignment

4.2.2 Formulating a mathematical model

Linkage subsystem mathematical modeling

The section primarily focuses on using geometric principles to develop a kinematic model for the linkage subsystem. Figure 4.7 illustrates the points, link lengths, and joint angles associated with this system [52].

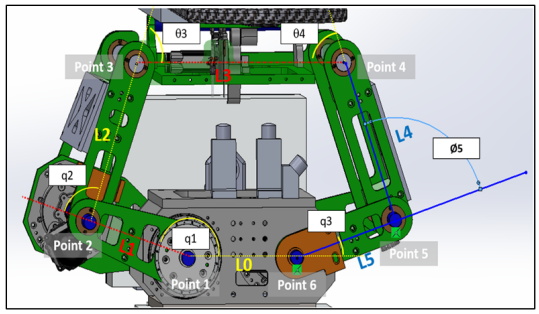

FIGURE 4.7: Linkage Subsystems Joints, Lengths and Angles

We assumed that all the angles are measured counterclockwise:

- $q_1 = 0$ when $L1$ is on $L0$.
- $q_2 = 0$ when $L2$ is along the same line of $L1$.
- $q_3 = 0$ when $L5$ is along the same line with $L0$.
- $\theta_3 = 0$ when $L3$ is along the same line of $L2$.
- $\theta_4 = 0$ when $L3$ is along the same line of $L4$.
- $\theta_5 = 0$ when $L4$ is along the same line of $L5$.

We specify a coordinate frame for each joint as follows:

$$\begin{pmatrix} x_0 \\ y_0 \end{pmatrix} = \begin{pmatrix} \cos q1 & -\sin q1 \\ \sin q1 & \cos q1 \end{pmatrix} \begin{pmatrix} x_1 \\ y_1 \end{pmatrix} + \begin{pmatrix} 0 \\ 0 \end{pmatrix} \tag{4.5}$$

$$\begin{pmatrix} x_1 \\ y_1 \end{pmatrix} = \begin{pmatrix} \cos q2 & -\sin q2 \\ \sin q2 & \cos q2 \end{pmatrix} \begin{pmatrix} x_2 \\ y_2 \end{pmatrix} + \begin{pmatrix} L1 \\ 0 \end{pmatrix} \tag{4.6}$$

$$\begin{pmatrix} x_2 \\ y_2 \end{pmatrix} = \begin{pmatrix} \cos \theta_3 & -\sin \theta_3 \\ \sin \theta_3 & \cos \theta_3 \end{pmatrix} \begin{pmatrix} x_3 \\ y_3 \end{pmatrix} + \begin{pmatrix} L2 \\ 0 \end{pmatrix} \tag{4.7}$$

where

$$\begin{pmatrix} x_0 \\ y_0 \end{pmatrix} = \begin{pmatrix} \cos q3 & -\sin q3 \\ \sin q3 & \cos q3 \end{pmatrix} \begin{pmatrix} x_6 \\ y_6 \end{pmatrix} + \begin{pmatrix} L0 \\ 0 \end{pmatrix} \tag{4.8}$$

$$\begin{pmatrix} x_6 \\ y_6 \end{pmatrix} = \begin{pmatrix} \cos \theta_5 & -\sin \theta_5 \\ \sin \theta_5 & \cos \theta_5 \end{pmatrix} \begin{pmatrix} x_5 \\ y_5 \end{pmatrix} + \begin{pmatrix} L5 \\ 0 \end{pmatrix} \tag{4.9}$$

$$\begin{pmatrix} x_5 \\ y_5 \end{pmatrix} = \begin{pmatrix} \cos \theta_4 & -\sin \theta_4 \\ \sin \theta_4 & \cos \theta_4 \end{pmatrix} \begin{pmatrix} x_4 \\ y_4 \end{pmatrix} + \begin{pmatrix} L4 \\ 0 \end{pmatrix} \tag{4.10}$$

$$\begin{pmatrix} x_4 \\ y_4 \end{pmatrix} = \begin{pmatrix} \cos 180 & -\sin 180 \\ \sin 180 & \cos 180 \end{pmatrix} \begin{pmatrix} x_3 \\ y_3 \end{pmatrix} + \begin{pmatrix} L3 \\ 0 \end{pmatrix} \tag{4.11}$$

From equations (4.5 to 4.11) and figure 4.7 we determined each point position as follows:

Point 1

$$\begin{pmatrix} x_0 \\ y_0 \end{pmatrix}_1 = \begin{pmatrix} \cos q1 & -\sin q1 \\ \sin q1 & \cos q1 \end{pmatrix} \begin{pmatrix} 0 \\ 0 \end{pmatrix} + \begin{pmatrix} 0 \\ 0 \end{pmatrix} = \begin{pmatrix} 0 \\ 0 \end{pmatrix} \tag{4.12}$$

Point 2

$$\begin{pmatrix} x_0 \\ y_0 \end{pmatrix}_2 = \begin{pmatrix} \cos q1 & -\sin q1 \\ \sin q1 & \cos q1 \end{pmatrix} \begin{pmatrix} L1 \\ 0 \end{pmatrix} = \begin{pmatrix} L1 \cos q1 \\ L1 \sin q1 \end{pmatrix} \tag{4.13}$$

Point 3

$$\begin{pmatrix} x_1 \\ y_1 \end{pmatrix}_3 = \begin{pmatrix} \cos q2 & -\sin q2 \\ \sin q2 & \cos q2 \end{pmatrix} \begin{pmatrix} L2 \\ y_2 \end{pmatrix} + \begin{pmatrix} L1 \\ 0 \end{pmatrix} = \begin{pmatrix} L2 \cos q2 + L1 \\ L2 \sin q2 \end{pmatrix} \tag{4.14}$$

$$\begin{aligned}\begin{pmatrix} x_0 \\ y_0 \end{pmatrix}_3 &= \begin{pmatrix} \cos q1 & -\sin q1 \\ \sin q1 & \cos q1 \end{pmatrix} \begin{pmatrix} L2\cos q2 + L1 \\ L2\sin q2 \end{pmatrix} \\ &= \begin{pmatrix} L2\cos q1\cos q2 + L1\cos q1 - L2\sin q1\sin q2 \\ L2\sin q1\cos q2 + L1\sin q1 + L2\cos q1\sin q2 \end{pmatrix}\end{aligned} \tag{4.15}$$

Point 6

$$\begin{pmatrix} x_0 \\ y_0 \end{pmatrix}_6 = \begin{pmatrix} \cos q3 & -\sin q3 \\ \sin q3 & \cos q3 \end{pmatrix} \begin{pmatrix} 0 \\ 0 \end{pmatrix} + \begin{pmatrix} L0 \\ 0 \end{pmatrix} = \begin{pmatrix} L0 \\ 0 \end{pmatrix} \tag{4.16}$$

Point 5

$$\begin{pmatrix} x_6 \\ y_6 \end{pmatrix}_5 = \begin{pmatrix} \cos\theta_5 & -\sin\theta_5 \\ \sin\theta_5 & \cos\theta_5 \end{pmatrix} \begin{pmatrix} 0 \\ 0 \end{pmatrix} + \begin{pmatrix} L5 \\ 0 \end{pmatrix} = \begin{pmatrix} L5 \\ 0 \end{pmatrix} \tag{4.17}$$

$$\begin{pmatrix} x_0 \\ y_0 \end{pmatrix}_5 = \begin{pmatrix} \cos q3 & -\sin q3 \\ \sin q3 & \cos q3 \end{pmatrix} \begin{pmatrix} L5 \\ 0 \end{pmatrix} + \begin{pmatrix} L0 \\ 0 \end{pmatrix} = \begin{pmatrix} L5\cos q3 + L0 \\ L5\sin q3 \end{pmatrix} \tag{4.18}$$

Therefore, **Point 4**

$$\begin{pmatrix} x_5 \\ y_5 \end{pmatrix}_4 = \begin{pmatrix} \cos\theta_4 & -\sin\theta_4 \\ \sin\theta_4 & \cos\theta_4 \end{pmatrix} \begin{pmatrix} 0 \\ 0 \end{pmatrix} + \begin{pmatrix} L4 \\ 0 \end{pmatrix} = \begin{pmatrix} L4 \\ 0 \end{pmatrix} \tag{4.19}$$

$$\begin{pmatrix} x_6 \\ y_6 \end{pmatrix}_4 = \begin{pmatrix} \cos\theta_5 & -\sin\theta_5 \\ \sin\theta_5 & \cos\theta_5 \end{pmatrix} \begin{pmatrix} L4 \\ 0 \end{pmatrix} + \begin{pmatrix} L5 \\ 0 \end{pmatrix} \quad = \quad \begin{pmatrix} L4\cos\theta_5 + L5 \\ L4\sin\theta_5 \end{pmatrix} \tag{4.20}$$

$$\begin{aligned}\begin{pmatrix} x_0 \\ y_0 \end{pmatrix}_4 &= \begin{pmatrix} \cos q3 & -\sin q3 \\ \sin q3 & \cos q3 \end{pmatrix} \begin{pmatrix} L4\cos\theta_5 + L5 \\ L4\sin\theta_5 \end{pmatrix} + \begin{pmatrix} L0 \\ 0 \end{pmatrix} \\ &= \begin{pmatrix} L4\cos q3\cos\theta_5 + L5\cos q3 - L4\sin q3\sin\theta_5 + L0 \\ L4\sin q3\cos\theta_5 + L5\sin q3 + L4\cos q3\sin\theta_5 \end{pmatrix}\end{aligned} \tag{4.21}$$

Intersection of Two Circles

In the domain of kinematics and mechanical geometry, a well-accepted technique for determining the location of a specific point within a linkage mechanism involves the intersection of two circles [53]. Here, we can pinpoint the position of Point 4 using these intersecting circles methodology. The scenario involves two circles: the first centered at Point 3 with a radius of L3, and the second centered at Point 5 with a radius of L5. The intersection of these two circles yields two potential points, namely Point 4 and Point 6.

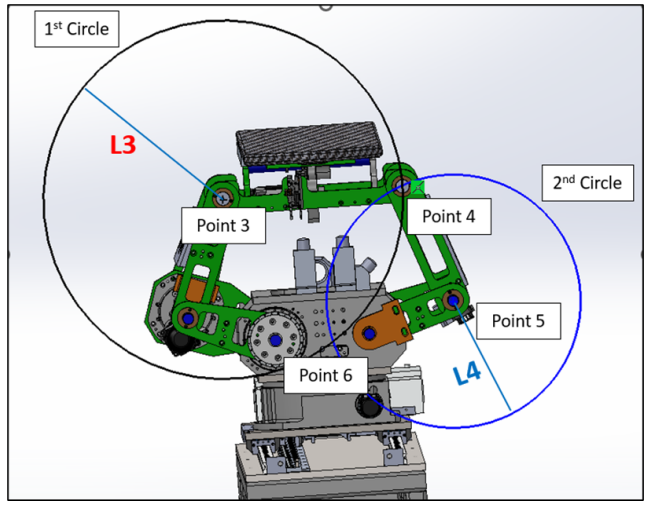

FIGURE 4.8: Two Circles Intersection

Consider two circles:

- Circle 1, centered at Point 3 ($C_3 = (x_3, y_3)$) with radius L_3.
- Circle 2, centered at Point 5 ($C_5 = (x_5, y_5)$) with radius L_5.

The equations of these circles are:

$$(x - x_3)^2 + (y - y_3)^2 = L_3^2 \tag{4.22}$$

$$(x - x_5)^2 + (y - y_5)^2 = L_5^2 \tag{4.23}$$

To find the intersection points, we can subtract two circle equations and simplify. This will give a linear equation in x and y.

Out of the two intersection points, the one with the greater y-coordinate is considered the upper intersection point. We choose this as Point 4, and the other intersection point is disregarded.

These represent possible locations of the mechanical joint or linkage. However, due to the physical constraints and design of our mechanical system, the existence of Point 6 would suggest a mechanically unfeasible configuration. Therefore, Point 6 can be categorically eliminated from our options, leaving us with the valid position, Point 4.

After that, to ascertain the orientation of the upper arm of the linkage mechanism 4.9, we must calculate the value of ϕ_3. This angle ϕ_3 is a critical parameter that provides insights into the inclination of the upper arm, thereby enabling a comprehensive understanding of the system's kinematics. The determination of ϕ_3 is a crucial step in accurately modeling and analyzing the mechanical system.

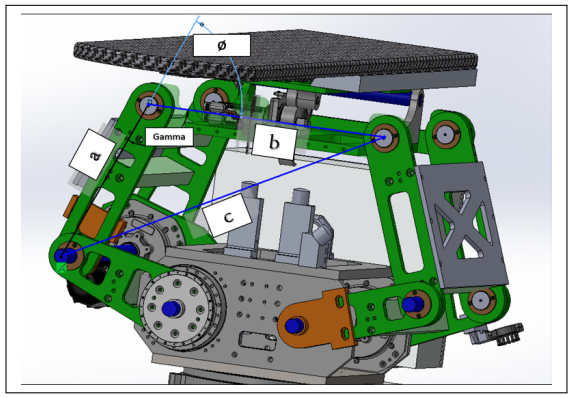

FIGURE 4.9: Upper Joint Angle Calculation

$$c = \sqrt{(P4(x) - P2(x))^2 + (P4(y) - P2(y))^2} \tag{4.24}$$

$$\Gamma = \text{arc}\left(\frac{a^2 + b^2 - c^2}{2 \times a \times b}\right) \tag{4.25}$$

$$\phi_3 = 180^\circ - \Gamma \tag{4.26}$$

Table Pitching mathematical modeling

Table angle or pitching angle controlled by servo motor and CAM as shown in the following figure 4.10

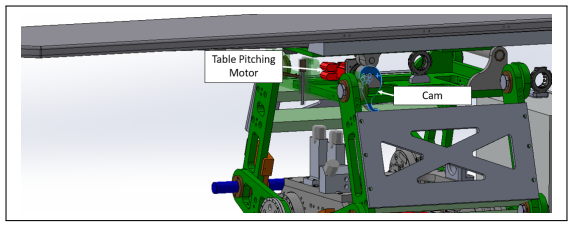

FIGURE 4.10: Table Pitching Design

In order to transition from point TP to point TE, it is necessary to calculate the length L10, based on the angle input as per the given table 4.1 and figure 4.15.

Then, after determining all needed parameters from figure 4.3 we can create the DH table as follows:

Utilize the Denavit-Hartenberg (DH) parameters

With the essential parameters and points now determined, we can utilize the Denavit-Hartenberg (DH) parameters. This allows us to transition from one frame to the subsequent frame, ultimately leading us to the final transformation matrix representing our PPS.

DH Matrix Formulation

The standard DH transformation matrix, denoted as A_i, is constructed using the given parameters a, α, d, and θ [48]:

$$A_i = \begin{bmatrix} \cos(\theta) & -\sin(\theta) & 0 & 0 \\ \sin(\theta) & \cos(\theta) & 0 & 0 \\ 0 & 0 & 1 & 0 \\ 0 & 0 & 0 & 1 \end{bmatrix} \begin{bmatrix} 1 & 0 & 0 & 0 \\ 0 & 1 & 0 & 0 \\ 0 & 0 & 1 & d \\ 0 & 0 & 0 & 1 \end{bmatrix} \begin{bmatrix} 1 & 0 & 0 & a \\ 0 & 1 & 0 & 0 \\ 0 & 0 & 1 & 0 \\ 0 & 0 & 0 & 1 \end{bmatrix} \begin{bmatrix} 1 & 0 & 0 & 0 \\ 0 & \cos(\alpha) & -\sin(\alpha) & 0 \\ 0 & \sin(\alpha) & \cos(\alpha) & 0 \\ 0 & 0 & 0 & 1 \end{bmatrix}$$

Linear Rail Subsystem

The transformation matrix for the linear rail subsystem, denoted as T_o, is:

$$T_o = A_i \Big|_{\substack{a=0, \\ \alpha=0, \\ d=0, \\ \theta=0}}$$

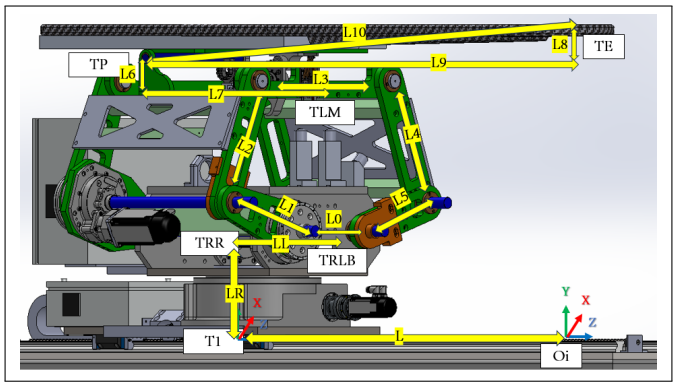

FIGURE 4.11: PPS Length Parameters need for DH

$$T_1 = A_i \Big|_{\substack{a=0,\\ \alpha=0,\\ d=-L+Lin,\\ \theta=0}}$$

$$T_0^1 = \begin{bmatrix} 1 & 0 & 0 & 0 \\ 0 & 1 & 0 & 0 \\ 0 & 0 & 1 & \text{Lin} - L \\ 0 & 0 & 0 & 1 \end{bmatrix} \tag{4.27}$$

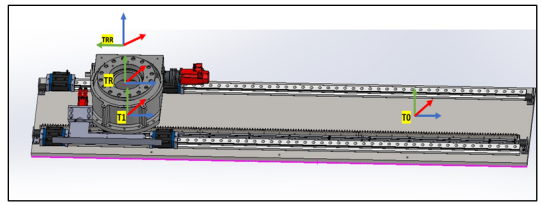

FIGURE 4.12: Linear Rail Frames

Rotary Base to the Height of the Linkage

Two transformation matrices are derived: 1. T_R representing a rotation about the θ-axis by $-\frac{\pi}{2}$ and no translation along the x-axis:

$$T_R = A_i \Big|_{\substack{a=0,\\ \alpha=0,\\ d=0,\\ \theta=-\frac{\pi}{2}}}$$

2. T_{RR} representing a rotation about the 'Rott' angle and a translation along the z-axis by LR:

$$T_{RR} = A_i \Big|_{\substack{a=0,\\ \alpha=0,\\ d=LR,\\ \theta=Rot}}$$

$$T_R^{RR} = \begin{bmatrix} 1 & 0 & 0 & 0 \\ 0 & 0 & 1 & 0 \\ 0 & -1 & 0 & 0 \\ 0 & 0 & 0 & 1 \end{bmatrix} \tag{4.28}$$

$$T_{RR}^{RLB} = \begin{bmatrix} \cos(Rot) & -\sin(Rot) & 0 & 0 \\ \sin(Rot) & \cos(Rot) & 0 & 0 \\ 0 & 0 & 1 & LR \\ 0 & 0 & 0 & 1 \end{bmatrix} \tag{4.29}$$

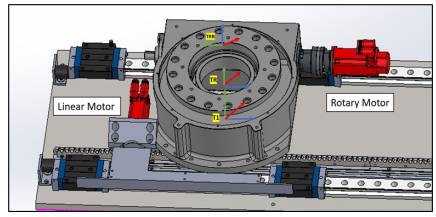

FIGURE 4.13: Linear Rail Frame Assignment

Linkage Subsystem

The linkage subsystem of the PPS consists of multiple stages of transformation:

1. First, no translation along the x-axis and a rotation of $\frac{\pi}{2}$ about the x-axis:

$$T_{RLB} = A_i \Big|_{\substack{a=0,\\ \alpha=\frac{\pi}{2},\\ d=0,\\ \theta=0}}$$

$$T_{RLB}^{L1} = \begin{bmatrix} 1 & 0 & 0 & 0 \\ 0 & 0 & -1 & 0 \\ 0 & 1 & 0 & 0 \\ 0 & 0 & 0 & 1 \end{bmatrix} \tag{4.30}$$

2. Second, a translation of $\frac{L0}{2}$ along the x-axis, translation of LL along the z-axis, and a rotation of π about the z-axis:

$$T_{L1} = A_i \Big|_{\substack{a=\frac{L0}{2}, \\ \alpha=0, \\ d=LL, \\ \theta=\{\pi}}$$

3. Next, we move the first link by controlling the 1st motor $q1$. This involves a translation of $L1$ along the x-axis and a rotation of $-\pi + q1$ about the z-axis:

$$T_{L2} = A_i \Big| \begin{array}{l} a=L1, \\ \alpha=0, \\ d=0, \\ \theta=pi+q1 \end{array}$$

$$T_{L1}^{L2} = \begin{bmatrix} -1 & 0 & 0 & -\frac{L0}{2} \\ 0 & -1 & 0 & 0 \\ 0 & 0 & 1 & LL \\ 0 & 0 & 0 & 1 \end{bmatrix} \tag{4.31}$$

4. After this, we control the second link with the 2nd motor $q2$. This step comprises a translation of $L2$ along the x-axis and a rotation of $q2$ about the z-axis:

$$T_{L12} = A_i \Big|_{\substack{a=L2, \\ \alpha=0, \\ d=0, \\ \theta=q2}}$$

$$T_{L3}^{LM} = \begin{bmatrix} \cos(q2) & -\sin(q2) & 0 & L2\cos(q2) \\ \sin(q2) & \cos(q2) & 0 & L2\sin(q2) \\ 0 & 0 & 1 & 0 \\ 0 & 0 & 0 & 1 \end{bmatrix} \tag{4.32}$$

5. Lastly, we move to the middle of the upper arm based on the $\phi 3$ value. This involves a translation of $\frac{L3}{2}$ along the x-axis and a rotation of $\phi 3$ about the z-axis:

$$T_{LM} = A_i \Big|_{\substack{a=\frac{L3}{2}, \\ \alpha=0, \\ d=0, \\ \theta=\phi 3}}$$

$$T_{LM}^{P} = \begin{bmatrix} \cos(\theta_3) & -\sin(\theta_3) & 0 & \frac{L3\cos(\theta_3)}{2} \\ \sin(\theta_3) & \cos(\theta_3) & 0 & \frac{L3\sin(\theta_3)}{2} \\ 0 & 0 & 1 & 0 \\ 0 & 0 & 0 & 1 \end{bmatrix} \tag{4.33}$$

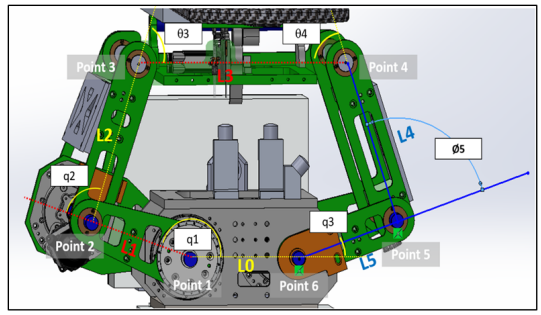

FIGURE 4.14: Linkage needed parameters for DH

Moving to the table pitching frame

we transition from T_{LM} to T_P. This involves a translation of $L6$ along the x-axis, a rotation of $\frac{\pi}{2}$ about the z-axis, a translation of $L7$ along the z-axis, and another rotation of $\frac{\pi}{2}$ about the z-axis:

$$T_P = A_i \Big|_{\substack{a=L6, \\ \alpha=\frac{\pi}{2}, \\ d=L7, \\ \theta=\frac{\pi}{2}}}$$

$$T_P^E = \begin{bmatrix} 0 & 0 & 1 & 0 \\ 1 & 0 & 0 & L6 \\ 0 & 1 & 0 & L7 \\ 0 & 0 & 0 & 1 \end{bmatrix} \tag{4.34}$$

Transitioning from the pitching axis to the endpoint

we use T_{PE}. The translation along the x-axis is determined by the hypotenuse of $L9$ and $L8$. The rotation about the z-axis is defined as $\frac{\pi}{2}$ minus the table angle ('Tabang') and the arctangent of the ratio $\frac{L9}{L8}$. This angle is derived from the pitching encoder:

$$T_{PE} = A_i \Big|_{\substack{a=\sqrt{(L9)^2+(L8)^2}, \\ \alpha=0, \\ d=0, \\ \theta=\left(\frac{\pi}{2}-\text{Tabang}-\arctan\left(\frac{L9}{L8}\right)\right)}}$$

$$T_E^{E1} = \begin{bmatrix} \cos(\text{TabAng} - \theta_6 + \frac{\pi}{2}) & -\sin(\text{TabAng} - \theta_6 + \frac{\pi}{2}) & 0 & L10\cos(\text{TabAng} - \theta_6 + \frac{\pi}{2}) \\ \sin(\text{TabAng} - \theta_6 + \frac{\pi}{2}) & \cos(\text{TabAng} - \theta_6 + \frac{\pi}{2}) & 0 & L10\sin(\text{TabAng} - \theta_6 + \frac{\pi}{2}) \\ 0 & 0 & 1 & 0 \\ 0 & 0 & 0 & 1 \end{bmatrix} \tag{4.35}$$

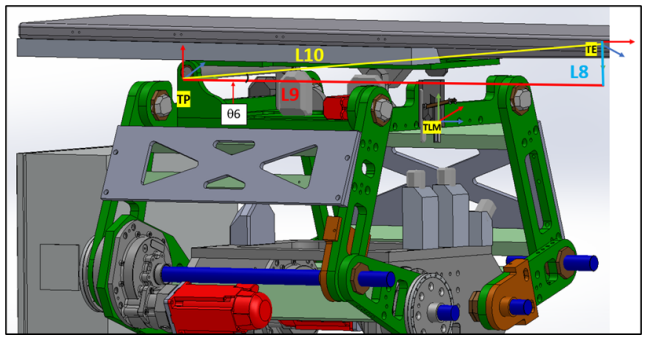

FIGURE 4.15: Moving from table pitching axis to End Point

Additional frames are integrated to align with the reference direction:

In Figure 4.15, it is evident that the TE coordinate does not align with the reference coordinate shown in Figure 4.2. To correct this orientation, several rotational matrices need to be applied as follows:

- $TE1$: Rotation about the z-axis is determined by $-\frac{\pi}{2}$ minus the arctangent of the ratio $\frac{L9}{L8}$. No translations are considered for this frame.

$$TE1 = A_i \Big|_{\substack{a=0,\\ \alpha=0,\\ d=0,\\ \theta=-\left(-\frac{\pi}{2}\arctan\left(\frac{L9}{L8}\right)\right)}}$$

- $TE2$: A rotation of $-\frac{\pi}{2}$ about the x-axis. No translations or other rotations are involved.

$$TE2 = A_i \Big|_{\substack{a=0,\\ \alpha=-\frac{\pi}{2},\\ d=0,\\ \theta=0}}$$

- TE: A rotation of $-\frac{\pi}{2}$ about the z-axis. Again, no translations or other rotations are considered.

$$TE = A_i \Big|_{\substack{a=0,\\ \alpha=0,\\ d=0,\\ \theta=-\frac{\pi}{2}}}$$

$$T_{E1}^{E2} = \begin{bmatrix} \cos(\theta_6 - \frac{\pi}{2}) & -\sin(\theta_6 - \frac{\pi}{2}) & 0 & 0 \\ \sin(\theta_6 - \frac{\pi}{2}) & \cos(\theta_6 - \frac{\pi}{2}) & 0 & 0 \\ 0 & 0 & 1 & 0 \\ 0 & 0 & 0 & 1 \end{bmatrix} \tag{4.36}$$

$$T_{E2}^{E3} = \begin{bmatrix} 1 & 0 & 0 & 0 \\ 0 & 0 & 1 & 0 \\ 0 & -1 & 0 & 0 \\ 0 & 0 & 0 & 1 \end{bmatrix} \tag{4.37}$$

$$T_{E3}^{0} = \begin{bmatrix} 0 & 1 & 0 & 0 \\ -1 & 0 & 0 & 0 \\ 0 & 0 & 1 & 0 \\ 0 & 0 & 0 & 1 \end{bmatrix} \tag{4.38}$$

TABLE 4.1: DH Parameters for the Linkage from origin frame to the end-point frame

Frame	a_i	α	d_i	θ
Linear Rail subsystem				
T0	0	0	0	0
T1	0	0	$-L + \text{Lin}$	0
TR	0	$-\pi/2$	0	0
TRR	0	0	LR	Rot
Linkage subsystem				
TRLB	0	$\pi/2$	0	0
TL1	$L0/2$	0	LL	π
TL2	L1	0	0	$-\pi + q1$
TL3	L2	0	0	$q2$
TLM	$L3/2$	0	0	θ_3
Table Top subsystem				
TP	L6	$\pi/2$	L7	$\pi/2$
TE	L10	0	0	$\pi/2 + \text{Table Angle} - \theta_6$
Euler Rotation Matrices				
TE1	0	0	0	$-\pi/2 - \theta_6$
TE2	0	$-\pi/2$	0	0
TE3	0	0	0	$-\pi/2$

Following table 4.1 outlines the Denavit-Hartenberg (DH) parameters for the PPS system. These parameters are essential for representing the kinematic transformations between adjacent frames of the system. Each row describes a specific transformation with the respective a_i, α_i, d_i, and θ_i parameters, as stipulated by Equation 4.4.

$$T_o^E = T_o \cdot T_1 \cdot T_R \cdot T_{RR} \cdot T_{RLB} \cdot T_{L1} \cdot T_{L2} \cdot T_{L3} \cdot T_{LM} \cdot T_P \cdot T_E \cdot T_{E1} \cdot T_{E2} \cdot T_{E3} \quad (4.39)$$

The 4×4 matrix T_o^E is a homogeneous transformation matrix commonly used in the field of robotics and computer graphics to represent both the position and orientation of a body in space.

The matrix T_o^E is given by [54]:

$$T_o^E = \begin{bmatrix} \mu_x & O_x & \alpha_x & p_x \\ \mu_y & O_y & \alpha_y & p_y \\ \mu_z & O_z & \alpha_z & p_z \\ 0 & 0 & 0 & 1 \end{bmatrix}$$

1. **Position (Translation Vector)**:

   The elements p_x, p_y, and p_z in the fourth column represent the position of the target point with respect to the origin. They give the x, y, and z coordinates of the point in the base or reference frame. In the context of robotics, this would be the position of the end effector or tool tip relative to the base or reference frame.

2. **Orientation (Rotation Matrix)**:

   - The 3×3 matrix on the top-left corner of T_o^E represents the orientation of the body in space. The columns

     $$\begin{bmatrix} \mu_x \\ \mu_y \\ \mu_z \end{bmatrix}, \begin{bmatrix} O_x \\ O_y \\ O_z \end{bmatrix},$$

     and

     $$\begin{bmatrix} \alpha_x \\ \alpha_y \\ \alpha_z \end{bmatrix}$$

     are unit vectors that represent the orientation of the body's local x, y, and z axes, respectively, in the base frame [55].
   - These vectors are often called the rotation axes, and their magnitude is always 1. The orientation of the body can be described using various representations like Euler angles, rotation matrices, or quaternions. In this matrix format, the orientation is represented using the rotation matrix [56].

and we can extract eualr angles from the following

$$\mathbf{R}_{\text{xzy}} = \mathbf{R}_{\text{y}} \cdot \mathbf{R}_{\text{z}} \cdot \mathbf{R}_{\text{x}} \tag{4.40}$$

$$\mathbf{R}_{\text{xzy}} = \begin{bmatrix} \cos\beta\cos\gamma & -\cos\beta\sin\gamma\cos\alpha + \sin\beta\sin\alpha & \cos\beta\sin\gamma\sin\alpha + \sin\beta\cos\alpha \\ \sin\gamma & \cos\gamma\cos\alpha & -\cos\gamma\sin\alpha \\ -\sin\beta\cos\gamma & \sin\beta\sin\gamma\cos\alpha + \cos\beta\sin\alpha & -\sin\beta\sin\gamma\sin\alpha + \cos\beta\cos\alpha \end{bmatrix} \tag{4.41}$$

By substitution in the matrices of each link and multiply them we get the final matrix which gives the information for both motions as:

$$\mu_x = \cos(q1 + q2 + \theta_3) \times \cos(Rot) \tag{4.42}$$

$$\mu_y = \sin(q1 + q2 + \theta_3) \tag{4.43}$$

$$\mu_z = -\cos(q1 + q2 + \theta_3) \times \sin(\text{Rot}) \tag{4.44}$$

$$\begin{aligned} O_x = {} & \sin(\text{Rot}) \times \sin(\text{TabAng}) \\ & - \cos(\text{Rot}) \times \cos(\text{TabAng}) \times \cos(q1) \times \cos(q2) \times \sin(\theta_3) \\ & - \cos(\text{Rot}) \times \cos(\text{TabAng}) \times \cos(q1) \times \cos(\theta_3) \times \sin(q2) \\ & - \cos(\text{Rot}) \times \cos(\text{TabAng}) \times \cos(q2) \times \cos(\theta_3) \times \sin(q1) \\ & + \cos(\text{Rot}) \times \cos(\text{TabAng}) \times \sin(q1) \times \sin(q2) \times \sin(\theta_3) \end{aligned} \tag{4.45}$$

$$O_y = \frac{\cos(\text{TabAng} + q1 + q2 + \theta_3)}{2} + \frac{\cos(q1 - \text{TabAng} + q2 + \theta_3)}{2} \tag{4.46}$$

$$\begin{aligned} O_z = {} & \cos(\text{Rot}) \cdot \sin(\text{TabAng}) \\ & + \cos(\text{TabAng}) \cdot \sin(\text{Rot}) \cdot \cos(q1) \cdot \cos(q2) \cdot \sin(\theta_3) \\ & + \cos(\text{TabAng}) \cdot \sin(\text{Rot}) \cdot \cos(q1) \cdot \cos(\theta_3) \cdot \sin(q2) \\ & + \cos(\text{TabAng}) \cdot \sin(\text{Rot}) \cdot \cos(q2) \cdot \cos(\theta_3) \cdot \sin(q1) \\ & - \cos(\text{TabAng}) \cdot \sin(\text{Rot}) \cdot \sin(q1) \cdot \sin(q2) \cdot \sin(\theta_3) \end{aligned} \tag{4.47}$$

$$
\begin{aligned}
\boldsymbol{a_x} = & \cos(\text{TabAng}) \cdot \sin(\text{Rot}) \\
& + \cos(\text{Rot}) \cdot \sin(\text{TabAng}) \cdot \cos(q1) \cdot \cos(q2) \cdot \sin(\theta_3) \\
& + \cos(\text{Rot}) \cdot \sin(\text{TabAng}) \cdot \cos(q1) \cdot \cos(\theta_3) \cdot \sin(q2) \\
& + \cos(\text{Rot}) \cdot \sin(\text{TabAng}) \cdot \cos(q2) \cdot \cos(\theta_3) \cdot \sin(q1) \\
& - \cos(\text{Rot}) \cdot \sin(\text{TabAng}) \cdot \sin(q1) \cdot \sin(q2) \cdot \sin(\theta_3)
\end{aligned} \tag{4.48}
$$

$$
\boldsymbol{a_y} = \frac{\sin(q1 - \text{TabAng} + q2 + \theta_3)}{2} - \frac{\sin(\text{TabAng} + q1 + q2 + \theta_3)}{2} \tag{4.49}
$$

$$
\begin{aligned}
\boldsymbol{a_z} = & \cos(\text{Rot}) \cos(\text{TabAng}) \\
& - \sin(\text{Rot}) \sin(\text{TabAng}) \cos(q1) \cos(q2) \sin(\theta_3) \\
& - \sin(\text{Rot}) \sin(\text{TabAng}) \cos(q1) \cos(\theta_3) \sin(q2) \\
& - \sin(\text{Rot}) \sin(\text{TabAng}) \cos(q2) \cos(\theta_3) \sin(q1) \\
& + \sin(\text{Rot}) \sin(\text{TabAng}) \sin(q1) \sin(q2) \sin(\theta_3)
\end{aligned} \tag{4.50}
$$

$$
\begin{aligned}
\boldsymbol{p_x} = & \, L7 \sin(\text{Rot}) - \frac{L0 \cos(\text{Rot})}{2} + LL \sin(\text{Rot}) \\
& + L1 \cos(\text{Rot}) \cos(q1) + L10 \sin(\text{Rot}) \cos(\text{TabAng} - \theta_6) \\
& - L6 \sin(q1 + q2 + \theta_3) \cos(\text{Rot}) \\
& + L2 \cos(\text{Rot}) \cos(q1) \cos(q2) - L2 \cos(\text{Rot}) \sin(q1) \sin(q2) \\
& + L10 \sin(q1 + q2 + \theta_3) \cos(\text{Rot}) \sin(\text{TabAng} - \theta_6) \\
& + \frac{L3 \cos(q1 + q2) \cos(\text{Rot}) \cos(\theta_3)}{2} \\
& - \frac{L3 \sin(q1 + q2) \cos(\text{Rot}) \sin(\theta_3)}{2}
\end{aligned} \tag{4.51}
$$

$$\begin{aligned} p_y = & LR + L2\sin(q1+q2) + L1\sin(q1) \\ & + L6\cos(q1+q2+\theta_3) \\ & + \frac{L3\sin(q1+q2+\theta_3)}{2} \\ & - \frac{L10\sin(\text{TabAng}+q1+q2+\theta_3-\theta_6)}{2} \\ & + \frac{L10\sin(q1-\text{TabAng}+q2+\theta_3+\theta_6)}{2} \end{aligned} \tag{4.52}$$

$$\begin{aligned} p_z = & \text{lin} - L + L7\cos(\text{Rot}) + LL\cos(\text{Rot}) + \frac{L0\sin(\text{Rot})}{2} \\ & - L1\sin(\text{Rot})\cos(q1) + L10\cos(\text{Rot})\cos(\text{TabAng}-\theta_6) \\ & + L6\sin(q1+q2+\theta_3)\sin(\text{Rot}) + \frac{L3\sin(q1+q2)\sin(\text{Rot})\sin(\theta_3)}{2} \\ & - L2\sin(\text{Rot})\cos(q1)\cos(q2) + L2\sin(\text{Rot})\sin(q1)\sin(q2) \\ & - L10\sin(q1+q2+\theta_3)\sin(\text{Rot})\sin(\text{TabAng}-\theta_6) \\ & - \frac{L3\cos(q1+q2)\sin(\text{Rot})\cos(\theta_3)}{2} \end{aligned} \tag{4.53}$$

From equation 4.40 we can extract eualr angles using 4.54, 4.55 and 4.56.

$$\begin{aligned} \alpha &= \tan^{-1}\left(\frac{\sin\alpha}{\cos\alpha}\right) \\ &= \tan^{-1}\left(\frac{\cos\gamma\cdot\sin\alpha}{\cos\alpha\cdot\cos\gamma}\right) \\ &= \tan^{-1}\left(\frac{-\mathbf{R}_{\text{xzy},2,3}}{\mathbf{R}_{\text{xzy},2,2}}\right) \\ &= \tan^{-1}\left(\frac{-\mathbf{R}_{2,3}}{\mathbf{R}_{2,2}}\right) \end{aligned} \tag{4.54}$$

$$\begin{aligned}\beta &= \tan^{-1}\left(\frac{\sin\beta}{\cos\beta}\right)\\ &= \tan^{-1}\left(\frac{\cos\gamma\cdot\sin\beta}{\cos\beta\cdot\cos\gamma}\right)\\ &= \tan^{-1}\left(\frac{-\mathbf{R}_{\text{xzy},3,1}}{\mathbf{R}_{\text{xzy},1,1}}\right)\\ &= \tan^{-1}\left(\frac{\mathbf{R}_{3,1}}{\mathbf{R}_{1,1}}\right)\end{aligned} \tag{4.55}$$

$$\begin{aligned}\gamma &= \tan^{-1}\left(\frac{\sin\gamma}{\cos\gamma}\right)\\ &= \tan^{-1}\left(\frac{\sin\gamma}{\sqrt{(\cos\alpha\cdot\cos\gamma)^2+(-\cos\gamma\cdot\sin\alpha)^2}}\right)\\ &= \tan^{-1}\left(\frac{\mathbf{R}_{\text{xzy},2,1}}{\sqrt{\mathbf{R}^2_{\text{xzy},2,2}+\mathbf{R}^2_{\text{xzy},2,3}}}\right)\\ &= \tan^{-1}\left(\frac{\mathbf{R}_{2,1}}{\sqrt{\mathbf{R}^2_{2,2}+\mathbf{R}^2_{2,3}}}\right)\end{aligned} \tag{4.56}$$

$$\begin{aligned}\text{Pitch} =& \frac{180}{\pi}\cdot\text{atan2}\left(\sin(\text{TabAng}+q1+q2+th3)/2\right.\\ &-\sin(q1-\text{TabAng}+q2+th3)/2,\\ &\cos(\text{TabAng}+q1+q2+th3)/2\\ &\left.+\cos(q1-\text{TabAng}+q2+th3)/2\right)\end{aligned} \tag{4.57}$$

$$\begin{aligned}\text{Yaw} =& \frac{180}{\pi}\cdot\text{atan2}\left(-\cos(q1+q2+th3)\cdot\sin(\text{Rot}),\right.\\ &\left.\cos(q1+q2+th3)\cdot\cos(\text{Rot})\right)\end{aligned} \tag{4.58}$$

$$\text{Roll} = \frac{180}{\pi} \cdot \text{atan2}\left(\sin(q1 + q2 + th3),\right.$$
$$\sqrt{\left(\frac{\cos(TabAng + q1 + q2 + th3)}{2} + \frac{\cos(q1 - TabAng + q2 + th3)}{2}\right)^2}$$
$$\left. + \left(\frac{\sin(TabAng + q1 + q2 + th3)}{2} - \frac{\sin(q1 - TabAng + q2 + th3)}{2}\right)^2\right) \tag{4.59}$$

Forward kinematics plays a pivotal role in deducing the end effector's pose, comprising both its position and orientation, based on the provided joint parameters within the context of a PPS.

Inputs considered:

- Linear displacement: Linear.
- Rotary displacement: $\text{Rotary}_{\text{rot}}$.
- Angles of the three linkage-driven joints: q_1, q_2, q_3.
- Table Pitching Angle: $\theta_{\text{TableAngle}}$.

Outcomes derived:

- Target Point position in Cartesian coordinates: $\mathbf{P} = [x, y, z]^T$.
- Target Point orientation expressed as pitch (α), yaw (β), and roll (γ): $\mathbf{O} = [\alpha, \beta, \gamma]^T$.

This forward kinematic study serves as solid evidence that our equations and calculations are accurate, ensuring the patient's precise alignment within the PPS, and thereby guaranteeing the reliability and accuracy of the entire system.

4.2.3 Inverse Kinematics

The aim of this subsection is to delve deep into the intricacies of inverse kinematics as it applies to the PPS, elucidating the mathematical models, methodologies, and algorithms that enable the PPS to achieve its precise positioning capabilities.

Solution Techniques for Inverse Kinematics

Inverse kinematics, given its computational complexity and intricacies, can be approached using several methods [57], [58]. These methods are typically categorized based on their approach—algebraic, geometric, or iterative[59], [60], [61].

While the above methods offer different pathways to solve the IK problem, the optimal choice often depends on the specific application, the robot's structure, and computational constraints [62]. For the PPS, we'll further investigate and determine which method best fits our needs and system architecture.

Advantages of Geometric Methods for the PPS

Geometric methods, as mentioned, employ a graphical interpretation of the robot's structure and its workspace [63]. While each method of inverse kinematics carries its own benefits and shortcomings, the geometric approach stands out in several respects, particularly for systems like the PPS [64], [65].

4.2.4 Inverse Kinematics Study of Subsystems

In the context of our project, dealing with multiple subsystems and a high degree of freedom (DOF) presents a complex kinematic scenario. To effectively handle this complexity and ensure precise control and positioning, we employ the geometric method for our kinematic analysis [66]. This approach allows us to decompose the multilayered system into simpler geometric entities, making the analysis more manageable and straightforward while ensuring the accuracy and reliability of our computations.

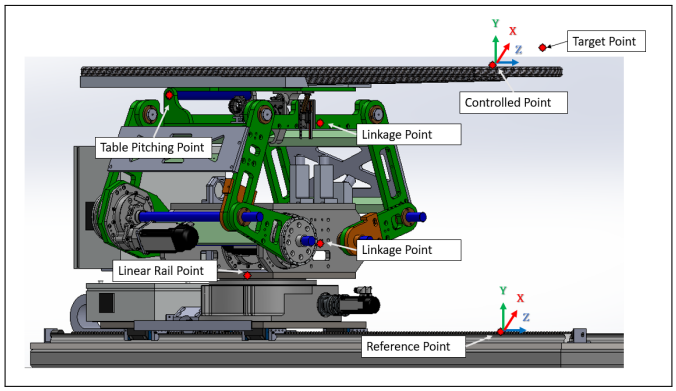

FIGURE 4.16: Inverse Kinematics main Points

Description of Points and Rotations in the PPS

In the context of the Patient Positioning System (PPS), specific points and rotations are crucial in accurately establishing and calculating positional data within the system.

Controlled Point (CP)

The Controlled Point (CP) in the PPS, specifically located at the center of the bed, plays a pivotal role due to its known coordinates relative to the origin frame. This point is expressed as:

$$\mathbf{CP} = (x, y, z) = (0, L_{home}, 0) \tag{4.60}$$

in Cartesian coordinates, and its orientation is described using the Pitch, Yaw, and Roll angles as

$$(\alpha, \beta, \gamma) = (0, 0, 0). \tag{4.61}$$

Rotations in the PPS

- **Pitch (Rotation around X-axis):** The Pitch rotation, denoted as α or simply as "Pitch", is the rotation about the x-axis. Positive values correspond to an upward rotation, while negative values indicate a downward rotation.
- **Yaw (Rotation around Y-axis):** The Yaw rotation, represented as β or "Yaw", involves rotation about the y-axis. When viewed from above, positive and negative Yaw angles correspond to counter-clockwise and clockwise rotations, respectively.
- **Roll (Rotation around Z-axis):** Denoted as γ or "Roll", this rotation around the z-axis involves positive angles for counterclockwise rotations and negative angles for clockwise rotations.

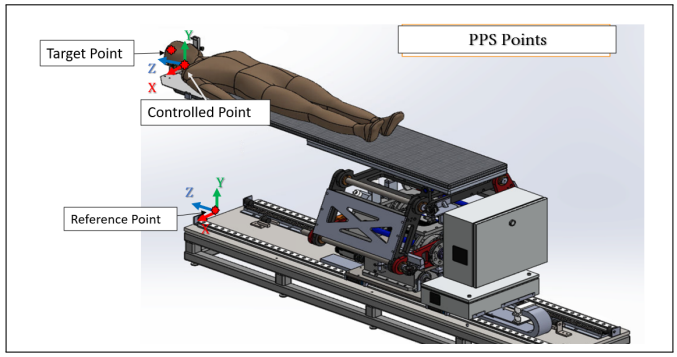

FIGURE 4.17: PPS's Control, Target and Reference Points

Reference Point

The *Reference Point* serves as the origin frame in the PPS, from which all other points, coordinates, and orientations are defined. Rotations (Pitch, Yaw, and Roll) and translations (in x, y, z) within the PPS are specified with respect to this fundamental point.

Target Point (TP)

The Target Point (TP) signifies the focal point for treatment in the PPS, representing the precise location of a tumor within the brain. Gamma radiation beams are directed towards this point to ensure targeted and effective treatment. It's crucial to note that the TP varies across patients, dependent on individual cases and the specifics of their treatment plan. The position and orientation of this point act as the primary input for our system, providing necessary details for subsequent kinematic calculations.

Mapping Target Point to Controlled Point

The foundational layer of the inverse kinematics process in the PPS aims to establish a correlation between the TP and the CP. By doing so, we can ensure that the desired treatment point, TP, is accurately aligned with the controlled point, CP, thus guaranteeing that the radiation beams are directed correctly for optimal treatment efficacy.
Ensuring the precise alignment of the Target Point (TP) with the Controlled Point (CP) in the Patient Positioning System (PPS) involves both positional and rotational transformations.

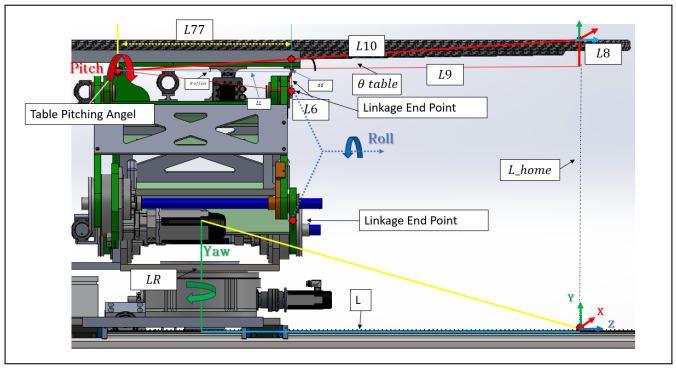

FIGURE 4.18: PPS Inverse Kinematics Geometry

Defining Displacement Inputs

Displacement represents the change in position of a point with respect to a reference. For the purpose of this analysis, the displacement values are defined as:

$$\Delta x = x_{\text{TargetToControl}} \tag{4.62}$$

$$\Delta y = d_{\text{Offset}} + y_{\text{TargetToControl}} \tag{4.63}$$

$$\Delta z = l_{\text{Offset}} + z_{\text{TargetToControl}} \tag{4.64}$$

Rotation Matrices

[67]

1. Rotation Matrix around the X-axis (Pitch)

$$R_x(\theta_{\text{Pitch}}) = \begin{bmatrix} 1 & 0 & 0 \\ 0 & \cos(\theta_{\text{Pitch}}) & -\sin(\theta_{\text{Pitch}}) \\ 0 & \sin(\theta_{\text{Pitch}}) & \cos(\theta_{\text{Pitch}}) \end{bmatrix} \tag{4.65}$$

2. Rotation Matrix around the Z-axis (Roll)

$$R_z(\theta_{\text{Roll}}) = \begin{bmatrix} \cos(\theta_{\text{Roll}}) & -\sin(\theta_{\text{Roll}}) & 0 \\ \sin(\theta_{\text{Roll}}) & \cos(\theta_{\text{Roll}}) & 0 \\ 0 & 0 & 1 \end{bmatrix} \tag{4.66}$$

3. Rotation Matrix around the Y-axis (Yaw)

$$R_y(\theta_{\text{Yaw}}) = \begin{bmatrix} \cos(\theta_{\text{Yaw}}) & 0 & \sin(\theta_{\text{Yaw}}) \\ 0 & 1 & 0 \\ -\sin(\theta_{\text{Yaw}}) & 0 & \cos(\theta_{\text{Yaw}}) \end{bmatrix} \tag{4.67}$$

Applying Rotations

For the new coordinates post each rotation[1]:

After X-axis rotation:

$$X_{\text{RotX}} = \Delta x \tag{4.68}$$

$$Y_{\text{RotX}} = \Delta y \cos(\theta_{\text{Pitch}}) - \Delta z \sin(\theta_{\text{Pitch}}) \tag{4.69}$$

$$Z_{\text{RotX}} = \Delta y \sin(\theta_{\text{Pitch}}) + \Delta z \cos(\theta_{\text{Pitch}}) \tag{4.70}$$

[1] **Pitch Rotation (X-axis)**: The point's initial rotation around the X-axis.
Roll Rotation (Z-axis): Following the first rotation, the point's new position is further rotated around the Z-axis.
Yaw Rotation (Y-axis): The point, having been rotated twice, undergoes a final rotation around the Y-axis.

After X and Z axes rotations:

$$X_{\text{RotXZ}} = X_{\text{RotX}} \cos(\theta_{\text{Roll}}) - Y_{\text{RotX}} \sin(\theta_{\text{Roll}}) \tag{4.71}$$

$$Y_{\text{RotXZ}} = X_{\text{RotX}} \sin(\theta_{\text{Roll}}) + Y_{\text{RotX}} \cos(\theta_{\text{Roll}}) \tag{4.72}$$

$$Z_{\text{RotXZ}} = Z_{\text{RotX}} \tag{4.73}$$

After X, Z, and Y axes rotations:

$$x_{\text{TP\_CP}} = -(X_{\text{RotXZ}} \cos(\theta_{\text{Yaw}}) + Z_{\text{RotXZ}} \sin(\theta_{\text{Yaw}})) \tag{4.74}$$

$$y_{\text{TP\_CP}} = -Y_{\text{RotXZ}} \tag{4.75}$$

$$z_{\text{TP\_CP}} = -(Z_{\text{RotXZ}} \cos(\theta_{\text{Yaw}}) - X_{\text{RotXZ}} \sin(\theta_{\text{Yaw}})) \tag{4.76}$$

This approach ensures that the TP aligns correctly with the CP, incorporating both positional and angular transformations.

Mapping Controlled Point to Linear Horizontal Rail

The equation below determines the effective length, L_{rail}[1], of the linear horizontal rail in the Patient Positioning System (PPS), as depicted in the following figure 4.18.

This linear rail system enables controlled linear movement of the main plate and the rotational alignment of the Linkage System via a rotary table 4.19, ensuring precise patient positioning.

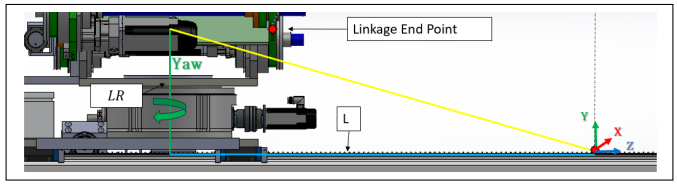

FIGURE 4.19: Linear Rail Inverse Geometry

$$L_{\text{rail}} = -\left(Z_{\text{base\_position}} + Z_{\text{linkage\_transform}} + X_{\text{linkage\_transform}} \cdot \tan(\theta_{\text{yaw}}) + X_{\text{base\_position}} \cdot \tan(\theta_{\text{yaw}}) + \frac{Z_{\text{rotary\_offset}}}{\cos(\theta_{\text{yaw}})}\right) \tag{4.77}$$

Here's a deeper insight into the components:

- L_{rail}: The effective length of the linear horizontal rail, indicating how extended or retracted the rail is.
- $Z_{\text{base\_position}}$: Represents the vertical position or height of the PPS base from a predetermined reference point.
- $Z_{\text{linkage\_transform}}$ and $X_{\text{linkage\_transform}}$: The vertical and horizontal offsets respectively caused by the transformations of the system's linkages.
- $\tan(\theta_{\text{yaw}})$: Here, the tangent function is used to translate the horizontal distance into a vertical offset based on the yaw angle. It essentially calculates how much vertical change is introduced for a given horizontal displacement when the system is rotated about its vertical axis.
- θ_{yaw}: The yaw angle, measured in radians, denotes the rotation of the system around its vertical axis.
- $Z_{\text{rotary\_offset}}$: A vertical offset from the rotary table joint. This value adjusts based on the rotation of the joint, ensuring precise patient positioning.

Mapping Controlled Point to Table Pitching Axis

Based on figure 4.20 the table angle can be calculated based on the following formula

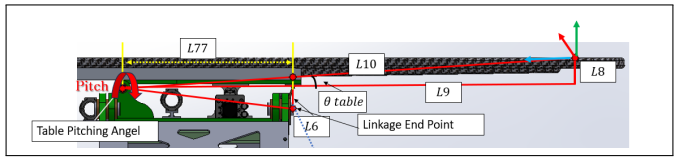

FIGURE 4.20: Table Angle Geometry

Given a right triangle where the opposite side is denoted as L_8 and the adjacent side as L_9, we can calculate the angle θ_{table} using the tangent function. The tangent

[1]The negative sign in front of the equation indicates that the rail's length extends in a direction opposite to the default coordinate system of the PPS.

of an angle in a right triangle is the ratio of the length of the opposite side to the length of the adjacent side.

$$\tan(\theta_{\text{table}}) = \frac{L_8}{L_9} \tag{4.78}$$

To find the angle θ_{table}, we use the inverse tangent function (also known as arctan or $\tan^{-1}$):

$$\theta_{\text{table}} = \arctan\left(\frac{L_8}{L_9}\right) \tag{4.79}$$

Due to the intricacies of the design, a minor angular offset affects the pitch axis. This deviation becomes evident upon closer inspection of the preceding figure. As illustrated in the subsequent figure (where the triangle is highlighted in blue), the triangle's two sides are denoted as dd and ll.

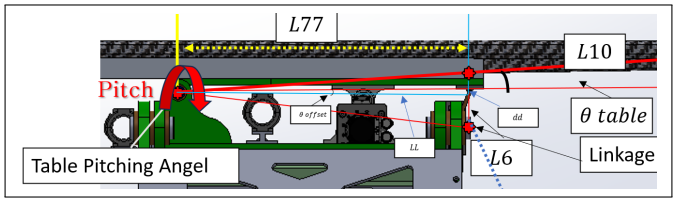

FIGURE 4.21: Zoomed-in view showcasing the blue triangle with sides dd and ll.

Using the Pythagorean theorem, the length of the third side, denoted as a, can be calculated as:

$$a = \sqrt{dd^2 + ll^2} \tag{4.80}$$

Subsequently, the angle θ_p, representing the pitch, is determined by:

$$\theta_p = \theta_{\text{offset}} - \theta_{\text{table}} \tag{4.81}$$

Where θ_{offset} is the initial angular deviation and θ_{table} is the angle calculated from the table's position.

Moreover

Given the relationship between the lengths L_{77}, a, and L_6 and the angles θ_{pitch} and θ_1, we can derive the angle θ_2 using the following steps:

1. Calculate the projection of the side a influenced by the angle θ_{pitch}:

$$a' = a\cos(\theta_p) \tag{4.82}$$

2. Compute the ratio of the adjusted length L_{77} to L_6:

$$R = \frac{L_{77} - a'}{L_6} \tag{4.83}$$

3. Determine the angle associated with this ratio using the arc cosine function:

$$\alpha = \arccos(R) \tag{4.84}$$

4. Finally, adjust this angle based on a reference or initial angle θ_p:

$$\theta_2 = -\alpha - \theta_p \tag{4.85}$$

Substituting the values from steps 1 to 3 into step 4, we get:

$$\theta_2 = -\left(\arccos\left(\frac{L_{77} - a\cos(\theta_p)}{L_6}\right)\right) - \theta_p$$

The vertical position

The vertical position, y_{point}, is influenced by several components. To determine y_{point}, we can use the following steps:

1. Determine the vertical contribution of the length a_1 given the angle θ_{pitch}:

$$y_1 = a_1 \sin(\theta_{\text{pitch}}) \tag{4.86}$$

2. Calculate the vertical effect of the length L_6 inclined by the combined angles θ and θ_2:

$$y_2 = L_6 \sin(\theta + \theta_2) \tag{4.87}$$

3. Consider a constant vertical offset, d_1.

4. Combine all the above contributions to get the final vertical position:

$$y_{\text{point}} = y_1 + y_2 + d_1 \tag{4.88}$$

Using the expressions from steps 1 to 3 in step 4, we arrive at:

$$y_{\text{point}} = a_1 \sin(\theta_{\text{pitch}}) + L_6 \sin(\theta + \theta_2) + d_1$$

4.2.5 Linkage Inverse Kinematics

In our inverse kinematics framework, we focus on accurately determining the joint angles—q_1, q_2, and q_3—to ensure the top bar is aligned with the target locations

both rapidly and precisely. This model accepts the mid-point position as its input, translating it into the necessary joint angles for output. Consequently, the robotic linkage can optimally position its midpoint via appropriate motor commands.

Many methodologies address the complexities of linkage inverse kinematics, as explored in references [68] and [69]. Nonetheless, our strategy draws inspiration predominantly from the geometric methods elaborated in [70] and [71].

Central to our analysis is the assumption that $L3$'s midpoint, represented as $P0$, remains fixed, which is illustrated in Figure 4.22.

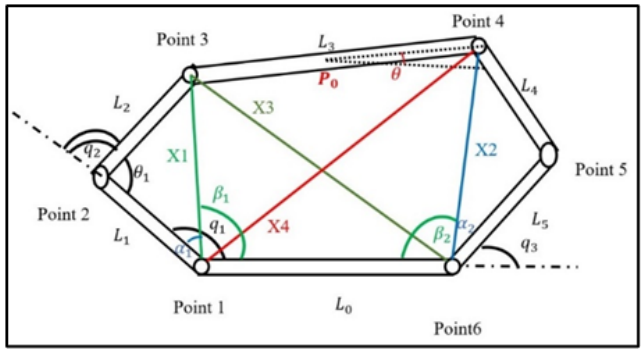

FIGURE 4.22: Linkage inverse Kinematic study strategy

4.2.6 Mathematical Formulation

We begin by making an assumption that Point 1 serves as the origin.

For the given system, the slope m is described as:

$$m = \tan\theta \tag{4.89}$$

Using this slope, we can express y_3 and y_4 by:

$$y - y_p = m(x - x_p) \tag{4.90}$$

$$y_3 = m(x_3 - x_{p0}) + y_{p0} \tag{4.91}$$

$$y_4 = m(x_4 - x_{p0}) + y_{p0} \tag{4.92}$$

The geometric constraints on the system yield:

$$(y_{p0} - y_3)^2 + (x_{p0} - x_3)^2 = \left(\frac{L3}{4}\right)^2 \tag{4.93}$$

$$m^2(x_{p0} - x_3)^2 + (x_{p0} - x_3)^2 = \left(\frac{L3}{4}\right)^2 \tag{4.94}$$

From these constraints, we can determine x_3 and x_4:

$$x_3 = x_{p0} - \frac{L3}{2\sqrt{1+m^2}} \tag{4.95}$$

$$(y_4 - y_3)^2 + (x_4 - x_3)^2 = L3^2 \tag{4.96}$$

$$m^2(x_4 - x_3)^2 + (x_4 - x_3)^2 = L3^2 \tag{4.97}$$

$$(1+m^2) + (x_4 - x_3)^2 = L3^2 \tag{4.98}$$

$$x_4 = x_3 + \frac{L3}{\sqrt{1+m^2}} \tag{4.99}$$

We can determine x_{p0}, y_{p0} based on the coordinates x_3, x_4, y_3 and y_4. Subsequently, all the X's can be represented as:

$$x_1 = \sqrt{x_3^2 + y_3^2} \tag{4.100}$$

$$x_2 = \sqrt{(x_4 - L0)^2 + y_4^2} \tag{4.101}$$

$$x_3 = \sqrt{(x_3 - L0)^2 + y_3^2} \tag{4.102}$$

$$x_4 = \sqrt{x_4^2 + y_4^2} \tag{4.103}$$

Considering vector addition:

$$\vec{L1} + \vec{L2} = \vec{X1} \tag{4.104}$$

$$L2^2 = X1^2 + L1^2 - 2L1X1\cos\alpha_1 \tag{4.105}$$

Thus, α_1 can be expressed as:

$$\alpha_1 = \cos^{-1}\left(\frac{L1^2 - L2^2}{2L1X1}\right) \tag{4.106}$$

From our constraints:

$$X1^2 = L1^2 + L2^2 + 2L1L2\cos\theta_1 \tag{4.107}$$

Which allows us to express θ_1:

$$\theta_1 = \cos^{-1}\left(\frac{X1^2 + L1^2 - L2^2}{2L1L2}\right) \tag{4.108}$$

Using the representation in Figure 4.22, we can define:

$$\vec{L0} + \vec{X1} = \vec{X3} \tag{4.109}$$

$$X3^2 = L0^2 + X1^2 + 2L0X1\cos\beta_1 \tag{4.110}$$

This allows us to define β_1:

$$\beta_1 = \cos^{-1}\left(\frac{X3^2 + L0^2 - X1^2}{2L0X1}\right) \tag{4.111}$$

Based on Figure 6, $q1$ and $q2$ can be expressed as:

$$q_2 = \theta_1 - \pi \tag{4.112}$$
$$q_1 = \alpha_1 + \beta_1 \tag{4.113}$$

Using the constraints:

$$\vec{L5} + \vec{L4} = \vec{X2} \tag{4.114}$$
$$L4^2 = X2^2 + L5^2 - 2X2L5\cos\alpha_2 \tag{4.115}$$

This yields:

$$\alpha_2 = \cos^{-1}\left(\frac{X2^2 + L5^2 - L4^2}{2X2L5}\right) \tag{4.116}$$

Again, referring to Figure 4.22:

$$\vec{L0} + \vec{X2} = \vec{X4} \tag{4.117}$$
$$X4^2 = L0^2 + X2^2 + 2L0X2\cos\beta_2 \tag{4.118}$$

This results in:

$$\beta_2 = \cos^{-1}\left(\frac{X4^2 - L0^2 - X2^2}{2L0X2}\right) \tag{4.119}$$

Lastly, the final rotation angle q_3 can be determined as:

$$q_3 = \pi - \alpha_2 - \beta_2 \tag{4.120}$$

The equations delineated herein provide a thorough examination of the inverse kinematics for a particular linkage. Integrating these insights with additional subsystems is imperative to formulate a comprehensive inverse kinematics solution for the entirety of the Patient Positioning System (PPS).

Inverse kinematics is instrumental in determining the requisite joint parameters to achieve the desired pose for the end effector based on its position and orientation within the PPS framework.

Inputs considered:

- Desired Target Point position in Cartesian coordinates: $\mathbf{P} = [x, y, z]^T$.

- Desired orientation represented as pitch (α), yaw (β), and roll (γ): $\mathbf{O} = [\alpha, \beta, \gamma]^T$.

Outcomes derived:

- Linear displacement: Linear Motor.
- Rotary displacement: Rotary Motor.
- Angles of the three linkage-driven joints: q_1, q_2, q_3.
- Table Pitching Angle: $\theta_{\text{TableAngle}}$.

This inverse kinematic study validates our mathematical formulations and computational methods, guaranteeing the optimal alignment of the patient within the PPS. This assurance underpins the robustness and precision of the entire positioning system.

4.3 Patient Positioning System Components

This section delves into the heart of the PPS's control architecture. It sheds light on the design intricacies and operational protocols that enable the PPS to achieve its desired movements, even under the most stringent requirements. From single to dual-loop control strategies, from the selection of appropriate motor drives and controllers to the firmware that acts as the brain of the system, every component plays a crucial role in the orchestration of the PPS's movements. Moreover, the integration of *SPiiPlus MMI Application* , which acts as an interface, further amplifies the system's robustness, allowing for enhanced user interaction and system monitoring.

4.3.1 PPS Control: An Insight into Hardware and Firmware

The Patient Positioning System (PPS) stands as a testament to the confluence of state-of-the-art hardware and cutting-edge firmware, collaborating seamlessly to achieve unparalleled precision in radiosurgery. As a nexus of technological advancements, the PPS integrates a multitude of components, each playing an indispensable role in its operation. From the intricate details of motor drives to the sophisticated algorithms of motion controllers and the unparalleled command management of the firmware, each facet contributes to the system's impeccable performance.

Hardware Architecture

Motors

The motor stands as the central component of our Precision Positioning System (PPS), translating electronic commands into meticulous mechanical actions [72].

This section elucidates the servo motors employed, their characteristics, and their significance in the PPS.

Introduction to Servo Motors

Servo motors serve as rotary actuators designed for exact angular position control [73]. The configuration includes a motor paired with a sensor offering position feedback. This arrangement requires a corresponding servo drive, which, with the aid of the feedback sensor, offers precision control of the motor's angular position [74].

Working Mechanism

A standard servo mechanism is characterized by:

- A servo motor combined with feedback apparatus like hall effect sensors, encoders, or resolvers.
- A drive amplifier responsible for powering and governing the motor.
- Essential cabling establishing a connection between the motor and drive [75].

In operation, the drive powers the motor, and the feedback apparatus continuously observes the rotor's velocity and positioning. Feedback is then relayed to the control circuits in the drive, which in response, refines the power dynamics to the motor, assuring impeccable execution of programmed movements [76].

Servo motors, while diversified in nature, universally incorporate feedback systems [77]. Their precision in reacting to directives from the drive pertaining to position, speed, and velocity is paramount for a spectrum of industrial applications, spanning robotics to metal formation [78].

Historical Context and Diversity

Historically, the term "servo" was first coined in 1859 by Joseph Facort, who introduced a feedback mechanism in steam navigation [79]. Modern-day servo mechanisms amalgamate a motor, feedback apparatus, and control electronics. Their categorization is based on motor type, operational nature, and feedback devices [80]. Their adaptability is evident in their use across varied fields, from DIY activities to state-of-the-art machining centers [81].

Embedded Loop System in Servo Mechanism

Servo mechanisms embrace a hierarchical loop system: current (or torque), velocity, and position loops. Each is underpinned by precision feedback components, ensuring synchronous and real-time adjustments to cater to commanded parameters

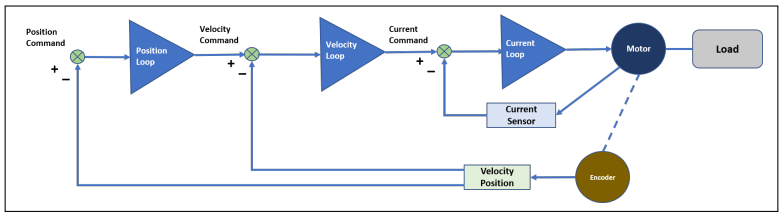

FIGURE 4.23: Diagram illustrating the embedded loops in a servo motor.

[82]. For instance, the base, current loop, which is proportional to torque, enables acceleration. A dedicated current sensor communicates with the control electronics, ensuring the motor's operation aligns with the desired parameters. Similarly, the velocity and position loops maintain the required synchronization to achieve seamless servo control [83].

AKM Servo Motor

For the precision positioning system (PPS) in our project, we utilize various AKM servo motors from Kollmorgen [84].

FIGURE 4.24: Kollmorgen Motor (AKM Family).

Each of these motors plays a pivotal role in the overall functioning and accuracy of the PPS.

Motor Drives

Motor drives are pivotal, regulating the power supply to the motor and translating electronic signals into mechanical actions. Dive into the design features, their operation, and how they synergize with motors to guarantee precise control [85].

The UDMPM is a dual and single axis, universal EtherCAT drive. The UDMPM is powered by a single phase 85 to 265Vac (or 120 to 375Vdc) and provides continuous/peak current options of 2.5A/5A, 5A/10A, and 7.5A/15A.

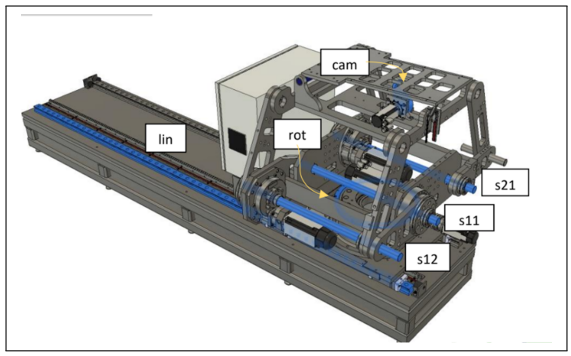

FIGURE 4.25: Motors Position on PPT

FIGURE 4.26: UDMPM ACS Drive

Secondary Encoders

To maintain the pinnacle of precision and to have redundancy, secondary encoders are incorporated into the PPS. These devices offer real-time feedback on motor positioning, allowing for instantaneous adjustments. Discuss their role, the technology behind them, and their importance in systems demanding high reliability [86].

FIGURE 4.27: Renishaw Optical Encoder

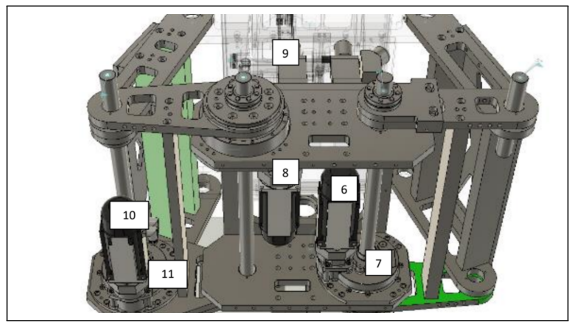

FIGURE 4.28: Secondary Encoders Located

Motion Controller

A motion controller is a device that determines and manages the path or route that a machine part should take (this is known as motion planning). If the system is a closed-loop type, the controller uses feedback to make adjustments, ensuring precise control of the movement [87].

ACS SPiiPlusES Motion Controllers: Developed by ACS, is a motion controller designed to function within EtherCAT-based control systems [88].

FIGURE 4.29: ACS SPiiPlusES Motion Controller

Firmware Integration

SPiiPlus MMi Application

The SPiiPlus MMi application transcends its role as just firmware; it's the brain of the PPS's operations. Serving as the bridge between hardware intricacies and user commands, this application is fundamental for error-free operations [89]. Delve into its user-friendly interface, its diagnostic capabilities, real-time monitoring features, and how it ensures every hardware component functions in harmony [90].

4.4 Control Algorithms for Patient Positioning System

4.4.1 Control Architecture

The control architecture of the Patient Positioning System (PPS) is a critical component that ensures the system's precision, safety, and effectiveness [91]. It comprises various layers of control strategies designed to manage the system's 6-DOF robotic movements with extreme accuracy [92]. This section aims to elucidate the underlying principles and operational protocols that constitute the control architecture of the PPS.

The architecture is primarily broken down into two types of control loops: Single-loop and Dual-loop control [93]. While Single-loop control is more straightforward and primarily deals with simple feedback systems, Dual-loop control offers an additional layer of control, making the system more robust and accurate [94].

4.4.2 Single-loop Control

Single-loop control systems are the most straightforward type of control mechanism in the realm of automatic control systems [95]. They involve a single feedback loop where the system's output is monitored by a sensor, such as an encoder [96]. The sensor's measurements are then compared to a predefined setpoint or desired state. Any discrepancy or error between the setpoint and the sensor data triggers the control system to adjust the system's output accordingly [97].

The primary advantage of single-loop control lies in its simplicity. With only one loop, the system is easier to design, implement, and troubleshoot. It also typically has faster response times due to the direct nature of the feedback loop and the fewer components involved [98]. However, this simplicity comes at the cost of flexibility and the ability to handle more complex, interrelated system dynamics [99].

Understanding PID Control

The PID controller is one of the most commonly utilized feedback controllers in industrial control systems [100]. The control law in a PID controller is a linear combination of three essential components:

- **P (Proportional)**: Provides correction based on the **present** error.
- **I (Integral)**: Delivers correction based on the accumulation of **past** errors, yielding zero steady-state error.

- **D (Derivative)**: Offers correction based on the rate of change of the error, producing a prediction of **future** behavior.

The control output U for a PID controller is generally described by the equation:

$$U(t) = K_p e(t) + K_i \int_0^t e(\tau)d\tau + K_d \frac{d}{dt}e(t)$$

Where $U(t)$ is the control output, $e(t)$ is the error signal, and K_p, K_i, and K_d are the proportional, integral, and derivative gains, respectively.

Cascaded Control Loops

Cascaded control loops are commonly used in advanced control systems [101]. These loops are arranged hierarchically and consist of the following:

- Current Loop: This is the innermost control loop and is responsible for regulating the current in the system.
- Velocity Loop: This loop controls the speed of the system and receives its command from the outer position loop.
- Position Loop: This is the outermost loop and generates a command that is fed into the velocity loop.

The hierarchical arrangement works as follows:

1. The Position Loop generates a command for the Velocity Loop.
2. The Velocity Loop, in turn, generates a command for the Current Loop.

The block diagram in Figure 4.30 illustrates the cascading relationship between these loops.

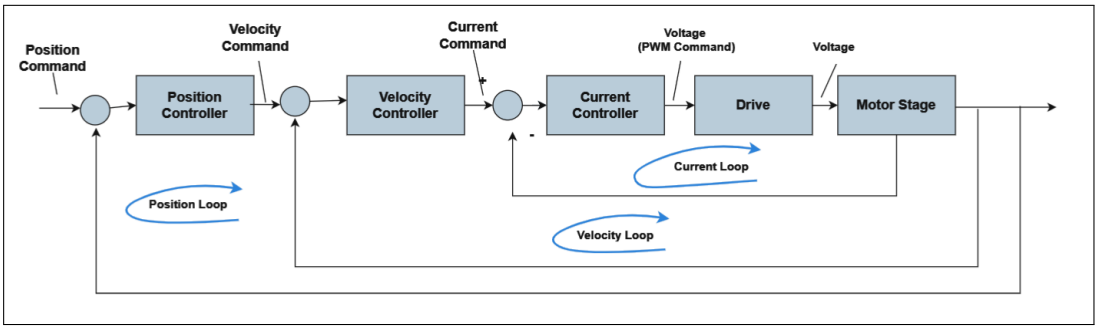

FIGURE 4.30: Block diagram illustrating cascaded control loops.

Benefits of Cascaded Control Loops

Cascaded control loops offer several advantages, particularly in terms of response speed and bandwidth [102]. Generally, the inner loops should have faster response times and higher bandwidth compared to the outer loops.

- An inner loop should be faster than an outer loop.
- Current response should be faster than velocity response.
- Velocity response should be faster than position response.

Faster here implies higher bandwidth, meaning the inner loops operate in a higher frequency zone compared to the outer loops.

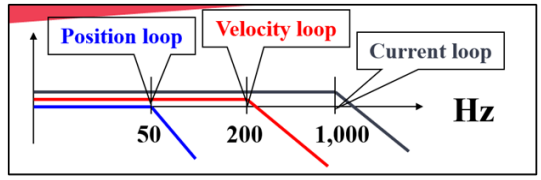

FIGURE 4.31: Control Loops Bandwidths

Typical Values of Bandwidth

The typical bandwidth values for these loops, from the high-frequency zone to the low-frequency zone, are as follows:

- **Current Loop**: 0.5 kHz to 1 kHz
- **Velocity Loop**: 50 Hz to 200 Hz
- **Position Loop**: 10 Hz to 50 Hz

Cascaded Control Loops Transfer Functions

Each closed loop in a cascaded control system functions as a low-pass filter within the overarching control architecture. A higher bandwidth of an inner loop typically enhances the stability of the subsequent outer loop.

The current control loop forms the foundational layer of our control system, ensuring the precision regulation of the motor's current and, consequently, its torque output. The current controller is typically configured as a Proportional-Integral (PI) controller. The corresponding control strategy is depicted in Figure 4.32.

The transfer function for the PI current controller is given by:

$$G_{current}(s) = K_{p\_current} + \frac{K_{i\_current}}{s} \tag{4.121}$$

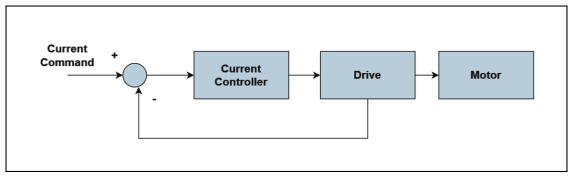

FIGURE 4.32: Current Loop Command.

where $K_{p\_current}$ and $K_{i\_current}$ denote the proportional and integral gains, respectively. The drive and motor dynamics are collectively modeled as a first-order linear system:

$$G_{motor}(s) = \frac{K_{motor}}{\tau_{motor}s + 1} \tag{4.122}$$

where K_{motor} is the motor gain, and τ_{motor} is the motor time constant. The overall closed-loop transfer function, describing the system's response to the current command input, is thus formulated as:

$$T_{current}(s) = \frac{G_{current}(s) \cdot G_{motor}(s)}{1 + G_{current}(s) \cdot G_{motor}(s)} \tag{4.123}$$

Following the current control loop, the velocity control loop regulates the motor's speed to match the desired velocity command. Figure 4.33 illustrates the schematic of the velocity control loop.

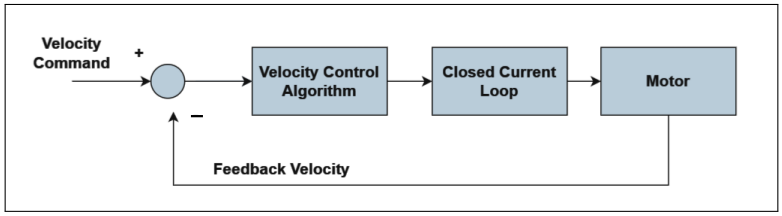

FIGURE 4.33: Velocity Command.

The velocity control algorithm, often a Proportional-Integral (PI) controller, computes the necessary current command to achieve the target velocity based on the feedback velocity. The transfer function for the velocity controller is typically expressed as:

$$G_{velocity}(s) = K_{p\_velocity} + \frac{K_{i\_velocity}}{s} \tag{4.124}$$

where $K_{p\_velocity}$ is the proportional gain and $K_{i\_velocity}$ is the integral gain for the velocity control.

The closed-loop transfer function, taking into account the dynamics of the current loop defined in Equation (4.123), can be represented as:

$$T_{velocity}(s) = \frac{G_{velocity}(s) \cdot T_{current}(s)}{1 + G_{velocity}(s) \cdot T_{current}(s)} \tag{4.125}$$

This equation describes the response of the velocity control loop to velocity command inputs, accounting for the motor's current response as an integral part of the control system.

The outermost layer of control is the position loop, which ensures that the motor's output shaft reaches and maintains the desired position. The position control loop and its elements are depicted in Figure 4.34.

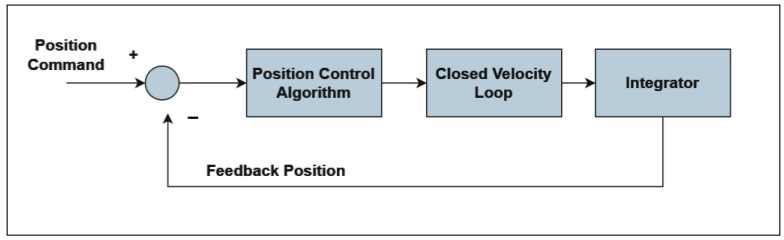

FIGURE 4.34: Position Command.

The position control algorithm typically employs a Proportional-Integral (PI) approach to generate the required velocity command based on the position error, which is the difference between the position command and the feedback position. The transfer function for the position controller is given by:

$$G_{position}(s) = K_{p\_position} + \frac{K_{i\_position}}{s} \tag{4.126}$$

where $K_{p\_position}$ and $K_{i\_position}$ are the proportional and integral gains, respectively.

An integrator is used to accumulate the velocity command over time, contributing to the position change. The closed-loop transfer function, incorporating the velocity loop from Equation (4.125), can be modeled as:

$$T_{position}(s) = \frac{G_{position}(s) \cdot s \cdot T_{velocity}(s)}{1 + G_{position}(s) \cdot s \cdot T_{velocity}(s)} \tag{4.127}$$

Equation (4.127) captures the dynamics of the position control loop, detailing how the system achieves precise positioning through the integration of velocity commands over time.

Single-loop Control with ACS

In a single-loop control architecture, the same feedback from the motor is utilized for both position and velocity control [97]. This approach simplifies the control scheme while still offering a level of performance that may be sufficient for certain applications.

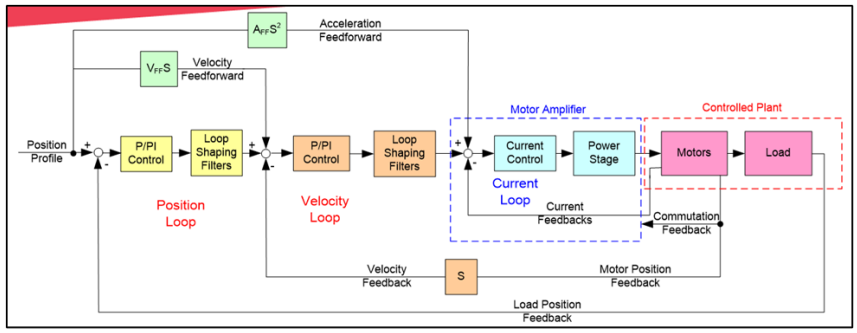

FIGURE 4.35: Full Control Scheme

4.4.3 Dual-loop Control

Dual Loop control is often employed to mitigate issues arising from mechanical slack between the motor and the load, often observed in systems like belt-driven mechanisms [103]. Unlike Single Loop control, which can experience diminished dynamic performance due to such slack and backlash, Dual Loop control remains largely unaffected and maintains performance [104].

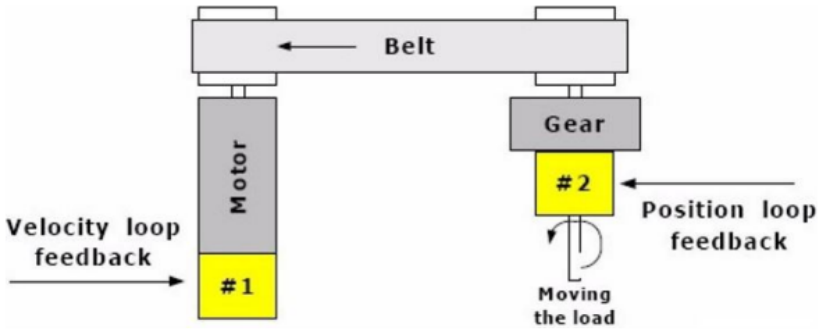

FIGURE 4.36: Dual Loop System

Dual loop Basics: In Dual Loop control, users have the flexibility to assign feedback either from multiple channels or from an analog input directly to the axis [105]. However, there is a condition that both the axis and the channels should be

connected to the same Servo Processor. Dual Loop control relies on at least two distinct sources of feedback:

- Load position feedback: Serves as the input for the Position Loop.
- Motor position feedback: Acts as the input for the Velocity Loop, as well as for the motor's commutation.

In our PPS, we employ dual-loop control for several reasons: to overcome backlash, achieve enhanced accuracy, and implement safety procedures.

4.38 A block diagram illustrating the different components involved in a Dual Loop control system is provided for better understanding.

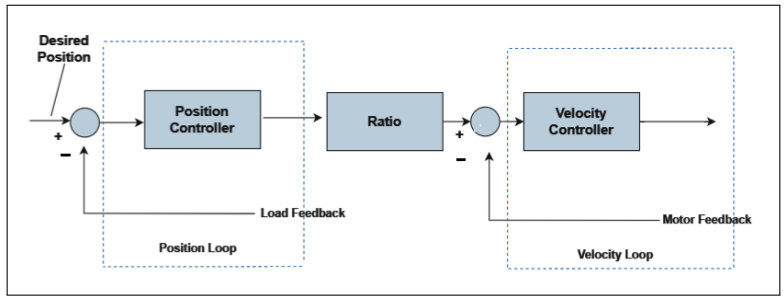

FIGURE 4.37: Controller in Dual Loop Block Diagram.

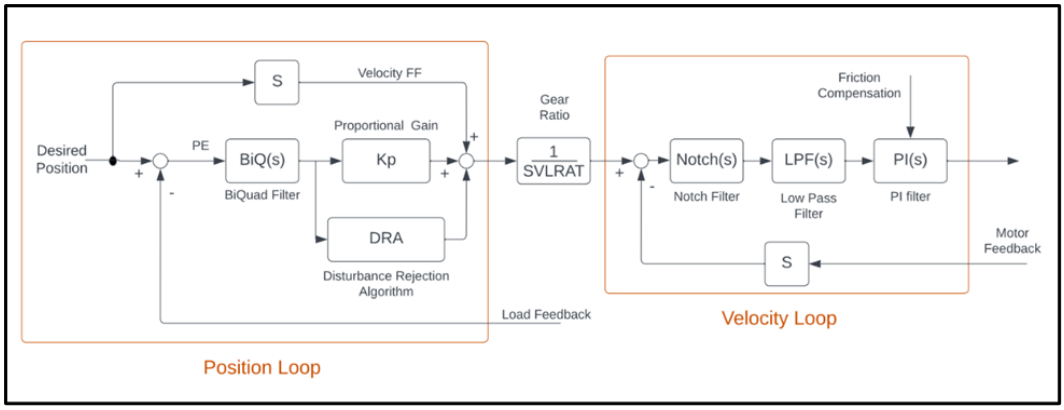

FIGURE 4.38: Controller in Dual Loop Block Diagram

In our PPS, we employ dual-loop control for several reasons: to overcome backlash, achieve enhanced accuracy, and implement safety procedures. The following Figure 4.38 A block diagram illustrating the different components involved in a Dual Loop control system is provided for better understanding.

Configuring Dual Loop Control Procedure

The setup procedure is primarily split into two key sections:

1. Single Loop Control Setup (incorporating both AXIS and LOAD configurations)
2. Dual Loop Control Setup

The setup procedure is categorized into two distinct phases:

1. Setting up Single Loop Control, encompassing both **AXIS** and **LOAD** configurations.
2. Configuration for Dual Loop Control.

The designation "**AXIS**" represents the drive axis that is physically attached to the motor phases, while "**LOAD**" denotes the feedback channel for the load. It's essential to understand that the motor feedback's axis might be distinct from the drive control's axis.

For our specific scenario:

- Motor phases are connected to axis 0.
- The motor encoder is similarly connected to axis 0.
- Conversely, the load encoder is connected to axis 1.

Axis and Load Setup

The Adjuster Wizard is used for single loop tuning

- Make sure `MFLAGS(AXIS)` bit 20 (#DUALLOOP) is set to OFF. If it's not, this can be corrected by entering the command **MFLAGS(AXIS).20=0** in the Communication Terminal.

- Open the Adjuster Wizard and select AXIS (according to the motor phases connection):
- Select the task Setup new System or Controller then click Next 4.39.
- Fill in the details in the Initialization window and click Next 4.40.
- In the Single Loop Setup (AXIS and LOAD) window: Axis Structure window setup AXIS as a single loop axis with the motor's feedback. The feedback topology should be Single, on motor.In the User Units, choose Count – Encoder Count.[1] 4.41.

- In the Components window: Motor – fill in the details according to the motor datasheet. Drive – fill in the details according to the drive datasheet. Feedback – fill in the details according to the motor encoder datasheet. Calculate parameters and apply changes 4.42.

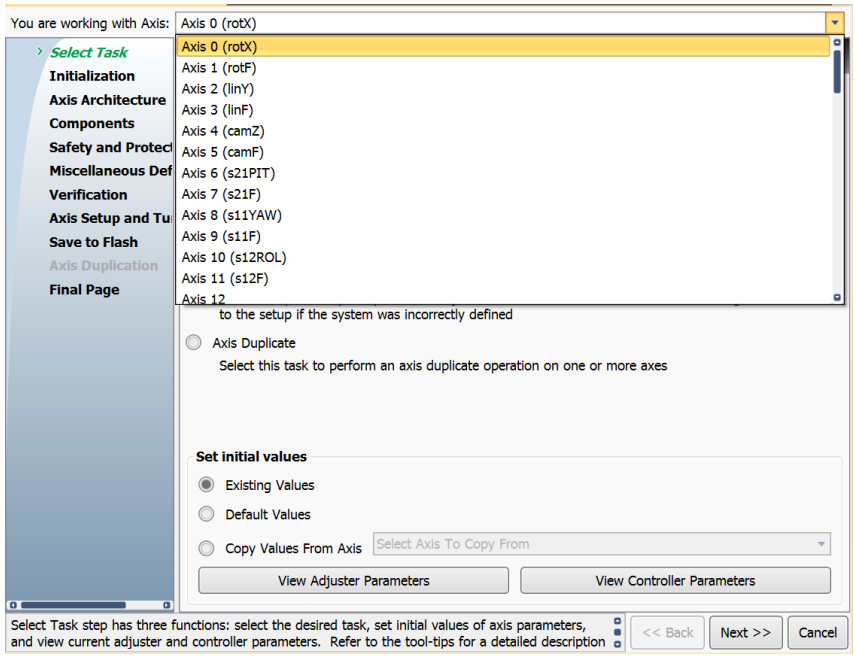

FIGURE 4.39: Select AXIS

Proceed with the process, including Axis Setup, tuning and save to flash [2].

Dual Loop Setup

Disable the axis and follow these steps:

1. Calculate **SLVRAT**, which describes the ratio between the load and motor readings. Set **SLVRAT(AXIS)** value in the Communication Terminal.
    - *Calculate SLVRAT using both theoretical and manual methods, to verify the correction.*
    - **Manual calculation:**

[1]The standard units of the encoder are counts. For the initial tuning, work with counts only. Changing the units will be explained in the next steps.

[2](Current Loop, Commutation, Position and Velocity Loops: Setting, Basic Tuning)

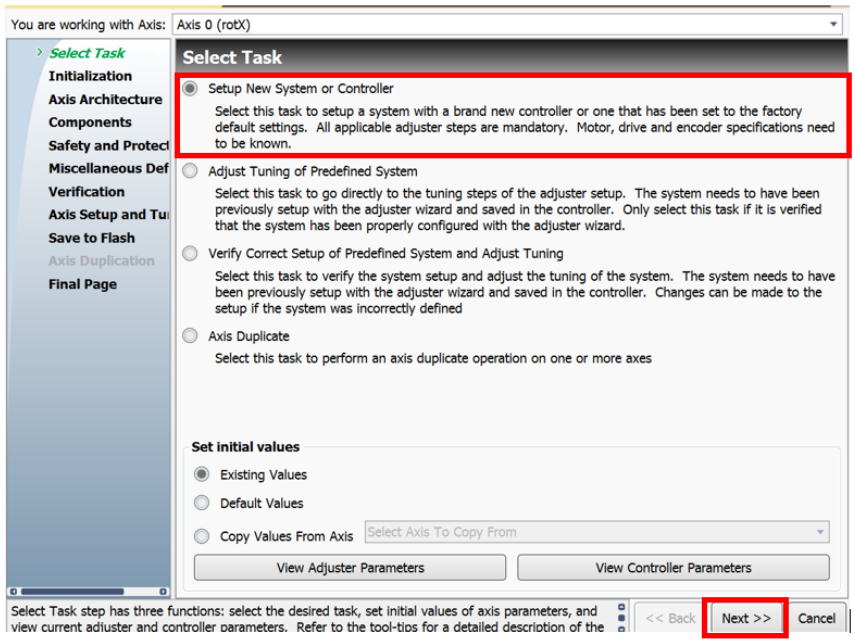

FIGURE 4.40: Setup New System or Controller

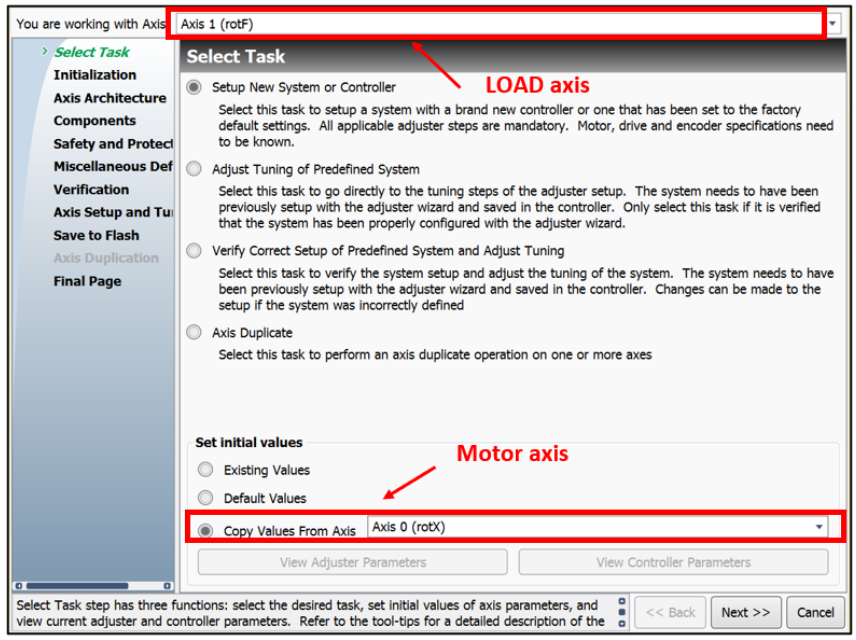

FIGURE 4.41: Setup the Load Axis

– Zero feedback position of both `AXIS` and `LOAD`:
`SET FPOS(AXIS)=0`, `SET FPOS(LOAD)=0`.

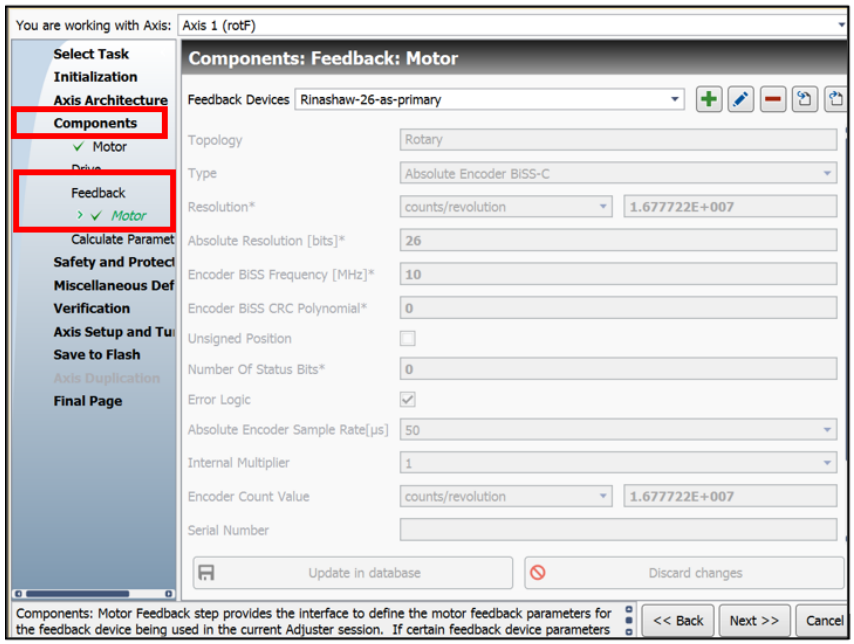

FIGURE 4.42: Setup the Load Feedback

– Move the system an arbitrary distance[1].

$$\text{SLVRAT(AXIS)} = \frac{\text{Load feedback}}{\text{Motor feedback}} = \frac{\text{FPOS(LOAD)}}{\text{FPOS(AXIS)}} \tag{4.128}$$

.

- **Theoretical calculation:**

$$\text{SLVRAT(AXIS)} = \frac{\text{Load feedback}}{\text{Motor feedback}} \times \text{Gear ratio} \tag{4.129}$$

  – Remember that feedbacks are assumed to be of the same polarity. If not, **SLVRAT** should be given a negative value [2].

- **Set EFAC(AXIS)** value according to the LOAD resolution. **EFAC(AXIS)** defines the factor converting encoder counts to the actual physical LOAD user units.
- Route the load feedback as the position feedback of the desired axis, by changing SLPROUT(AXIS) in the Communication Terminal.

[1] both feedbacks should be expressed in encoder counts

[2] Verify that feedbacks (load and motor) have the samempolarity. Positive increment leads to positive readings of the load. Otherwise, polarity of one of the encoders should be changed (Changing the hardware wiring is recommended).

```
SLPROUT(0)=101
```

If you need to read the motor feedback, it can be assigned to another axis, using **SLPROUT** as shown

- **Set MFLAGS(AXIS)** bit 20 **(#DUALLOOP)** ON by entering the command **MFLAGS(AXIS).20=1** in the Communication Terminal (this sets AXIS to Dual Control) [3].
- From this point, the Load Feedback is used for the Position Loop and the Motor Feedback is used for Commutation and the Velocity Loop.

Resolution Ratio Verification

The dual feedback configuration uses two feedback sources. It is important to properly set the resolution ratio of these feedbacks. The "Resolution Ratio Verification" feature of the scope allows the user set this ratio based on Frequency Response Measurement [4].

Basic Verification The section depicted in 4.43 contains the resolution ratio **(SLVRAT)** currently set in the controller and an automatically calculated value based on frequency response measurement. If both values are close enough – a green LED is displayed; otherwise, a red LED is displayed.

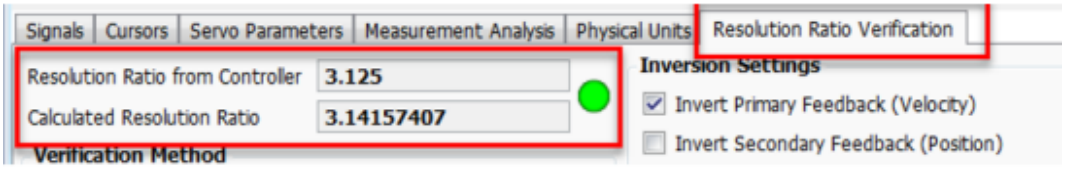

FIGURE 4.43: Resolution Ratio Verification Tab

Inversion Setting If the resolution ratio value in the controller and the calculated value have similar absolute values but opposite signs, the encoder polarity should be inverted. The user may invert either the motor or the load polarity. Either inversion will have a similar effect on the resolution ratio calculation. The user should select which encoder should be inverted based on the application requirement of positive or negative directions.

Automatic or Manual Calculation The range where the resolution ratio Is being calculated can be set automatically or manually.

[3] Switching to dual loop mode changes the servo architecture by moving BiQuad filter (enabled by MFLAGS(0).16=1) from velocity to position loop.

[3] To ensure the proper operation of the system both the absolute value and the polarity should be correct.

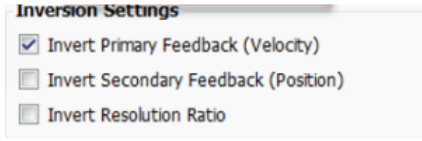

FIGURE 4.44: Resolution Ratio Inversion Setting

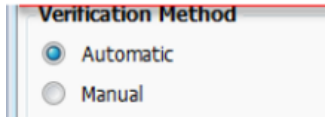

FIGURE 4.45: Choice of Verification Methods

4.4.4 Tuning of the Patient Positioning System

Radiosurgical interventions rely fundamentally on the meticulous and precise positioning of the patient, a responsibility entrusted to the Patient Positioning System (PPS). The fine-tuning of the PPS is imperative, serving as the cornerstone for achieving optimal alignment precision. This section is dedicated to delineating the systematic tuning methodologies employed to refine the PPS for its critical role in clinical applications.

Overview of Tuning Procedures

Tuning the PPS is a multifaceted process that encompasses calibration and meticulous adjustment, aiming to ensure exact patient placement. It involves a sequence of methodical steps designed to enhance the system's responsiveness, ensure pinpoint accuracy, and maintain structural stability [106]. The overriding objective of these procedures is to minimize positional discrepancies, thereby guaranteeing the safety and comfort of the patient throughout the radiosurgical process.

Achieving Precision through Advanced Control Mechanisms

Following the standard tuning process, the application of a dual-loop control algorithm represents a significant advancement in the quest for ultra-precise positioning. This sophisticated control strategy is pivotal in compensating for mechanical system variances, such as backlash and other hardware inconsistencies, that can compromise precision [107]. Through its implementation, the PPS achieves a heightened level of accuracy, essential for the delivery of successful radiosurgical treatment.

Enhancing PPS Tuning with ACS Motion Control Tools

The precision of the Patient Positioning System (PPS) is further augmented by utilizing cutting-edge tools provided by ACS Motion Control. Known for their advanced solutions in motion control technology, ACS Motion Control offers a suite of tools that are integral to fine-tuning the PPS for optimal performance.

ACS and FRF: A Synergistic Approach to System Tuning

The Frequency Response Function (FRF) analysis, a prominent feature in the ACS toolbox, is a potent instrument for assessing the dynamic characteristics of the PPS. Alongside the oscilloscope tool, the FRF analysis enables a comprehensive understanding of the system's response to various frequencies, which is pivotal in adjusting the control loops for precision movements [108].

Scope for Precision Tuning

Using the oscilloscope function from ACS Motion Control's suite, we gain real-time insights into the system's behavior [109]. This allows for immediate and precise calibration adjustments, ensuring that every motion is executed with the utmost accuracy [110]. The combined use of FRF analysis and the oscilloscope is central to the fine-tuning process, guaranteeing that the PPS operates at its highest potential to support the critical demands of radiosurgery.

4.4.5 Steps for tuning the Patient Positioning System

The optimization of the Patient Positioning System (PPS) is a methodical procedure that ensures precision in patient alignment, crucial for the efficacy of radiosurgical interventions. The tuning process involves configuring primary and virtual axes, calibrating loops, and verifying system responses to achieve optimal performance. The following subsections detail the systematic approach undertaken.

Axis Configuration

Configuration begins with the designation of primary and secondary (virtual) axes for the system. The primary motor for the rotary motion is labeled as Axis 0, with its virtual axis as Axis 1. This pattern extends to Axis 10 and 11, which delineate the upper limits of the system's axes. Each axis undergoes a rigorous tuning protocol to ensure accuracy and responsiveness.

Current Loop Tuning

The initial phase of tuning entails the current loop. Using the oscilloscope, the step response and overshoot are measured to determine the proportional (P) and

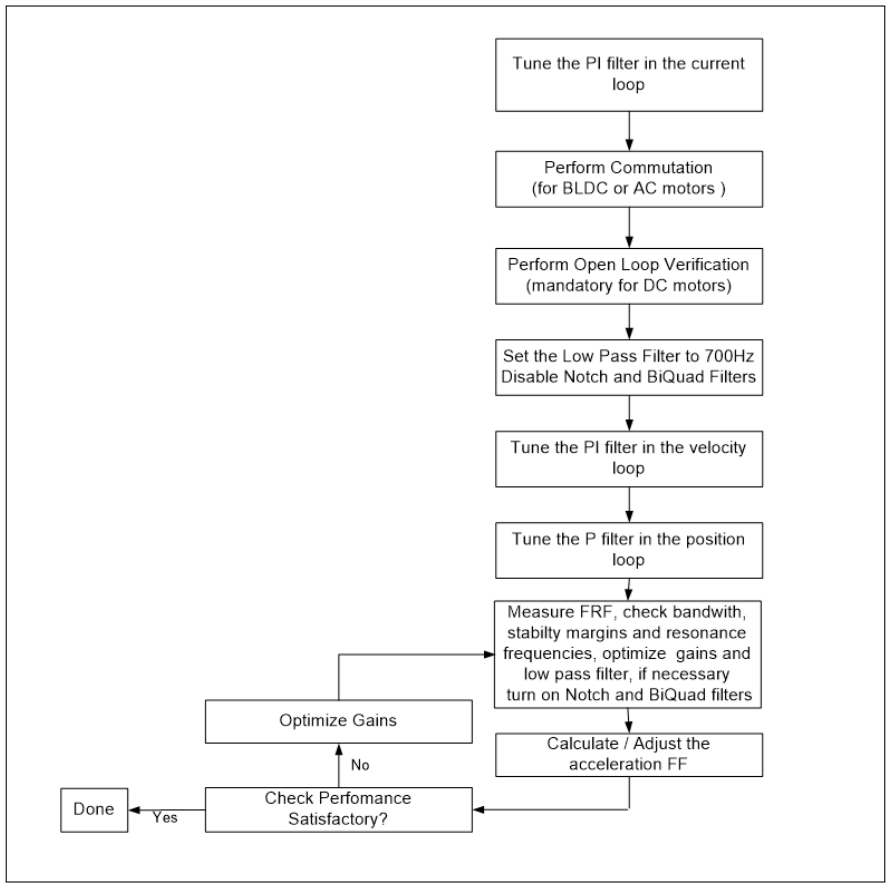

FIGURE 4.46: System Tuning Flow Chart

integral (I) gains [111]. This process is vital for setting the foundation for subsequent loop tuning. by following the flowchart 4.47 using SpiiPlus MMI 4.48 we can achieve a stable tuned system.

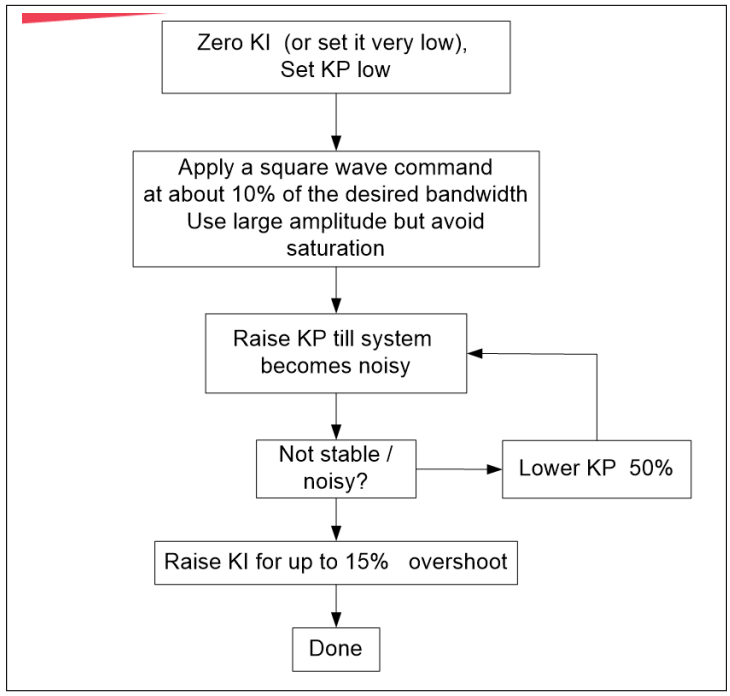

FIGURE 4.47: Current Loop Tuning Flow Chart

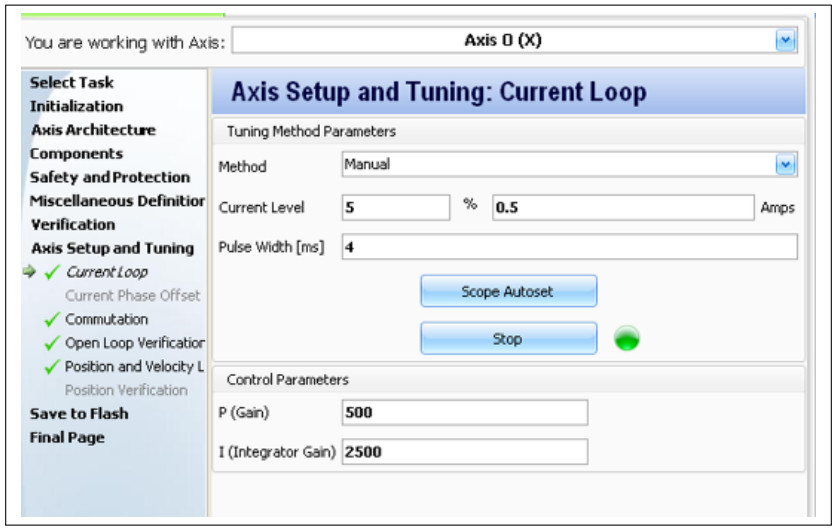

FIGURE 4.48: Current Loop Tuning using SPiiPlus MMI

Open Loop Verification

Following the current loop tuning, open loop verification is conducted using the Frequency Response Function (FRF). This step assesses the system's behavior without feedback control to ensure the open loop system operates as expected.

Velocity Loop Tuning

Subsequent to the current loop, the velocity loop tuning is performed. This step involves fine-tuning to match the desired velocity profile and to achieve the required parameters for system functionality.

Position Loop Tuning

Position loop tuning is the final step in the single-loop calibration process. Here, the emphasis is on achieving precise positional accuracy, a crucial aspect of the PPS where even minute deviations can have significant impacts.

Dual Loop Implementation

Upon satisfactory single-loop tuning, a dual-loop control strategy is implemented. This advanced control method utilizes both velocity and position feedback to correct errors and enhance system accuracy.

Tuning Dual Loops

The dual loops for velocity and position are then tuned. This advanced calibration ensures that the PPS can maintain accuracy under dynamic conditions, compensating for factors like backlash and system nonlinearities.

Each step in the tuning process builds upon the previous one, leading to a refined and highly accurate Patient Positioning System.

4.4.6 Comparison of Control Systems

The control architecture is a pivotal element of the Patient Positioning System (PPS), integral to its precision, safety, and efficacy. It employs advanced control strategies to accurately manage the system's 6-DOF (Degrees of Freedom) robotic movements. This section delves into the control architecture, highlighting its core principles and operational mechanisms. Our focus is on two types of control loops: Single-loop and Dual-loop. Single-loop control offers straightforward feedback mechanisms, while Dual-loop control introduces an additional control layer, enhancing system robustness and accuracy [96].

4.5 Safety Protocols and System Integration

Radiosurgery demands high precision, where the Patient Positioning System (PPS) is crucial for accurate radiation delivery and patient safety [112]. This section outlines the safety considerations, potential hazards, and technological advancements in PPS to enhance patient safety [113].

The PPS ensures sub-millimeter accuracy through advanced immobilization techniques, reproducible positioning, and integration with imaging systems for dynamic tumor tracking [114]. Key aspects include patient comfort and rigorous quality control to maintain system performance.

Safety in radiosurgery involves managing involuntary patient movements, stringent equipment maintenance, and calibration protocols to prevent dosimetric errors [115, 116]. Effective communication and synchronized efforts are essential to preempt safety oversights.

Accurate patient placement is vital to avoid radiation-induced damage to healthy tissues and ensure sufficient dosage to the target tumor [117, 118]. Systematic positioning verification before and during procedures enhances treatment efficacy and minimizes harm.

Technological advancements in PPS include real-time imaging for continuous target visualization and movement detection sensors for immediate corrective action [119]. Automatic shutdown features halt radiation delivery upon misalignment detection, acting as a safeguard [120].

Our PPS implementation prioritizes safety with emergency stops, fault detection, limit sensors, and rigorous initialization procedures [121]. Operator training ensures competent system handling and prompt issue rectification. A backup power system preserves patient safety during external power failures, underscoring system resilience [122].

Fault Classification

Faults within the PPS can be broadly classified into two categories Figure 4.49:

1. Axis Faults: Pertaining to motor motion. These faults primarily arise from issues related to the mechanical components responsible for movement.
2. System Faults: Directly associated with the controller program. These faults can originate from software glitches, erroneous commands, or disruptions in the control processes.

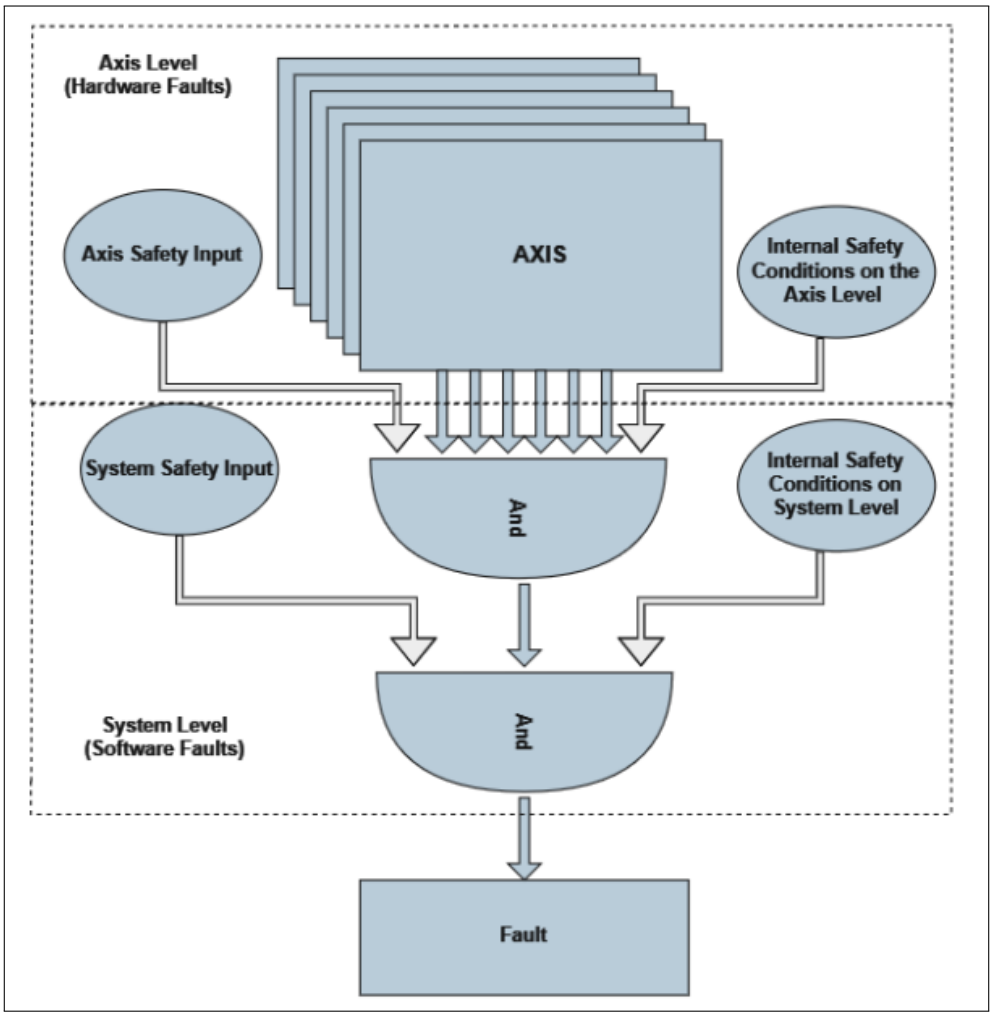

FIGURE 4.49: ACS Fault Handling.

4.5.1 PPS Internal Safety Conditions

In the Patient Positioning System (PPS), the "internal safety condition" refers to the system's built-in checks and measures that monitor operational states. If any irregularities or deviations are detected, the PPS automatically takes preventive actions to ensure safe operation, such as halting movements or triggering alerts as shown in Figure 4.50. This ensures the machinery operates without causing unexpected hazards or errors.

We have detailed this intricate process through various safety conditions and have visually represented their workings in a flowchart, as discussed below:

1. Primary/Secondary Encoder Slipping Check: Both the primary and secondary encoders undergo rigorous checks for position and velocity slipping (Figure

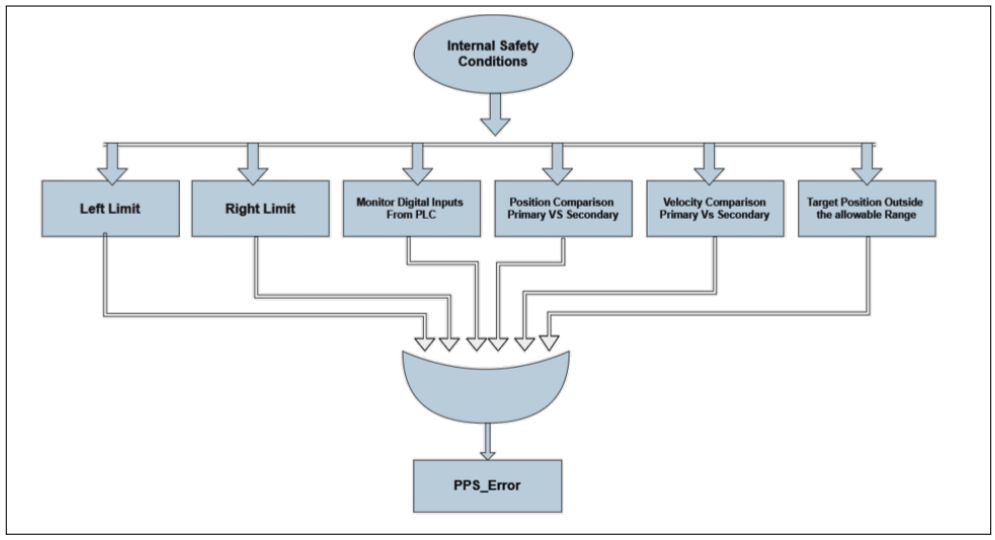

FIGURE 4.50: Internal safety Conditions Diagram.

4.55). Any discrepancies observed between expected and actual readings flag an immediate safety alert [123].

2. Target Position Monitoring: It is vital that the machine's target position stays within an allowable range. For a sequential understanding of how this monitoring occurs, please consult the flowchart in Figure 4.52.

3. Digital Inputs from PLC Monitoring: Digital inputs from the PLC (Programmable Logic Controller) are continuously monitored. The flowchart in Figure 4.53 further elucidates this monitoring process.

4. Left/Right Limit Check: This safety feature ensures that the machine operates within the defined left and right boundaries (Figure 4.54).

The importance of safety and fault handling in the Patient Positioning System (PPS) for radiotherapy cannot be overstated. The incorporation of emergency stops, continuous monitoring for fault detection, and limit sensors ensures the system can promptly respond to any anomalies, thereby safeguarding patient and operator well-being.

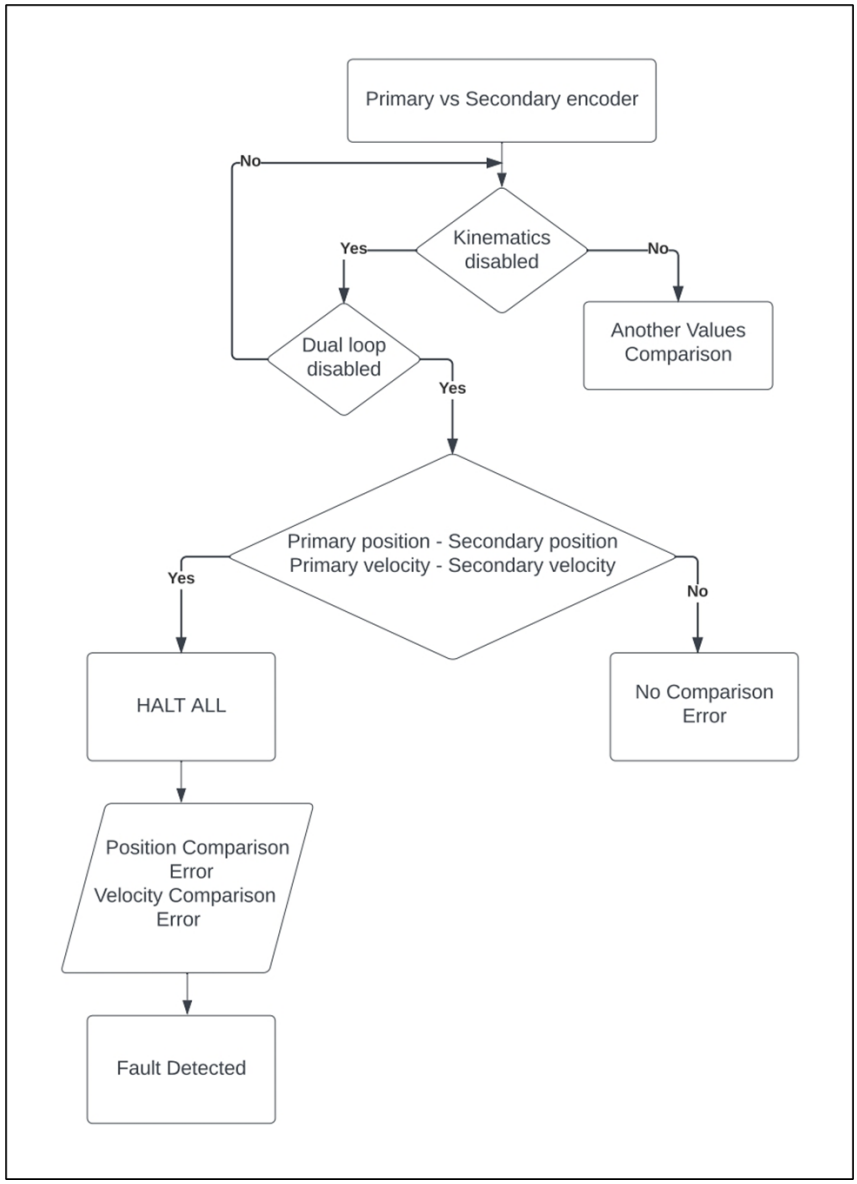

FIGURE 4.51: Slipping check Flowchart.

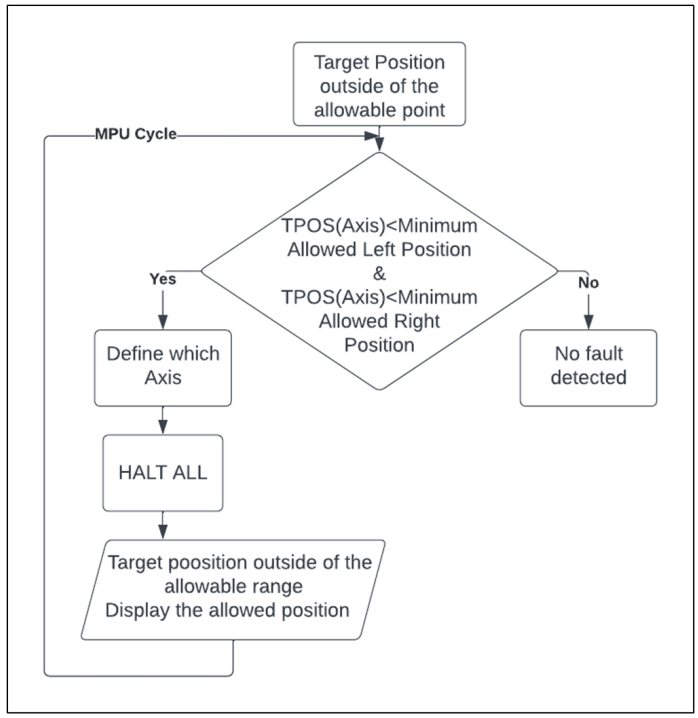

FIGURE 4.52: Target Position check Flowchart.

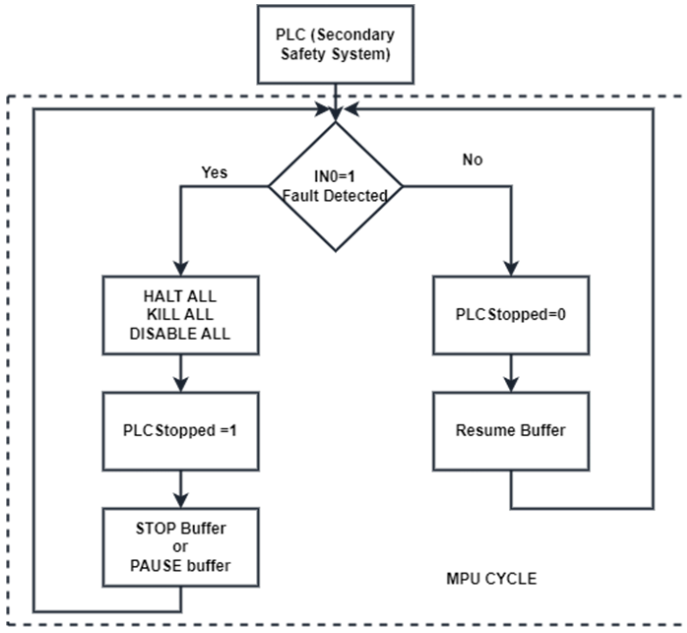

FIGURE 4.53: Monitoring Input from PLC.

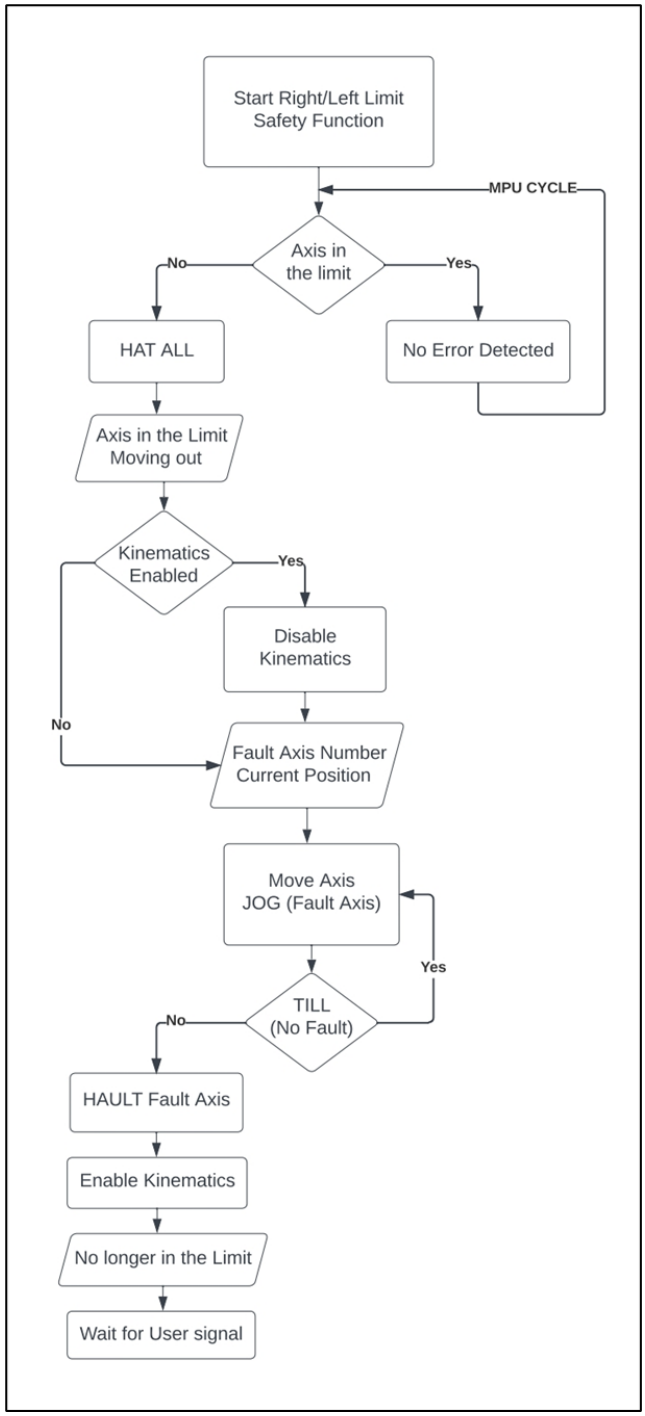

FIGURE 4.54: Left/Right Limit checking flowchart

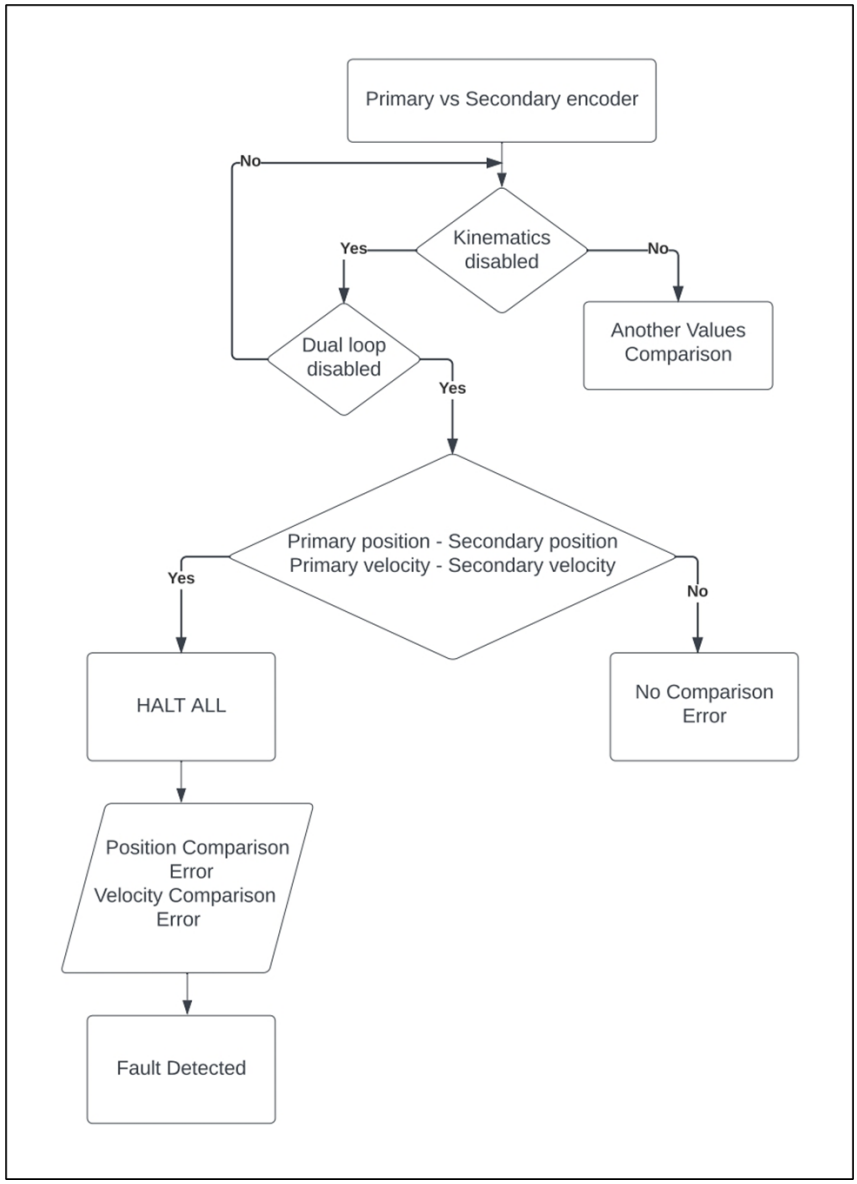

FIGURE 4.55: Slipping check Flowchart

4.6 Testing and Measurement

This section outlines the testing and measurement procedures used to validate the precision and reliability of the Patient Positioning System (PPS) in stereotactic radiosurgery. It includes the description of the Optical Tracking System (OTS), the integration of Motive software, and the detailed specifications of the equipment used. The Optical Tracking System (OTS) is a ceiling and wall mounted camera vision system that accurately tracks the position of the optical markers mounted on the Stereotactic Immobilization System (SIS) [124]. The OTS incorporates 3 optical cameras (Manufacturer: OptiTrack | model: Primex 41) and 6 spherical optical markers (Manufacturer: OptiTrack | Model: MKR127M4-10).

TABLE 4.2: Primex 41 Camera Technical Specifications

Specification	Value
Resolution	4.1 MP
3D Accuracy	±0.10mm
Native Frame Rate	180 FPS

FIGURE 4.56: OptiTrack Camera

4.6.1 OptiTrack PrimeX 41 Camera

The OptiTrack PrimeX 41 camera represents a breakthrough in motion capture technology, offering high-resolution, high-speed 3D tracking capabilities. With a resolution of 4.1 megapixels, it delivers precise and accurate tracking data with an impressive 3D accuracy of ±0.10mm. Operating at a native frame rate of 180 frames per second, the PrimeX 41 captures rapid movements seamlessly, making it an indispensable tool for applications requiring meticulous motion analysis [125]. Its advanced imaging and tracking algorithms ensure data fidelity, enabling users to conduct sophisticated biomechanical research and industrial motion analysis with confidence [126].

FIGURE 4.57: OptiTrack Cameras

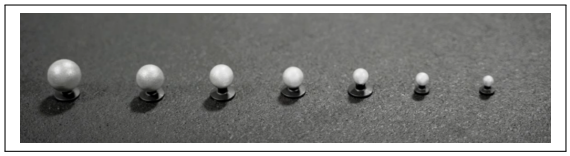

FIGURE 4.58: OptiTrack Cameras Markers

4.6.2 Integration of Motive Software in Patient Positioning Systems

The precision of radiosurgical interventions is greatly enhanced by the incorporation of advanced motion capture technologies. In our Patient Positioning System (PPS), we leverage the capabilities of Motive software, which interfaces seamlessly with OptiTrack camera systems. This software is pivotal in monitoring and capturing the intricate movements of retroreflective markers, which are strategically placed on the patient to provide real-time spatial data [127].

Motive Software's Functional Attributes

Motive software is renowned for its streamlined setup and user-friendly interface, enabling rapid deployment within clinical settings [128]. Its support for larger capture volumes is particularly beneficial in creating an extensive tracking environment, essential for the diverse range of movements exhibited by patients during radiosurgery procedures [129].

- **Accuracy:** The software's precision in tracking ensures that the PPS can achieve and maintain the sub-millimeter alignment necessary for accurate radiation targeting [130].
- **Real-time Tracking:** Motive's real-time data processing capabilities allow for instantaneous adjustments in patient positioning, thereby mitigating the risks of radiation misdelivery [131].
- **Versatility:** The utility of Motive extends beyond patient tracking, contributing to the refinement of robotic movements, enhancing ergonomic assessments, and aiding in the development of patient-specific treatment protocols.

TABLE 4.3: Technical Specifications for MKR127M4-10 Markers

Specification	Detail
Diameter	12.7mm
Thread	M4x0.7mm | 4.5mm depth
Reflective Tape	3M 7610

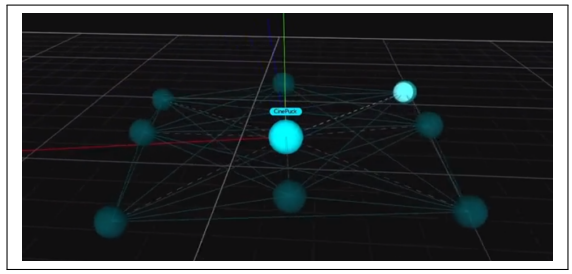

FIGURE 4.59: OptiTrack Cameras Marker

- **Data Integrity:** Clean and reliable data output from Motive ensures that the clinicians have access to high-fidelity information for decision-making during radiosurgical procedures.

4.6.3 Data Collection and Analysis

Data collection is a critical component of validating the accuracy and reliability of the PPS. The process involves several key steps:

1. **Setup:** The OptiTrack cameras are calibrated and positioned to ensure optimal coverage of the patient area. The retroreflective markers are affixed to specific points on the patient's immobilization system.

2. **Data Acquisition:** During the procedure, the cameras continuously capture the positions of the markers. Motive software processes this data in real-time, providing instantaneous feedback on the patient's position.

3. **Data Recording:** All positional data is recorded for subsequent analysis. This includes the spatial coordinates of each marker and any deviations from the desired alignment.

4. **Analysis:** The recorded data is analyzed to evaluate the system's performance. Key metrics include positional accuracy, system response time, and the consistency of marker tracking throughout the procedure.

5. **Validation:** The analysis results are compared against predefined benchmarks to validate the PPS's performance. Any discrepancies are investigated, and the system is fine-tuned accordingly.

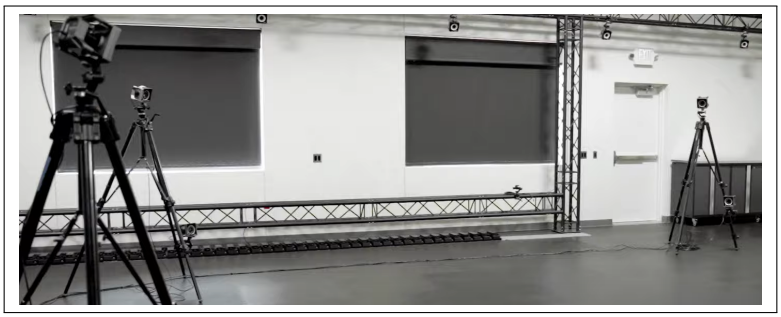

FIGURE 4.60: Setting OptiTrack Cameras

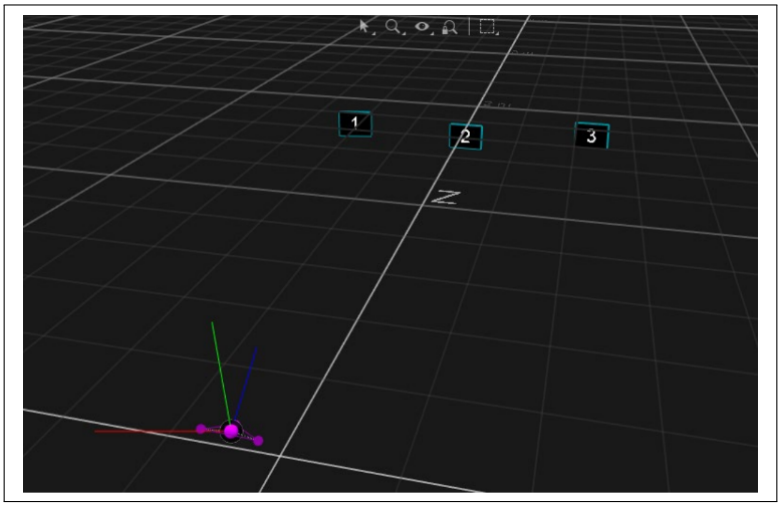

FIGURE 4.61: Motive OptiTrack Cameras View

The integration of advanced motion capture technologies such as the OptiTrack PrimeX 41 cameras and Motive software in the Patient Positioning System (PPS) significantly enhances the precision and reliability of radiosurgical interventions. These technologies ensure sub-millimeter accuracy, real-time tracking, and robust data integrity, thereby improving patient outcomes and safety in radiosurgery. The comprehensive testing and measurement procedures detailed in this section underscore the critical role of these advanced systems in modern medical procedures.

Chapter 5

Results and Validation

5.1 Range of Motion

The emphasis of this section is on the Range of Motion (ROM) inherent to this system. ROM is paramount in understanding the system's versatility, especially in accommodating diverse patient profiles. It's essential for ensuring patient comfort and the precision required during procedures, especially for minute adjustments like tumor misalignment.

5.2 Range of Motion in the Linkage System of the Patient Positioning System

The Patient Positioning System (PPS) incorporates the Linkage System, a central mechanism responsible for patient positioning in the two-dimensional plane. As discussed in detail in earlier chapters, this system comprises four linkage arms, three of which are active and one passive, designed meticulously for precision and adaptability.

Given the redundant encoding of the system's motors and its design principles, previously elaborated upon in the kinematic analyses section, the Linkage System boasts a robust and expansive ROM. This ROM not only underlines the system's adaptability but also its commitment to ensuring precise and safe medical interventions. For a deeper dive into the Linkage System's workings and principles, readers are referred back to the comprehensive kinematics discussion in previous chapters.

5.2.1 Analysis of Robotic Linkage Subsystem Behavior

The robotic linkage subsystem plays a paramount role in our setup's spatial operations, facilitating movements along the X and Y axes, and pivotal rotations about the Z-axis (Roll). It's essential to analyze its behavior, especially concerning its performance at extremities in the X and Y coordinates [1].

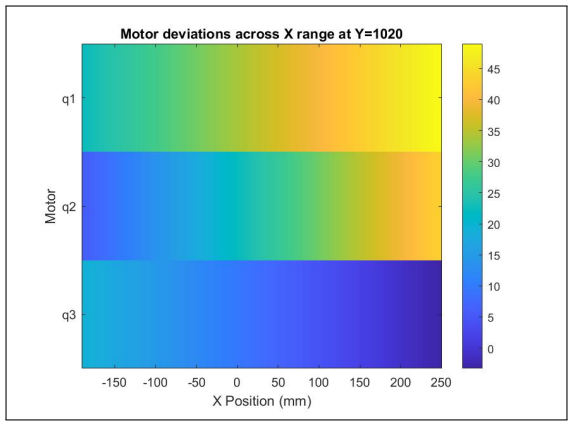

FIGURE 5.1: Motor deviations across X range at $Y = 1020$

Figure 5.1 presents the variations in joint angles—q_1, q_2, and q_3—as the linkage traverses the X axis while being at its minimum Y value (1020). The colormap accentuates the subtleties of the linkage's behavior at this configuration, showing how each motor's angular position is adjusted within its specific range of motion (ROM).

On the other hand, Figure 5.2 displays motor adjustments when the linkage moves along the X-axis with Y at its maximum value (1250). Here, the colormap provides insights into the nuanced motor operations, emphasizing the linkage's precision even at operational extremes.

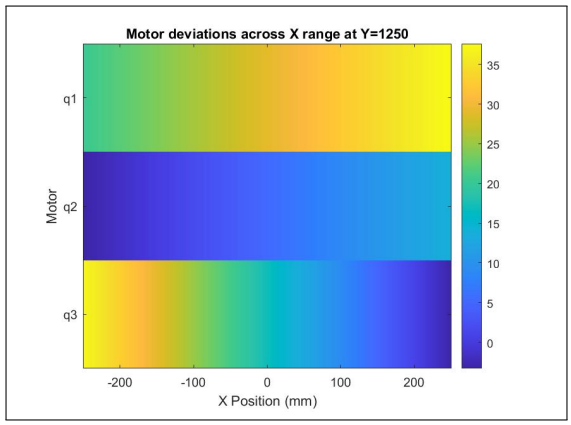

FIGURE 5.2: Motor deviations across X range at $Y = 1250$

Visualization of Parameters against Position and Orientation

The 3D scatter plots provide a comprehensive visualization of the relationship between the positional data (X, Y), the orientation (ROLL), and the parameters q_1, q_2, and q_3.

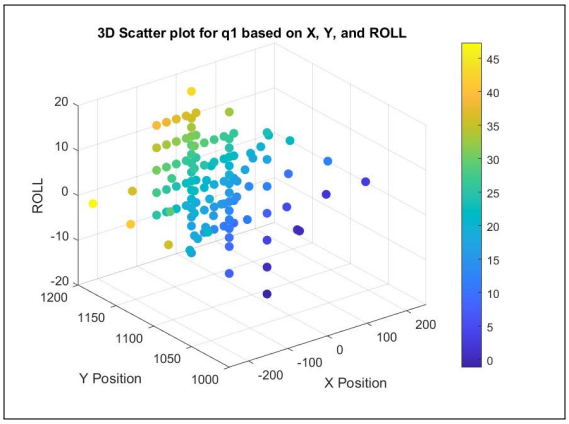

FIGURE 5.3: 3D scatter plot illustrating the variation of q_1 against X, Y positions and ROLL orientation. The color intensity indicates the magnitude of q_1 at a particular position and orientation.

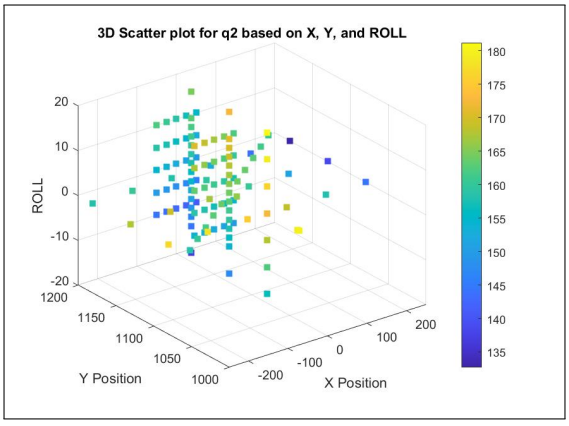

FIGURE 5.4: 3D scatter plot showing the variation of q_2 against X, Y positions and ROLL orientation. The color intensity indicates the magnitude of q_2 at a particular position and orientation.

[1]Square markers differentiate this from the q_1 plot, and the color gradient gives an understanding of q_2's behavior.

[2]Triangle markers provide a unique identification. The color variance highlights the patterns in q_3.

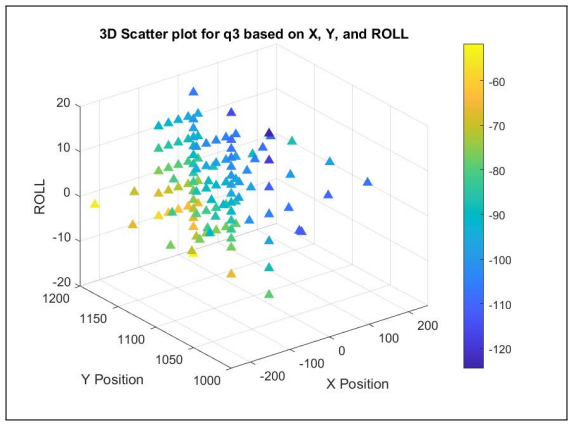

FIGURE 5.5: 3D scatter plot for q_3 variation against X, Y positions and ROLL orientation. The color intensity indicates the magnitude of q_2 at a particular position and orientation.

From the these figures 5.3, 5.4 and 5.5, it's clear to see the effects on q_1, q_2, and q_3 on the roll aspect.

[3]In the ROM section, the home position for each joint is considered as 0 to calculate or present the extent of movement in each joint. However, in this section, the actual data for each motor, q_1, q_2, and q_3, is provided, which is 0, 180, -112 in the home position respectively.

5.3 Range of Motion in Linear Rail Subsystem

Linear Rail Subsystem facilitates motion across the z-axis while also governing the Yaw rotation around the y-axis. This subsystem adeptly maneuvers the main plate vis-à-vis the bottom base plate via its rail system. Furthermore, a rotary table is employed to achieve the Yaw rotation of the Linkage System relative to the main plate. Such precise control in two distinct axes allows for the seamless and convenient positioning of the patient within the operational zone, as per our design references.

Subsystem Component	Motion Type[1]	Axis or Rotation
Linear Motor	Linear Motion ±1000 cm	z-axis
Rotary Motor	Rotational Motion ±35 degrees	Yaw (around y-axis)

TABLE 5.1: Movement Capabilities of the Linear-Rail

5.3.1 Analysis the Linear-Rail subsystem Behavior

The subsequent figure illustrates the alterations in the linkage motor upon applying Yaw rotation on the Y-axis, demonstrating the collaborative operation of the rotary base and linkage to achieve the desired position.

Visualization of Parameters against Position and Orientation

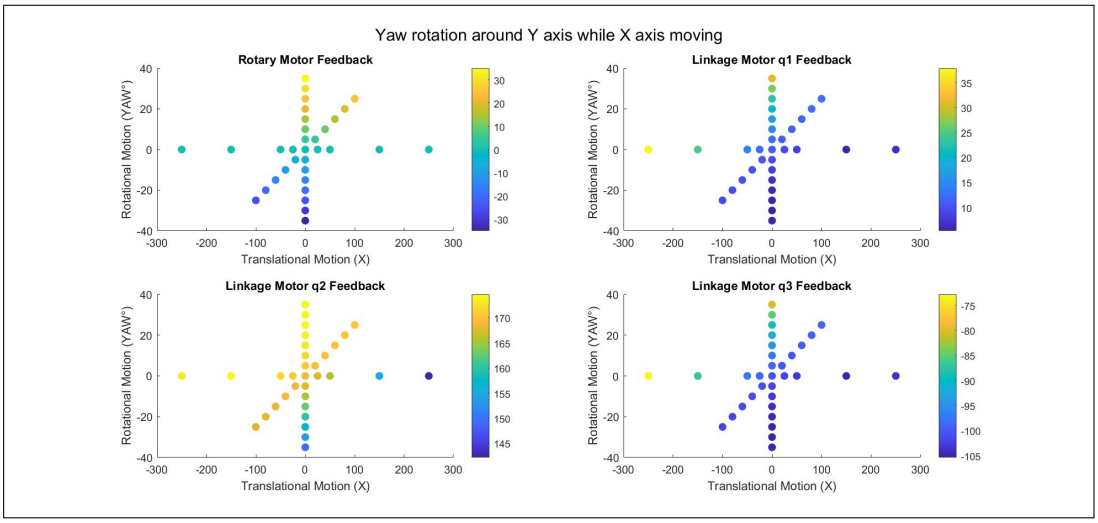

FIGURE 5.6: Spatial Distribution of Rotary and Linkage Motor Feedbacks (q1, q2, q3) as Functions of X-Position and Yaw Rotation.

[1]The Range of Motion (ROM) discussed in this section is evaluated with the kinematics activated

5.4 Table Tilt Range of Motion

The Tabletop facilitates movement along the Y-axis and introduces Pitch, a rotation about the X-axis. The range of motion for this rotation is $\pm 3^{\circ}$ on the X-axis, which directly influences the translation on the Y-axis.

The presented figure 5.7 provides a three-dimensional perspective of how the Y translation is influenced by two primary factors: the table's tilt (or angle) around the X-axis and the movement of the linkage motor. Specifically:

- The Y-axis motion is intricately connected with the tilt or pitching of the table. At a given Y position, introducing a tilt around the X-axis instigates a noticeable shift in the Y translation.
- To maintain the desired Y position while incorporating a tilt, the linkage motor's role becomes pivotal. The motor adjusts, often descending slightly, to counteract the effect of the tilt, ensuring the Y remains consistent despite the introduced table angle.

This intricate interplay between the table tilt and the linkage motor adjustment underlines the complexity of achieving precise translational movements in multi-faceted systems.

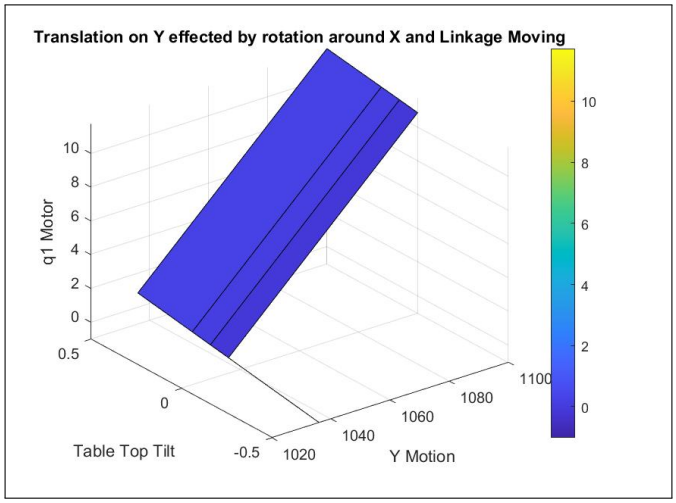

FIGURE 5.7: Translation on Y effected by rotation around X and Linkage Moving

5.5 Analysis of DualLoop vs SingleLoop Systems

This analysis aims to evaluate and compare the performance of two systems: DualLoop and SingleLoop, in terms of their precision in achieving target positions. The

data consists of target coordinates (X, Y, Z) and the corresponding errors from both systems in achieving those targets.

5.5.1 Statistical Analysis

In our exploration of the error behavior under two distinct control paradigms, Single Loop and Dual Loop, a myriad of descriptive statistics were gleaned to shed light on the efficiency and precision of each method. These statistics offer insights into the central tendencies and spread of the errors observed in the X, Y, and Z axes for both methods.

TABLE 5.2: Error Analysis for Single and Dual Loop Control Systems

Control System	Axis	Statistical Measures			
		Mean	Standard Deviation	Min	Max
Single Loop	X-axis	0.4752	0.5962	0.0	2.8304
	Y-axis	0.0444	0.0816	-0.0321	0.4307
	Z-axis	1.4713	2.4429	0.0	10.7805
Dual Loop	X-axis	0.0866	0.0582	0.0	0.3356
	Y-axis	0.0333	0.0430	-0.0213	0.2243
	Z-axis	0.0468	0.0339	0.0	0.2051

5.5.2 Visualization Analysis

Given the multi-faceted nature of our observations, we have employed a suite of visualization tools to present our findings. Each visualization caters to a specific aspect of our results, offering both a macro and micro perspective of the system's behavior.

Having evaluated the range of motion capabilities of the patient positioning system, the subsequent phase of our analysis ventured into assessing the efficacy of two control approaches: Single Loop Control and Dual Loop Control. By subjecting the positioning system to a series of motion sequences, we were able to juxtapose the errors that surfaced in the X, Y, and Z dimensions for both methodologies.

Visualizations were generated to provide a more intuitive understanding of the error distributions:

- **Boxplots**: These visualized the spread, median, and presence of outliers for the error values of both systems. The DualLoop system demonstrated tighter error distributions across all axes, suggesting better precision 5.8.

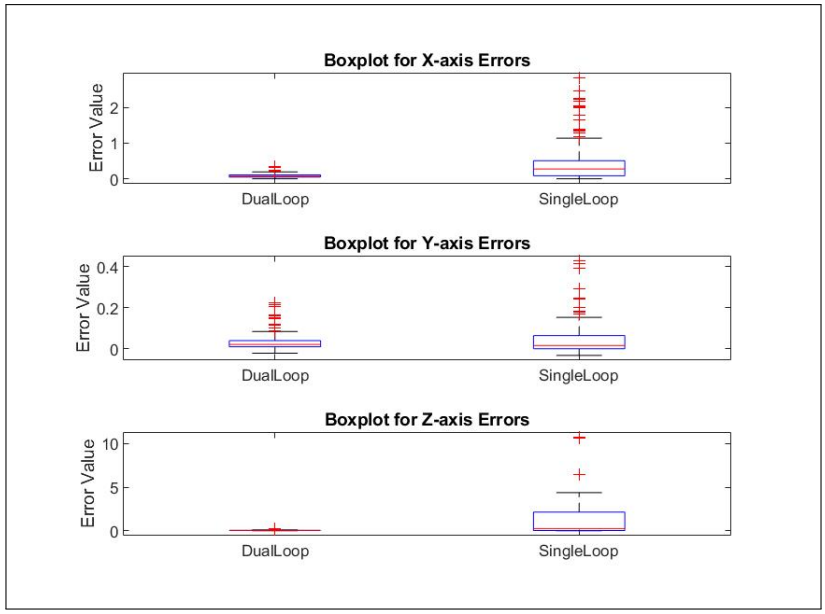

FIGURE 5.8: Box Plot.

- **Histograms**: Provided a frequency distribution of the error values, which reinforced the findings from the boxplots 5.9.
- **Error Trend Over Time**: By considering the rows as sequential measurements, we plotted the error trends to visualize any patterns or fluctuations over time 5.10.
- **Cumulative Distribution Function (CDF)**: This will depict the probability that the error will assume a value less than or equal to a particular magnitude 5.11.
- **Error Evaluation Bar Graph**: Compare the mean or median errors of the X, Y, and Z dimensions for both control methods 5.12.
- **Heatmap**: Visualize the error magnitude in a matrix format, potentially categorizing errors into bins (e.g., low, medium, high) for each sequence step 5.13.

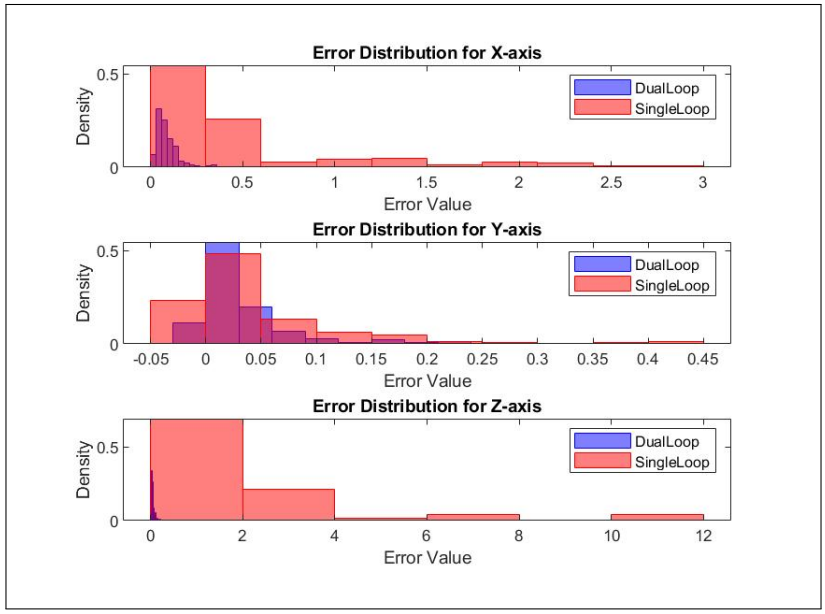

FIGURE 5.9: Histogram

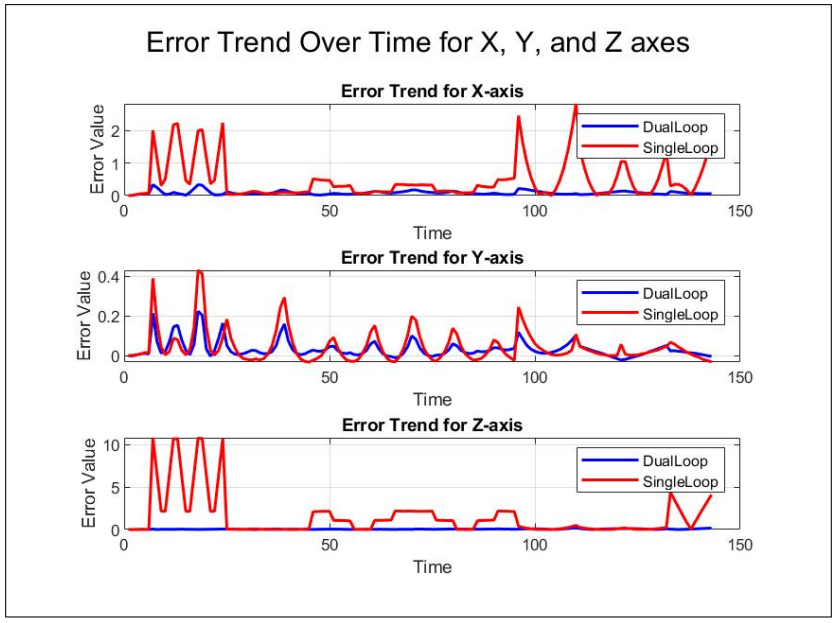

FIGURE 5.10: Error Over Time

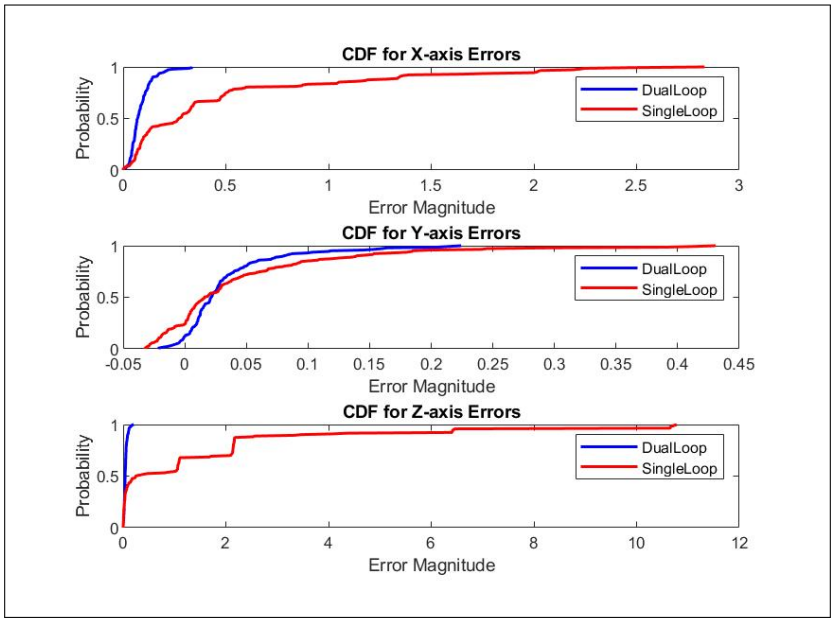

FIGURE 5.11: CDF

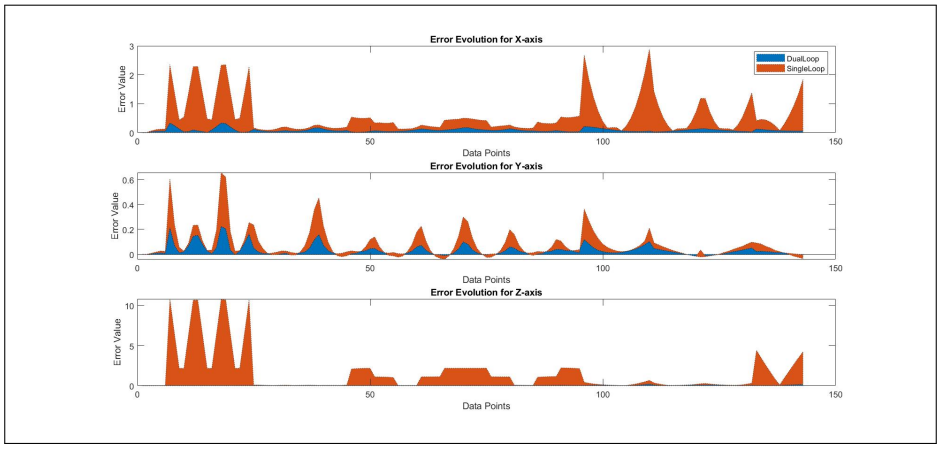

FIGURE 5.12: Error Evaluation

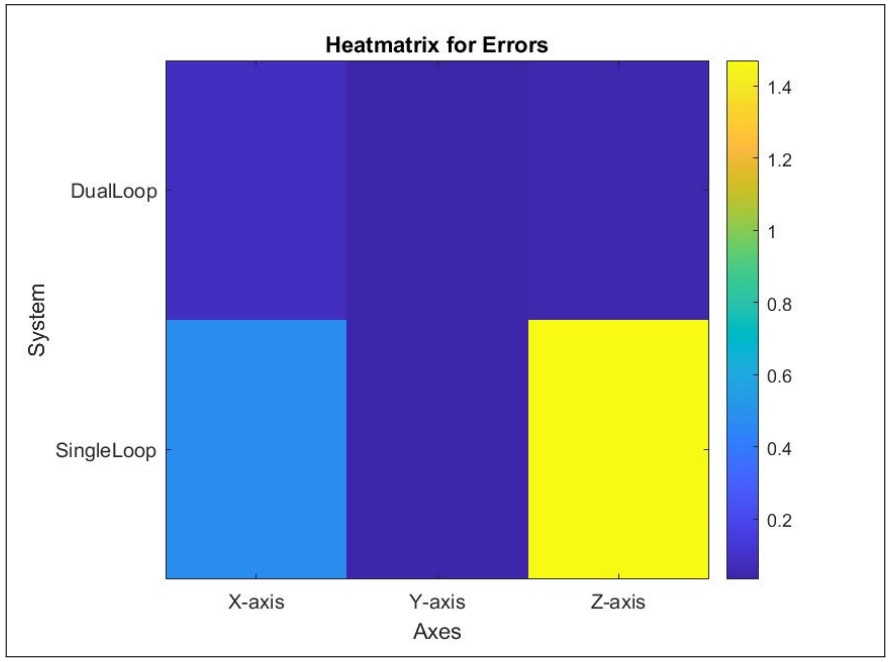

FIGURE 5.13: Heat Matrix

5.5.3 Line Fit (Main Visualization)

This method mainly used to Plot the observed errors against the expected values, fitting a regression line to depict the trend 5.14.

By subjecting the positioning system to a series of motion sequences, we were able to juxtapose the errors that surfaced in the X, Y, and Z dimensions for both methodologies.

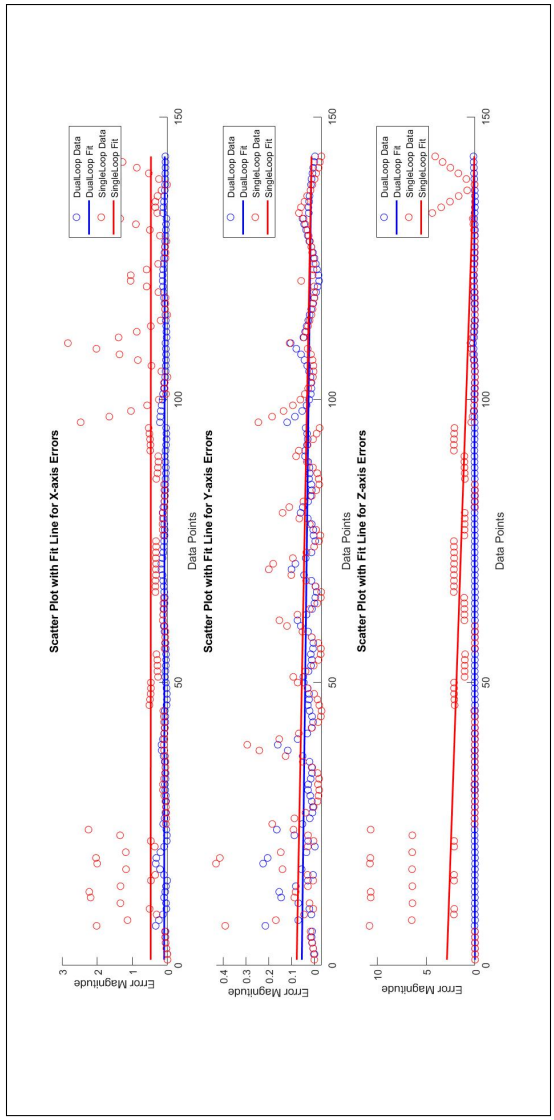

FIGURE 5.14: Scatter plot with fit line of Axes errors

Y-axis Motion: 1

Context: The system was observed primarily moving along the Y-axis, with all other parameters (X, Z, Pitch, Yaw, Roll) being constant.

Analysis:

- The Y-axis movement was substantial, indicating a prominent upward shift.
- The DualLoop mechanism's low errors during this phase suggest its ability to effectively manage pure Y-axis motion without interference from other stationary parameters.
- Pronounced errors in the SingleLoop approach highlight potential challenges in maintaining accuracy during Y-axis movements.

X-axis Motion: 2

Context: The system's movement was centered on the X-axis, spanning a notable range, while other parameters remained constant.

Analysis:

- The DualLoop mechanism showcased its capability in managing significant X-axis movements.
- On the other hand, the SingleLoop method displayed potential issues in maintaining stability during extensive linear displacements.

Adjusted X-axis Motion with Y Variations: 3

Context: With a slight decrease in the Y-axis position, the system continued its movement on the X-axis.

Analysis:

- A subtle shift in the Y-axis position might modify the system's dynamics.
- The DualLoop method's consistent low errors under this condition signify its resilience and adaptability.
- Variability in the SingleLoop method's errors denotes challenges in managing simultaneous Y and X-axis motion adjustments.

Roll Rotation: 4

Context: Linear movement on the X-axis was neutralized, and the system began its rotation around the Z-axis.

Analysis:

- The system performed a balanced rotation around the Roll axis.

- Minimal and stable errors in the DualLoop method emphasize its efficiency during such rotations.
- For the SingleLoop method, any fluctuations during these rotations could suggest issues in rotation management.

Yaw Rotation: 5

Context: Initiating a rotation around the Yaw axis, the system kept all linear movements (X, Y, Z) stationary.

Analysis:

- The DualLoop method's minimal errors underscore its efficacy in handling Yaw rotations.
- The SingleLoop approach, if experiencing error spikes, may find it challenging to manage Yaw rotations, more so if combined with other movements.

Combined X Motion and Yaw Rotation: 6

Context: Simultaneously, the system maintained its movement on the X-axis and persisted with Yaw rotation.

Analysis:

- This phase showcased the system's ability to manage both linear and rotational motions.
- The DualLoop method, with its sustained low errors, proves its proficiency in handling these combined motions.
- However, the SingleLoop method may struggle with managing the X-axis motion intertwined with Yaw rotations if it exhibits variable errors.

Pure Yaw Rotation with Neutral X-axis: 7

Context: Neutralizing the X-axis motion, the system continued its Yaw rotation.

Analysis:

- During this phase, the focus was solely on rotation.
- With consistent error rates, the DualLoop method displays its adeptness at managing pure Yaw rotations.
- For the SingleLoop method, any significant errors would reveal challenges in overseeing pure rotations.

Return to Initial Position with Adjustments: 8

Context: The system commenced its return to the starting positions, integrating slight adjustments on the Y-axis.

Analysis:

- This phase majorly involved stabilization.
- The DualLoop method's errors, if minimal, would indicate its capability to revert to the original position efficiently.
- Fluctuations in the SingleLoop method might reveal issues in final position stabilization.

Final Sequences: 9

Context: This section pertains to the end sequences of the motion, likely integrating various combined motions and rotations.

Analysis:

- Observations from these sequences offer insights into the system's behavior as it concludes its motions.
- Ideally, the DualLoop method would maintain its consistency, reaffirming its robustness.
- In contrast, the SingleLoop method, if showing pronounced or variable errors, may have challenges with complex motions or returning to starting positions.

Based on the dataset and the analyses conducted, the DualLoop system consistently showcases better precision and consistency across all dimensions. While the SingleLoop system is capable, its broader spread of errors, especially in the X and Z axes, make it less precise in those dimensions. For applications that demand high precision, the DualLoop system is the preferred choice.

5.6 System Safety Response Analysis

In this section, we present an analysis of the system's response to two critical events:

5.6.1 Encoder Slipping

Figure 5.15 illustrates the encoder readings over time, described as follows: 5.15 described as follows:

- The blue line represents the encoder readings across various time points.
- At time point 4 (marked by the red dashed line), a significant spike in the readings indicates the slipping event.
- Following this event, the encoder readings drop to zero, as shown by the portion of the graph following time point 4. This drop to zero, highlighted by the green dashed line, represents the system's 'kill motion' response, effectively stopping all motion for safety.
- These time points are measured instances that correspond to the data collection frequency, such as every second or millisecond, as defined by the system's monitoring capabilities.

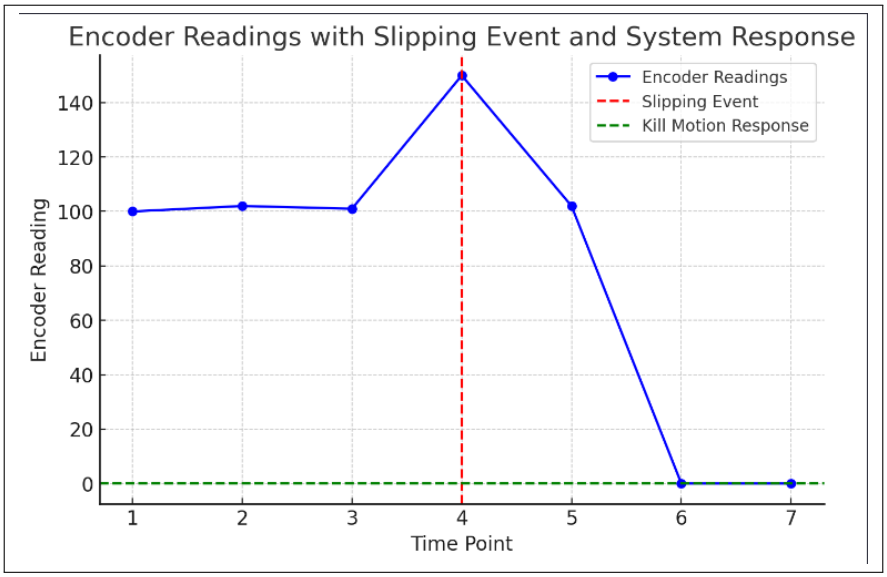

FIGURE 5.15: Primary Vs Secondary Encoder.

5.6.2 Left and Right Limits Test

Figure 5.16 presents two separate line graphs, each representing a scenario for the Left Limit Check and Right Limit Check of your system on the Z axis:

Left Limit Check

- Normal Operation: The blue line shows normal operation within the allowable range.
- Limit Breach: At time point 4 (red dashed line), the machine position drops below the minimum allowable limit (100), indicating a breach of the left limit.

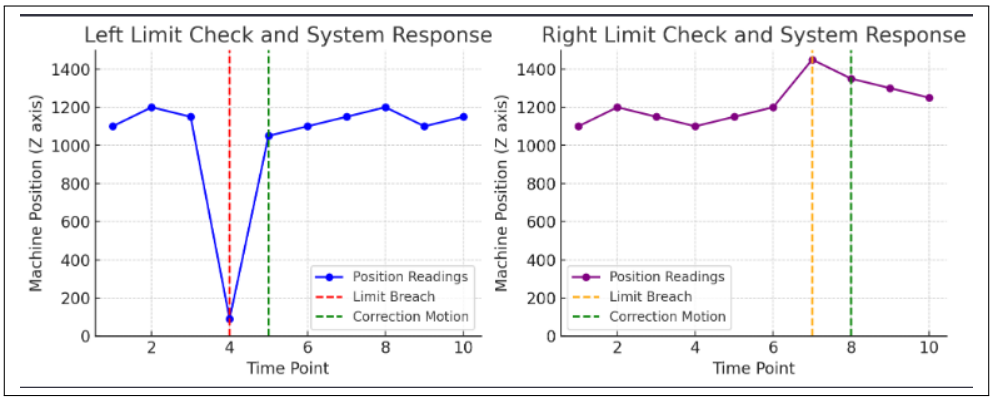

FIGURE 5.16: Left/Right Limits.

- Correction Motion: Immediately after the breach, at time point 5 (green dashed line), the system responds by applying a corrective motion, bringing the machine position back into the allowable range.

Right Limit Check

- Normal Operation: The purple line indicates normal operation within the allowable range.
- Limit Breach: At time point 7 (orange dashed line), the machine position exceeds the maximum allowable limit (1400), signaling a breach of the right limit.
- Correction Motion: Following this breach, at time point 8 (green dashed line), the system executes a corrective motion in the opposite direction, ensuring the machine returns to within the safe operating range.

These time points are measured instances that correspond to the data collection frequency, such as every second or millisecond, as defined by the system's monitoring capabilities.

Chapter 6

Conclusion and Future Work

This dissertation has comprehensively examined the Robotic Patient Positioning System (PPS) within Stereotactic Radiosurgery (SRS), focusing on kinematics, control mechanisms, safety protocols, and precision effectiveness. The critical analysis of the PPS, including its components and control algorithms, has provided significant insights into enhancing the accuracy and safety of cancer treatment technologies, particularly in brain cancer therapies.

The research has successfully demonstrated the PPS's capability to achieve high precision with an accuracy of up to 0.1mm, addressing a crucial need in SRS treatments. Through rigorous testing, both in simulations and real-world scenarios using the OptiTrack system, the dissertation validates the effectiveness of the PPS and its alignment with safety standards. The study not only fills a significant gap in existing literature but also lays a foundation for future advancements in medical treatment technology.

6.1 State-of-the-Art Design and Innovation

The design and research presented in this dissertation represent a cutting-edge advancement in the field of Stereotactic Radiosurgery (SRS), particularly in the development of the Robotic Patient Positioning System (PPS). The PPS is currently undergoing the patenting process, with the application number PCT/US2019/048205. This patent application underscores the novelty and uniqueness of the device, highlighting its potential for significant impact in medical technology.

This novel, state-of-the-art design is unique and patented, meaning that every study conducted on this device, from kinematics to control systems and safety protocols, represents a significant contribution to the scientific community. The research and development on this design are groundbreaking, as they are being done for the first time on this unique system, marking a significant advancement in SRS technology.

6.2 Scientific Contributions

This dissertation represents a comprehensive and multifaceted contribution to the field of Stereotactic Radiosurgery (SRS), particularly in the development and optimization of the Robotic Patient Positioning System (PPS). The key contributions of this research are outlined as follows, each accompanied by its respective scientific publication or output:

Thesis Outline

Thesis I:

Optimizing Range of Motion in Stereotactic Radiosurgery: A Comprehensive Analysis of the Patient Positioning System Design.

This thesis has presented a comprehensive analysis of the Patient Positioning System (PPS) used in Stereotactic Radiosurgery, highlighting its sophisticated design and functionality. The following points summarize the key findings:

- **Design and Components of PPS:** Detailed examination of the PPS, including its 6-degree-of-freedom robotic bed, Linear Rail System, Linkage System, and Tabletop, emphasizing their roles in precise patient alignment.
- **Linear Rail System Functionality:** Analysis of the Linear Rail System, underscoring its critical function in controlling two-axis movements and its contribution to the system's overall flexibility.
- **Linkage System Precision:** Exploration of the Linkage System's contribution to 2D patient positioning, with a focus on the precision offered by its four linkage arms and servo-driven gearboxes.
- **Tabletop Pitching Mechanism:** Discussion on the tabletop's pitching capabilities through the helical cam following system, crucial for effective patient positioning.
- **Kinematic Analysis and Range of Motion:** In-depth study of the kinematics and range of motion within the PPS, highlighting the robustness and precision of the Linkage System, especially at operational extremes.
- **Visualization and Analysis:** Utilization of 3D scatter plots to visualize the relationship between position, orientation, and linkage arm parameters, providing insights into the system's complex operations.
- **System Integration and Precision:** Final analysis of how different subsystems integrate to achieve precision in patient positioning, particularly focusing on the interplay between table tilt and linkage motor adjustments.

Thesis II:

Accurate Robotic Patient Positioning: Integrating Forward Kinematics in Advanced System Design.

In this comprehensive thesis, an in-depth analysis of forward kinematics within the Patient Positioning System (PPS) has been conducted, yielding significant outcomes that enhance the system's operational efficacy:

- **Linear and Rotary Displacements:** The thesis explores detailed computations of linear and rotary displacements, crucial for precise positioning within the PPS.
- **Joint Angle Calculations:** The study accurately determines the angles of the three linkage-driven joints (q_1, q_2, q_3), essential for the kinematic movement of the system.
- **Table Pitching Angle:** The analysis of the Table Pitching Angle ($\theta_{\text{TableAngle}}$) contributes significantly to the system's ability to adjust the patient's position with high accuracy.
- **End-Effector Position and Orientation:** The thesis includes the computation of the end-effector position in Cartesian coordinates ($\mathbf{P} = [x, y, z]^T$) and the derivation of the end-effector orientation, expressed in terms of pitch (α), yaw (β), and roll (γ): ($\mathbf{O} = [\alpha, \beta, \gamma]^T$).

These outcomes validate the precision of our kinematic models and computational methods, underscoring the capability of the PPS to align patients accurately for medical procedures. The results obtained from this forward kinematics analysis are pivotal in enhancing the PPS's performance in real-world medical applications.

Thesis III:

Geometric Approach to Inverse Kinematics in Multi-Subsystem Robotic Patient Positioning System

This thesis delves into the intricate geometric approach to inverse kinematics within the multi-subsystem of the Robotic Patient Positioning System (PPS). Significant advancements achieved in various aspects include:

- **End-Effector Position and Orientation:** Determination of the desired end-effector position in Cartesian coordinates ($\mathbf{P} = [x, y, z]^T$) and calculation of the required orientation expressed as pitch (α), yaw (β), and roll (γ) ($\mathbf{O} = [\alpha, \beta, \gamma]^T$).

- **Joint Angle Calculations:** Computation of angles for the three linkage-driven joints (q_1, q_2, q_3) of the PPS, crucial for precision in the system's movements.
- **Displacement Determination:** Evaluation of linear and rotary displacements using the Linear Motor and Rotary Motor, ensuring precise positional adjustments and alignment.
- **Table Pitching Angle Analysis:** Accurate measurement of the Table Pitching Angle ($\theta_{\text{TableAngle}}$) for rotational alignment of the patient positioning table.

These comprehensive outcomes underscore the precision and effectiveness of the inverse kinematics model used in the PPS. They play a crucial role in enhancing the system's performance, ensuring reliable and precise positioning for medical procedures, and contributing significantly to the field of medical robotics.

Thesis IV:

Advanced Motion Control in Robotic Patient Positioning System: Optimizing Performance Through Comparative Analysis of Single and Dual Control Loops

This thesis delves into the intricate world of control algorithms vital for the effective operation of the Patient Positioning System (PPS). The study entails a thorough investigation of single-loop and dual-loop control systems, focusing on their respective advantages and drawbacks within the PPS framework. A key aspect of this research is the exploration of how dual-loop control surpasses single-loop systems in precision and adaptation to mechanical system variances.

A significant portion of the thesis is dedicated to the utilization of advanced control mechanisms for precision tuning. This includes the deployment of ACS Motion Control tools, such as Frequency Response Function (FRF) analysis and the oscilloscope function, and their pivotal role in enhancing the calibration process and dynamic response analysis of the system.

Furthermore, the thesis outlines a systematic approach to optimize PPS performance. This approach encompasses a comprehensive process of configuration, calibration, and verification of the system's responses, emphasizing the practical application of theoretical control principles to boost system responsiveness and reliability.

In addition, the thesis presents a comparative analysis of DualLoop and SingleLoop systems. This section covers the necessity of error analysis in control systems, a statistical analysis of errors for both systems, and a variety of visualization techniques, such as boxplots and histograms, to illustrate error distributions. It also includes an in-depth examination of the systems' performance across different

movements and rotations.

Overall, the outcomes of this thesis are crucial in advancing the PPS toward achieving optimal performance in clinical settings. The research highlights the importance of sophisticated control strategies and their adaptability to future technological innovations, ensuring the system's efficiency, reliability, and readiness for emerging challenges.

Thesis V:

Developing Robust Safety Protocols for Radiosurgery within Patient Positioning System Framework

This thesis delves into the crucial role of safety protocols within the Patient Positioning System (PPS) in radiosurgery. Key aspects of the analysis include the identification of unique safety concerns intrinsic to radiosurgery, particularly the precision required in radiation delivery and the management of involuntary patient movements. The importance of precision positioning is highlighted, emphasizing the risks associated with mispositioning during radiosurgical procedures and outlining systematic approaches for verifying positioning accuracy.

Further, the thesis explores the advancements in PPS safety technology, such as the integration of real-time imaging and movement detection sensors, along with the development of automatic shutdown features to enhance safety in case of misalignments. The implementation and assurance of safety through emergency stops, fault detection capabilities, limit sensors, and daily initialization procedures are thoroughly detailed. Operator training is also prioritized to ensure competent system management and the prompt resolution of any issues.

Additionally, the thesis presents a structured approach to fault classification and handling, classifying faults into axis and system faults, and describing detailed fault handling procedures, including default responses and monitoring mechanisms. The monitoring of internal safety conditions is also presented, illustrating the system's built-in checks for operational states and anomalies and its capability to automatically take preventive actions to ensure safe operation and minimize potential hazards.

Overall, these outcomes significantly contribute to enhancing patient safety and system reliability in the field of radiosurgery. The development and implementation of robust safety protocols within the PPS framework underscore a commitment to advancing medical technology while prioritizing patient welfare and treatment efficacy.

6.3 Future Work

While this dissertation has made significant strides in understanding and optimizing the PPS for SRS, several avenues for future research have emerged:

1. **Expanded Clinical Trials:** Future work could involve more extensive clinical testing to further establish the efficacy and safety of the PPS in diverse medical scenarios.

2. **Adaptation for Other Cancer Treatments:** Exploring the adaptability of the PPS technology for other types of cancer treatments could broaden its applicability and impact.

3. **Technological Advancements:** Continuous improvements in technology, such as enhanced servo motors or more sophisticated control algorithms, could be integrated into the PPS to further refine its precision and functionality.

4. **Interdisciplinary Collaboration:** Engaging in collaborative efforts with experts from various fields, such as biomedical engineering and computer science, could yield innovative solutions and applications for the PPS.

6.4 Closing Remarks

In conclusion, this dissertation contributes substantially to the field of Stereotactic Radiosurgery, offering promising solutions for precise and safe patient positioning in cancer treatments. The potential of the PPS to revolutionize SRS practices and improve patient outcomes is immense, paving the way for a new era in medical technology and treatment efficacy.

Bibliography

[1] Chauncey Depew Leake. *The old Egyptian medical papyri*. Lawrence, Kan., University of Kansas Press, 1952.

[2] Rose J Papac. "Origins of cancer therapy." In: *The Yale journal of biology and medicine* 74.6 (2001), p. 391.

[3] Edmund S Meltzer and Gonzalo M Sanchez. *The Edwin Smith Papyrus: Updated translation of the trauma treatise and modern medical commentaries*. ISD LLC, 2014.

[4] Francis R Packard. "The Papyrus Ebers". In: *Annals of Medical History* 3.3 (1931), p. 360.

[5] Steven I Hajdu. "A note from history: landmarks in history of cancer, part 1". In: *Cancer* 117.5 (2011), pp. 1097–1102.

[6] Niki Papavramidou, Theodossis Papavramidis, and Thespis Demetriou. "Ancient Greek and Greco–Roman methods in modern surgical treatment of cancer". In: *Annals of surgical oncology* 17 (2010), pp. 665–667.

[7] Anna Di Lonardo, Sergio Nasi, and Simonetta Pulciani. "Cancer: we should not forget the past". In: *Journal of cancer* 6.1 (2015), p. 29.

[8] Emilie Savage-Smith and Roshdi Rashed. *Encyclopedia of the history of Arabic science*. 1996.

[9] Mohammad M Zarshenas and Afshin Mohammadi-Bardbori. "A medieval description of metastatic breast cancer; from Avicenna's view point". In: *The Breast* 31 (2017), pp. 20–21.

[10] Hossein Hosseinzadeh and Marjan Nassiri-Asl. "Avicenna's (Ibn Sina) the canon of medicine and saffron (Crocus sativus): a review". In: *Phytotherapy Research* 27.4 (2013), pp. 475–483.

[11] Harry Keil. "The historical relationship between the concept of tumor and the ending-oma". In: *Bulletin of the History of Medicine* 24.4 (1950), pp. 352–377.

[12] Timothy Jackson. *Celebrating 150 years of care at the Royal Marsden Hospital*. 2001.

[13] Heinz David. "Rudolf Virchow and modern aspects of tumor pathology". In: *Pathology-Research and Practice* 183.3 (1988), pp. 356–364.

[14] Edward Walter and Mike Scott. "The life and work of Rudolf Virchow 1821–1902:"Cell theory, thrombosis and the sausage duel"". In: *Journal of the Intensive Care Society* 18.3 (2017), pp. 234–235.

[15] Jan Willem Coebergh et al. "EUROCOURSE lessons learned from and for population-based cancer registries in Europe and their programme owners: Improving performance by research programming for public health and clinical evaluation". In: *European journal of cancer* 51.9 (2015), pp. 997–1017.

[16] John S Bertram. "The molecular biology of cancer". In: *Molecular aspects of medicine* 21.6 (2000), pp. 167–223.

[17] Eyal Bercovich and Marcia C Javitt. "Medical imaging: from roentgen to the digital revolution, and beyond". In: *Rambam Maimonides medical journal* 9.4 (2018).

[18] Richard Francis Mould. "The early history of x-ray diagnosis with emphasis on the contributions of physics 1895-1915". In: *Physics in Medicine & Biology* 40.11 (1995), p. 1741.

[19] Barron H Lerner. ""To see today with the eyes of tomorrow": a history of screening mammography". In: *Canadian bulletin of medical history* 20.2 (2003), pp. 299–321.

[20] Vincent T DeVita Jr and Edward Chu. "A history of cancer chemotherapy". In: *Cancer research* 68.21 (2008), pp. 8643–8653.

[21] Martin S Highley et al. "The nitrogen mustards". In: *Pharmacological Reviews* 74.3 (2022), pp. 552–599.

[22] Mark Clemons, Sarah Danson, and Anthony Howell. "Tamoxifen ('Nolvadex'): a review: Antitumour treatment". In: *Cancer treatment reviews* 28.4 (2002), pp. 165–180.

[23] Bettyann Kevles. *Naked to the bone: Medical imaging in the twentieth century*. Rutgers University Press, 1997.

[24] Vahe Petrosyan, Georgina Kane, and Phillip Ameerally. "Oral cancer treatment through the ages: Part 2". In: *Journal of Oral and Maxillofacial Surgery* 77.7 (2019), pp. 1484–1489.

[25] Apostolia-Maria Tsimberidou. "Targeted therapy in cancer". In: *Cancer chemotherapy and pharmacology* 76 (2015), pp. 1113–1132.

[26] Manfred Schuster, Andreas Nechansky, and Ralf Kircheis. "Cancer immunotherapy". In: *Biotechnology Journal: Healthcare Nutrition Technology* 1.2 (2006), pp. 138–147.

[27] AR Genazzani and M Gambacciani. "Hormone replacement therapy: the perspectives for the 21st century". In: *Maturitas* 32.1 (1999), pp. 11–17.

[28] Giovana Maria Fioramonti Calixto et al. "Nanotechnology-based drug delivery systems for photodynamic therapy of cancer: a review". In: *Molecules* 21.3 (2016), p. 342.

[29] Gou Watanabe and Norihiro Ishikawa. "da Vinci surgical system". In: *Kyobu geka. The Japanese journal of thoracic surgery* 67.8 (2014), pp. 686–689.

[30] Bin S Teh, Shiao Y Woo, and E Brian Butler. "Intensity modulated radiation therapy (IMRT): a new promising technology in radiation oncology". In: *The oncologist* 4.6 (1999), pp. 433–442.

[31] Allison M Campbell et al. "Gamma knife stereotactic radiosurgical thalamotomy for intractable tremor: a systematic review of the literature". In: *Radiotherapy and Oncology* 114.3 (2015), pp. 296–301.

[32] Edward A Monaco et al. "The past, present and future of Gamma Knife radiosurgery for brain tumors: the Pittsburgh experience". In: *Expert Review of Neurotherapeutics* 12.4 (2012), pp. 437–445.

[33] Nicolas Massager et al. "Clinical evaluation of targeting accuracy of gamma knife radiosurgery in trigeminal neuralgia". In: *International Journal of Radiation Oncology* Biology* Physics* 69.5 (2007), pp. 1514–1520.

[34] Jean Regis et al. "Safety and efficacy of Gamma Knife radiosurgery in hypothalamic hamartomas with severe epilepsies: A prospective trial in 48 patients and review of the literature". In: *Epilepsia* 58 (2017), pp. 60–71.

[35] G Luxton et al. "Mechanical malfunction of the Leksell gamma knife during patient treatment". In: *Stereotactic and Functional Neurosurgery* 66.1-3 (1996), pp. 35–40.

[36] Mark Ruschin et al. "Performance of a novel repositioning head frame for gamma knife perfexion and image-guided linac-based intracranial stereotactic radiotherapy". In: *International Journal of Radiation Oncology* Biology* Physics* 78.1 (2010), pp. 306–313.

[37] Andrew Wu et al. "Physics of gamma knife approach on convergent beams in stereotactic radiosurgery". In: *International Journal of Radiation Oncology* Biology* Physics* 18.4 (1990), pp. 941–949.

[38] Michael C Ferris and David M Shepard. "Optimization of gamma knife radiosurgery." In: *Discrete Mathematical Problems with Medical Applications* 55 (1999), pp. 27–44.

[39] R Lee MacDonald et al. "Real-time infrared motion tracking analysis for patients treated with gated frameless image guided stereotactic radiosurgery". In: *International Journal of Radiation Oncology* Biology* Physics* 106.2 (2020), pp. 413–421.

[40] Marc Levivier, Thierry Gevaert, and Laura Negretti. "Gamma Knife, CyberKnife, TomoTherapy: gadgets or useful tools?" In: *Current opinion in neurology* 24.6 (2011), pp. 616–625.

[41] Einar Osland Vik-Mo et al. “Gamma knife stereotactic radiosurgery for acromegaly”. In: *European Journal of Endocrinology* 157.3 (2007), pp. 255–263.

[42] Terence T Sio et al. “Comparing gamma knife and cyberknife in patients with brain metastases”. In: *Journal of applied clinical medical physics* 15.1 (2014), pp. 14–26.

[43] Jyothis John. “Cyber Knife”. In: *International Journal of Nursing Education and Research* 7.4 (2019), pp. 633–637.

[44] SJ Goetsch et al. “Physics of rotating gamma systems for stereotactic radiosurgery”. In: *International Journal of Radiation Oncology* Biology* Physics* 43.3 (1999), pp. 689–696.

[45] Bishwambhar Sengupta et al. “Intensity modulated operating mode of the rotating gamma system”. In: *Medical Physics* 45.5 (2018), pp. 2289–2298.

[46] Huan Liu et al. “Dosimetric Evaluation of a New Rotating Gamma System for Stereotactic Radiosurgery”. In: *arXiv preprint arXiv:2210.04386* (2022).

[47] Saadah Alaa and Géza Husi. “Hat szabadságfokos robotkarprototípus-modellezés Matlab által”. In: *Műszaki Tudományos Közlemények* 15 (2021), pp. 94–98.

[48] Alaa Saadah and Géza Husi. “Six DOF Robotic Arm Prototype Modelling By Matlab”. In: *Papers on Technical Science* 15 (2021), pp. 94–98.

[49] Alaa Saadah. “Computing the kinematics study of a 6 DOF industrial manipulator prototype by matlab”. In: *Recent Innovations in Mechatronics* 7.1. (2020), pp. 1–5.

[50] Sébastien Briot et al. “Homogeneous transformation matrix”. In: *Dynamics of Parallel Robots: From Rigid Bodies to Flexible Elements* (2015), pp. 19–32.

[51] Tao Zhang et al. “A novel method to identify DH parameters of the rigid serial-link robot based on a geometry model”. In: *Industrial Robot: the international journal of robotics research and application* 48.1 (2020), pp. 157–167.

[52] Alaa Saadah et al. “Kinematics Study for Linkage System (Parallel Robotics System): linkage system of patient positioning system PPS to accurately position a human body for radiosurgery treatment”. In: *2023 Advances in Science and Engineering Technology International Conferences (ASET)*. IEEE. 2023, pp. 1–6.

[53] Teun Koetsier. “Ludwig Burmester, Kinematics as Part of Geometry”. In: *A History of Kinematics from Zeno to Einstein: On the Role of Motion in the Development of Mathematics*. Springer, 2023, pp. 265–285.

[54] Omar Martínez and Ricardo Campa. “Comparing methods using homogeneous transformation matrices for kinematics modeling of robot manipulators”. In: *Multibody Mechatronic Systems: Papers from the MuSMe Conference in 2020 7*. Springer. 2021, pp. 110–118.

[55] Hao Ye et al. “Forward and inverse kinematics of a 5-DOF hybrid robot for composite material machining”. In: *Robotics and Computer-Integrated Manufacturing* 65 (2020), p. 101961.

[56] James Diebel et al. “Representing attitude: Euler angles, unit quaternions, and rotation vectors”. In: *Matrix* 58.15-16 (2006), pp. 1–35.

[57] Deepak Tolani, Ambarish Goswami, and Norman I Badler. “Real-time inverse kinematics techniques for anthropomorphic limbs”. In: *Graphical models* 62.5 (2000), pp. 353–388.

[58] Oscar Altuzarra et al. “Path analysis for hybrid rigid–flexible mechanisms”. In: *Mathematics* 9.16 (2021), p. 1869.

[59] Sabine Stifter. “Algebraic methods for computing inverse kinematics”. In: *Journal of Intelligent and Robotic Systems* 11 (1994), pp. 79–89.

[60] Xuewen Yang et al. “A geometric method for kinematics of delta robot and its path tracking control”. In: *2014 14th International Conference on Control, Automation and Systems (ICCAS 2014)*. IEEE. 2014, pp. 509–514.

[61] Serdar Kucuk and Zafer Bingul. “Inverse kinematics solutions for industrial robot manipulators with offset wrists”. In: *Applied Mathematical Modelling* 38.7-8 (2014), pp. 1983–1999.

[62] John J Craig. *Introduction to Robotics: Mechanics and Control. 4th*. 2018.

[63] Pierre Larochelle. “Synthesis of planar mechanisms for pick and place tasks with guiding positions”. In: *Journal of Mechanisms and Robotics* 7.3 (2015), p. 031009.

[64] Kwan Wu Chin, BR Von Konsky, and A Marriott. “Closed-form and generalized inverse kinematics solutions for the analysis of human motion”. In: *Proceedings of the 19th Annual International Conference of the IEEE Engineering in Medicine and Biology Society.'Magnificent Milestones and Emerging Opportunities in Medical Engineering'(Cat. No. 97CH36136)*. Vol. 5. IEEE. 1997, pp. 1911–1914.

[65] Vahid Nazari and Leila Notash. “Motion analysis of manipulators with uncertainty in kinematic parameters”. In: *Journal of Mechanisms and Robotics* 8.2 (2016), p. 021014.

[66] Serdar Kucuk and Zafer Bingul. *Robot kinematics: Forward and inverse kinematics*. INTECH Open Access Publisher London, UK, 2006.

[67] Gregory G Slabaugh. “Computing Euler angles from a rotation matrix”. In: *Retrieved on August* 6.2000 (1999), pp. 39–63.

[68] Robert J Webster III and Bryan A Jones. “Design and kinematic modeling of constant curvature continuum robots: A review”. In: *The International Journal of Robotics Research* 29.13 (2010), pp. 1661–1683.

[69] Juan Ignacio Valderrama-Rodríguez, José M Rico, and J Jesús Cervantes-Sánchez. "A screw theory approach to compute instantaneous rotation axes of indeterminate spherical linkages". In: *Mechanics Based Design of Structures and Machines* 50.8 (2022), pp. 2836–2876.

[70] Erik Brynjolfsson and Andrew McAfee. *The second machine age: Work, progress, and prosperity in a time of brilliant technologies*. WW Norton & Company, 2014.

[71] Jorge A Franco, Juan A Gallego, and Just L Herder. "Static Balancing of Four-Bar Linkages With Torsion Springs by Exerting Negative Stiffness Using Linear Spring at the Instant Center of Rotation". In: American Society of Mechanical Engineers. 2020.

[72] FU Jian et al. "Multi-level virtual prototyping of electromechanical actuation system for more electric aircraft". In: *Chinese Journal of Aeronautics* 31.5 (2018), pp. 892–913.

[73] Sayako Sakama, Yutaka Tanaka, and Akiya Kamimura. "Characteristics of hydraulic and electric servo motors". In: *Actuators*. Vol. 11. 1. MDPI. 2022, p. 11.

[74] Muhammad Ahmad Baballe et al. "Different Types of Servo Motors and Their Applications". In: *1st International Conference on Engineering and Applied Natural Sciences*. 2022, pp. 974–979.

[75] Recep Halicioglu, L Canan Dulger, and A Tolga Bozdana. "Mechanisms, classifications, and applications of servo presses: A review with comparisons". In: *Proceedings of the Institution of Mechanical Engineers, Part B: Journal of Engineering Manufacture* 230.7 (2016), pp. 1177–1194.

[76] Riccardo Marino, Sergei Peresada, and Patrizio Tomei. "Output feedback control of current-fed induction motors with unknown rotor resistance". In: *IEEE Transactions on Control Systems Technology* 4.4 (1996), pp. 336–347.

[77] Abdul Wali Abdul Ali, Fatin Asmida Abdul Razak, and Nasri Hayima. "A review on the AC servo motor control systems". In: *ELEKTRIKA-Journal of Electrical Engineering* 19.2 (2020), pp. 22–39.

[78] Riazollah Firoozian. *Servo motors and industrial control theory*. Springer, 2014.

[79] Anthony Thomas Fuller. "The early development of control theory. II". In: (1976).

[80] George W Younkin. *Industrial Servo Control Systems: Fundamentals And Applications, Revised And Expanded*. CRC press, 2002.

[81] PR Ouyang et al. "Micro-motion devices technology: The state of arts review". In: *The International Journal of Advanced Manufacturing Technology* 38 (2008), pp. 463–478.

[82] Fayez FM El-Sousy et al. "Adaptive neural-network optimal tracking control for permanent-magnet synchronous motor drive system via adaptive dynamic programming". In: *2020 IEEE industry applications society annual meeting*. IEEE. 2020, pp. 1–8.

[83] Ge Ou et al. "Robust integrated actuator control: experimental verification and real-time hybrid-simulation implementation". In: *Earthquake Engineering & Structural Dynamics* 44.3 (2015), pp. 441–460.

[84] Parag D Lalwani et al. "Advanced safety control system for industrial articulated robots". In: *2017 International conference of Electronics, Communication and Aerospace Technology (ICECA)*. Vol. 1. IEEE. 2017, pp. 241–245.

[85] Eryu Zhang and Xingang Miao. "Designation of laser rapid prototyping machine based on ACS motion controller". In: *2016 Chinese Control and Decision Conference (CCDC)*. IEEE. 2016, pp. 6328–6331.

[86] Lorenzo Iafolla et al. "Proof of concept of a novel absolute rotary encoder". In: *Sensors and Actuators A: Physical* 312 (2020), p. 112100.

[87] Xiaotian Li. "Model-Based Design of Brushless DC Motor Control and Motion Control Modelling for RoboCup SSL Robots". In: (2015).

[88] Supachock Tuntivivat and Pradya Prempraneerach. "Design and Construction and Motion Control of 6-Axis Robot Manipulator for Industrial Applications". In: *The Second TSME International Conference on Mechanical Engineering, Krabi, Thailand*. 2011, pp. 19–21.

[89] Xiao Yu Ge, Yong Xiao, and Li Hua Gu. "Motion Control Design for XY Positioning Platform". In: *Advanced Materials Research* 482 (2012), pp. 435–438.

[90] Junfeng Liang et al. "A novel 3D video oculography system for measuring cross-axis vestibulo-ocular reflex". In: *Medical Engineering & Physics* 96 (2021), pp. 41–45.

[91] Chiara Cimini et al. "A human-in-the-loop manufacturing control architecture for the next generation of production systems". In: *Journal of manufacturing systems* 54 (2020), pp. 258–271.

[92] Jingjing Xu et al. "A noncontact control strategy for circular peg-in-hole assembly guided by the 6-dof robot based on hybrid vision". In: *IEEE Transactions on Instrumentation and Measurement* 71 (2022), pp. 1–15.

[93] Tianyi He, Xiang Chen, and Guoming G Zhu. "A dual-loop robust control scheme with performance separation: Theory and experimental validation". In: *IEEE Transactions on Industrial Electronics* 69.12 (2022), pp. 13483–13493.

[94] Zhitai Liu et al. "Approximation-free robust synchronization control for dual-linear-motors-driven systems with uncertainties and disturbances". In: *IEEE Transactions on Industrial Electronics* 69.10 (2021), pp. 10500–10509.

[95] Zeng Meng et al. "Convergence control of single loop approach for reliability-based design optimization". In: *Structural and Multidisciplinary Optimization* 57 (2018), pp. 1079–1091.

[96] DV Sabarianand, P Karthikeyan, and T Muthuramalingam. "A review on control strategies for compensation of hysteresis and creep on piezoelectric actuators based micro systems". In: *Mechanical Systems and Signal Processing* 140 (2020), p. 106634.

[97] Hsiao-Ping Huang and Jyh-Cheng Jeng. "Monitoring and assessment of control performance for single loop systems". In: *Industrial & engineering chemistry research* 41.5 (2002), pp. 1297–1309.

[98] Yao Wang, Haitao Yu, and Yulei Liu. "Speed-current single-loop control with overcurrent protection for PMSM based on time-varying nonlinear disturbance observer". In: *IEEE Transactions on Industrial Electronics* 69.1 (2021), pp. 179–189.

[99] Cecil L Smith. *Advanced process control: beyond single loop control*. John Wiley & Sons, 2011.

[100] Michael A Johnson and Mohammad H Moradi. *PID control*. Springer, 2005.

[101] Carlos A Smith and Armando B Corripio. *Principles and practices of automatic process control*. John wiley & sons, 2005.

[102] MV Sadasivarao and M Chidambaram. "PID Controller tuning of cascade control systems". In: *Journal of the Indian Institute of Science* 86.4 (2006), p. 343.

[103] Xuan Yao, Zhaobo Chen, and Yinghou Jiao. "A dual-loop control approach of active magnetic bearing system for rotor tracking control". In: *IEEE Access* 7 (2019), pp. 121760–121768.

[104] JF Pan et al. "High-precision dual-loop position control of an asymmetric bilateral linear hybrid switched reluctance motor". In: *IEEE Transactions on Magnetics* 51.11 (2015), pp. 1–5.

[105] Yu Cao et al. "A Dual-Position Loop LLADRC Control Method Based on Harmonic Gear Drive". In: *Mathematical Problems in Engineering* 2022 (2022).

[106] Štefan Bucz and Alena Kozáková. "Advanced methods of PID controller tuning for specified performance". In: *PID Control for Industrial Processes* (2018), pp. 73–119.

[107] Zoran Miljković and Milica Petrović. "A Survey of Swarm Intelligence-based Optimization Algorithms for Tuning of Cascade Control Systems: Concepts, Models and Applications". In: *Plenary Session-Invited paper, Proceedings of the 5th International Conference-Mechnanical Engineering in XXI Century (MASING 2020), Niš, December 09-10, 2020*. University of Niš-Faculty of Mechanical Engineering. 2020, pp. 3–8.

[108] Artur Piščalov et al. “Investigation of position and velocity stability of the nanometer resolution linear motor stage with air bearings by shaping of controller transfer function”. In: *Symmetry* 12.12 (2020), p. 2062.

[109] Vilius Kavaliauskas. “Investigation of dynamic processes of precision positioning systems with linear motor”. PhD thesis. Vilniaus Gedimino technikos universitetas., 2021.

[110] Rakesh P Borase et al. “A review of PID control, tuning methods and applications”. In: *International Journal of Dynamics and Control* 9 (2021), pp. 818–827.

[111] Oluwasegun Ayokunle Somefun, Kayode Akingbade, and Folasade Dahunsi. “The dilemma of PID tuning”. In: *Annual Reviews in Control* 52 (2021), pp. 65–74.

[112] Ki Mun Kang et al. “Estimation of optimal margin for intrafraction movements during frameless brain radiosurgery”. In: *Medical physics* 40.5 (2013), p. 051716.

[113] David J Eaton and Kevin Alty. “Dependence of volume calculation and margin growth accuracy on treatment planning systems for stereotactic radiosurgery”. In: *The British Journal of Radiology* 90 (2017), p. 20170633.

[114] Martin J Murphy. “The importance of computed tomography slice thickness in radiographic patient positioning for radiosurgery”. In: *Medical Physics* 26.2 (1999), pp. 171–175.

[115] Indra J Das et al. “Quality and safety considerations in stereotactic radiosurgery and stereotactic body radiation therapy: An ASTRO safety white paper update”. In: *Practical Radiation Oncology* 12.4 (2022), e253–e268.

[116] Daniel M Trifiletti et al. “The evolution of stereotactic radiosurgery in neurosurgical practice”. In: *Journal of neuro-oncology* 151 (2021), pp. 451–459.

[117] Lindsey Claps et al. “Utilization of CBCT to improve the delivery accuracy of Gamma Knife radiosurgery with G-frame”. In: *Journal of Applied Clinical Medical Physics* 22.8 (2021), pp. 120–128.

[118] Fadi Al Saiegh et al. “Frameless Angiography–Based Gamma Knife Stereotactic Radiosurgery for Cerebral Arteriovenous Malformations: A Proof-of-Concept Study”. In: *World Neurosurgery* 164 (2022), e808–e813.

[119] David Krug et al. “Stereotactic body radiotherapy for ventricular tachycardia (cardiac radiosurgery) First-in-patient treatment in Germany”. In: *Strahlentherapie und Onkologie* 196 (2020), pp. 23–30.

[120] X Sharon Qi et al. “Quality and safety considerations in image guided radiation therapy: An ASTRO Safety White Paper update”. In: *Practical Radiation Oncology* 13.2 (2023), pp. 97–111.

[121] Ronald E Warnick et al. “Failure mode and effects analysis (FMEA) to enhance the safety and efficiency of Gamma Knife radiosurgery”. In: *Journal of Radiosurgery and SBRT* 7.2 (2020), p. 115.

[122] AA Sarchosoglou et al. “Failure modes in stereotactic radiosurgery. A narrative review”. In: *Radiography* 28.4 (2022), pp. 999–1009.

[123] Kun Wang et al. “Predicting fault slip via transfer learning”. In: *Nature Communications* 12.1 (2021), p. 7319.

[124] E Rezich et al. “Overview of SLOPE Laboratory Testing Capabilites for Planetary Mobility and Traction Studies at NASA Glenn Research Center”. In: *ASCE Earth and Space 2022*. 2022.

[125] Alexander M Morgan et al. “A NOVEL STUDY EXAMINING COGNITIVE-MOTOR INTERFERENCE AFTER ANTERIOR CRUCIATE LIGAMENT RECONSTRUCTION”. In: *ISBS Proceedings Archive* 41.1 (2023), p. 83.

[126] Takuto Yoshida et al. “A Survey of Ground Truth Measurement Systems for Indoor Positioning”. In: *Journal of Information Processing* 31 (2023), pp. 15–20.

[127] Marek Retinger et al. “Toward improving tracking precision in motion capture systems”. In: *2023 International Conference on Unmanned Aircraft Systems (ICUAS)*. IEEE. 2023, pp. 919–925.

[128] Isabella Chiurillo et al. “High-Accuracy Neuro-Navigation with Computer Vision for Frameless Registration and Real-Time Tracking”. In: *Bioengineering* 10.12 (2023), p. 1401.

[129] Vicente Perez-Sanchez et al. “Bio-inspired morphing tail for flapping-wings aerial robots using macro fiber composites”. In: *Applied Sciences* 11.7 (2021), p. 2930.

[130] Hui Meng and Hongsik Park. “Empathy Study in Animation-The Proposed Empathetic Gesture Guidance.” In: *International Journal of Contents* 19.1 (2023).

[131] Zhengtao Wei et al. “Experimental study on autonomous assembly of multiple spacecraft simulators in a spinning scenario”. In: *Acta Astronautica* 207 (2023), pp. 106–117.